

**INVESTIGATING THE MOLECULAR MECHANISM OF ACTION
OF *Clostridium perfringens* ENTEROTOXIN USING
STRUCTURE-FUNCTION AND OLIGOMERIC ANALYSES**

by

James Gilbert Smedley, III

Bachelor of Science, University of Delaware, 1999

Master of Science, Duquesne University, 2001

Submitted to the Graduate Faculty of
the School of Medicine in partial fulfillment
of the requirements for the degree of
Doctor of Philosophy

University of Pittsburgh

2007

UNIVERSITY OF PITTSBURGH
SCHOOL OF MEDICINE

This dissertation was presented

by

James Gilbert Smedley, III

It was defended on

March 23, 2007

and approved by

James A. Carroll, Ph.D., Molecular Genetics and Biochemistry

Michael Cascio, Ph.D., Molecular Genetics and Biochemistry

Michael A. Parniak, Ph.D., Molecular Genetics and Biochemistry

Dissertation Advisor: Bruce A. McClane, Ph.D., Molecular Genetics and Biochemistry

Copyright © by James Gilbert Smedley, III

2007

**INVESTIGATING THE MOLECULAR MECHANISM OF ACTION
OF *Clostridium perfringens* ENTEROTOXIN USING
STRUCTURE-FUNCTION AND OLIGOMERIC ANALYSES**

James Gilbert Smedley, III, M.S.

University of Pittsburgh, 2007

Clostridium perfringens, a Gram-positive and spore-forming anaerobe, is a significant pathogen of both humans and domestic animals. Among the many toxins produced by this bacterium, the *C. perfringens* enterotoxin (CPE) is one of the principal contributors to *C. perfringens* human disease via its role in both foodborne and non-foodborne gastrointestinal illness. Produced in massive quantities during sporulation in the intestine, CPE begins its action by binding to host cells and forming an SDS-sensitive small complex. At physiologic conditions, CPE then associates with additional proteins to form large SDS-resistant complexes in the plasma membrane, the formation of which coincide with membrane permeability alterations of the cell. The two species of large complex have been reported to have molecular masses of ~155 and ~200 kDa, and recent compositional analysis of the complexes has shown that the former complex contains both CPE and claudin, while the latter contains CPE, claudin, and occludin. Prior structure-function analysis of CPE has defined regions at the N- and C-termini involved with cytotoxic and binding activities of the toxin, respectively. Despite the important findings contributed from previous studies of CPE, several significant questions remain regarding the molecular aspects of CPE's mechanism of action. In this thesis dissertation, research is presented aimed to answer three specific structure-function and mechanistic questions about CPE action. Site-directed mutagenesis enabled the identification of two residues in the N-terminal cytotoxicity region of CPE that were crucial for the formation of the CPE large complexes, and likely function in oligomerization of the toxin. In addition, a novel pre-pore step was defined by deletion mutagenesis of a 25 amino acid region of CPE proposed to be involved in membrane insertion. Lastly, CPE was determined to have hexameric stoichiometry in both of the large complexes, prompting a reevaluation of their molecular masses. Several new insights into CPE activity have been gained by the work presented here within, and models for the molecular mechanism of action and structure-function relationships of CPE are updated.

TABLE OF CONTENTS

LIST OF TABLES.....	xii
LIST OF FIGURES.....	xiii
PREFACE.....	xvi
1.0 INTRODUCTION	1
1.1 <i>Clostridium perfringens</i>	1
1.1.1 General bacteriology.....	1
1.1.2 Genomic analysis of <i>C. perfringens</i>	2
1.1.3 <i>C. perfringens</i> toxins and associated diseases	2
1.1.3.1 Typing toxins of <i>C. perfringens</i>	3
1.1.3.2 Non-typing toxins of <i>C. perfringens</i>	4
1.2 <i>C. perfringens</i> ENTEROTOXIN.....	5
1.2.1 <i>C. perfringens</i> type A food poisoning and the discovery of CPE.....	5
1.2.2 Association of CPE with non-foodborne diarrheas	8
1.2.3 Beta2 toxin: an AAD/SD accessory toxin?	8
1.2.4 CPE Genetics.....	9
1.2.4.1 Gene structure and transcriptional regulation of <i>cpe</i>	9
1.2.4.2 Genetic locus of <i>cpe</i>	11
1.2.4.3 Molecular Koch's postulates and <i>cpe</i>	11
1.3 MECHANISM OF ACTION OF CPE.....	12
1.3.1 The enterotoxic consequences of CPE delivery in the small intestine....	12

1.3.2	Cellular toxicity induced by CPE	14
1.3.2.1	Cell culture models of CPE cytotoxicity.....	15
1.3.2.2	Cellular mechanism of death.....	17
1.3.3	Membranes and complexes: the molecular action of CPE	18
1.3.3.1	Receptor binding	19
1.3.3.2	Small complex formation by CPE	21
1.3.3.3	Large complex formation by CPE	22
1.3.3.4	Exploiting CPE:claudin interactions: clinical and therapeutic applications.....	24
1.4	CORRELATING CPE STRUCTURE WITH ACTIVITY.....	26
1.4.1	CPE biochemistry.....	26
1.4.2	Current knowledge of structure-function relationships within CPE	29
1.4.2.1	N-terminal activation region	29
1.4.2.2	N-terminal cytotoxicity region.....	31
1.4.2.3	C-terminal binding domain	33
1.5	THE β -BARREL PORE-FORMING TOXINS.....	36
1.5.1	Membrane-damaging proteins	36
1.5.2	β -PFTs: from water-soluble proteins to membrane-penetrating pores....	37
1.5.2.1	Structural attributes of the β -PFTs	38
1.6	QUESTIONS ADDRESSED IN THIS THESIS.....	41
1.6.1	Specific question #1 – Why is the N-terminal cytotoxicity region of CPE essential for its post-binding cytotoxicity activity?.....	41
1.6.2	Specific question #2 – Is there a region of CPE that is important for membrane insertion or pore formation?	42

1.6.3	Specific question #3 – What is the oligomeric state of CPE within the large complexes?	43
2.0	MATERIALS AND METHODS	45
2.1	BACTERIAL CULTURING	45
2.1.1	Bacterial strains, growth media, and media supplements	45
2.2	DNA PREPARATION AND MANIPULATION	45
2.2.1	Site-directed mutagenesis of <i>cpe</i>	45
2.2.2	Deletion mutagenesis of <i>cpe</i>	47
2.2.3	DNA Sequencing	47
2.3	PROTEIN BIOCHEMISTRY AND CHROMATOGRAPHY	49
2.3.1	Preparation of CPE	49
2.3.2	Enterokinase digestions of rCPE ₃₇₋₃₁₉	50
2.3.3	Limited trypsin proteolysis assay	50
2.3.3	Size exclusion chromatography	51
2.3.3	Ferguson plot analysis	52
2.4	CPE ACTIVITY CHARACTERIZATION	53
2.4.1	Morphologic damage assay	53
2.4.2	Competitive binding analysis	53
2.4.3	Small complex formation	54
2.4.4	Large complex formation	54
2.4.5	Heteromer gel shift assay with CPE large complexes	55
2.4.6	⁸⁶ Rb release experiments	56
2.4.7	Pronase resistance of large complex	56
2.4.8	Dissociation of CPE large complex from membranes	57
2.4.9	Heat denaturation of CPE large complex	57

2.5	IN VIVO ANALYSIS OF CPE ACTIVITY	58
2.5.1	Fluid accumulation in rabbit ileal loops	58
2.5.2	Histopathological analysis of CPE-treated ileal tissues.....	58
3.0	RESULTS	59
3.1	FINE-MAPPING OF THE N-TERMINAL CYTOTOXICITY REGION OF CPE	59
3.1.1	Alanine-scanning mutagenesis	59
3.1.1.1	Introduction of amino acid substitutions.....	59
3.1.1.2	Morphologic damage of Caco-2 cells by alanine variants of rCPE.....	60
3.1.1.3	Analysis pore-formation by the alanine-substituted rCPE variants.....	61
3.1.1.4	Competitive binding ability of the rCPE alanine variants	63
3.1.1.5	Small complex formation by the rCPE alanine variants	65
3.1.1.6	Large complex formation by the rCPE alanine variants	66
3.1.1.7	Analysis of gross conformational changes in rCPE alanine variants.....	67
3.1.2	Saturation mutagenesis of residues important for CPE action	68
3.1.2.1	Non-alanine substitutions at D48.....	69
3.1.2.2	Non-alanine substitutions at I51	70
3.1.2.3	Non-alanine substitutions at W50.....	70
3.1.3	Correlation between <i>in vitro</i> cytotoxicity and <i>in vivo</i> enterotoxicity	71
3.1.3.1	Fluid accumulation in the rabbit ileal loop model	71
3.2	SEARCH FOR A MEMBRANE INSERTION DOMAIN OF CPE	75
3.2.1	Amino acids 81-106 of CPE: a transmembrane stem domain?	75
3.2.1.1	Deletion mutagenesis of the putative TMD of CPE	76

3.2.1.2	Competitive binding analysis of the TM1 deletion variant	77
3.2.1.3	Cytotoxicity of the TM1 deletion variant	77
3.2.1.4	Pore-formation of the TM1 variant	78
3.2.1.5	Formation of SDS-resistant large complexes by the TM1 variant	80
3.2.1.6	Analysis of the TM1 pre-pore large complex	81
3.2.1.6.1	Pronase resistance of the TM1 large complex.....	81
3.2.1.6.2	Membrane dissociation of the TM1 large complex.....	82
3.2.1.6.3	Heat Denaturation of the TM1 Large Complex.....	84
3.2.2	Temporal questions regarding functional regions of CPE.....	85
3.2.2.1	Activity characterization of TM1-D48A	86
3.3	INVESTIGATING THE OLIGOMERIZATION OF CPE IN THE LARGE	
	COMPLEXES.....	87
3.3.1	Generation of rCPE molecular mass variants	87
3.3.2	Characterization of large complexes made by rCPE molecular mass	
	variants.....	88
3.3.3	Heteromeric CPE large complex gel shift analysis	90
3.3.4	Reassessment of the molecular mass of the CPE large complexes	92
3.3.4.1	Ferguson plot analysis of the CPE large complexes	94
3.3.4.2	Analysis of the large CPE complexes by size exclusion	
	chromatography	98
3.3.5	Exploration of dominant negative phenotypes from rCPE variants.....	100
3.3.5.1	Dominant negative effects of CPE oligomerization	101
3.3.5.2	Blocking of pore-formation by dominant negative variants.....	103
4.0	DISCUSSION.....	105

4.1	WHY IS THE N-TERMINAL CYTOTOXICITY REGION ESSENTIAL FOR POST-BINDING CYTOTOXIC ACTIVITY OF CPE?	107
4.1.1	Explanation of mutagenesis and rCPE variant phenotypes	107
4.1.1.1	D48 and I51: crucial for CPE cytotoxicity.....	107
4.1.1.2	Glycine to alanine: loss of flexibility	108
4.1.1.3	W50 is plays a structural role for CPE.....	109
4.1.2	N-terminal core cytotoxicity sequence: the latch hypothesis	110
4.1.3	<i>In vivo</i> validation of <i>in vitro</i> phenotypes.....	112
4.2	SEARCH FOR A REGION OF CPE INVOLVED IN MEMBRANE INSERTION	113
4.2.1	Identification of a pre-pore large complex state	113
4.2.2	Possible functions of CPE amino acids 81-106.....	114
4.2.2.1	Transmembrane stem domain	114
4.2.2.1.1	Probing the environment of residues in the putative TMD of CPE	118
4.2.2.2	Rim interactions with the membrane.....	122
4.2.2.3	Protein-protein interactions	123
4.2.3	Order of involvement of CPE functional regions	123
4.3	EXAMINATION OF THE OLIGOMERIC STATE OF CPE IN THE LARGE COMPLEXES	124
4.3.1	Determination the stoichiometry of CPE in the large complexes.....	125
4.3.2	Molecular mass and composition of the “~155 kDa” large complex	126
4.3.3	Molecular mass and composition of the “~200 kDa” large complex	127
4.3.4	Nomenclature change.....	128
4.3.5	Dominant negative variants of rCPE	129
4.3.5.1	Inhibition by blocking membrane insertion	129

4.3.5.2	Inhibition by chain termination	130
4.4	UPDATING STRUCTURE-FUNCTION RELATIONSHIPS OF CPE	131
4.4.1	N-terminal activation region.....	131
4.4.2	N-terminal core cytotoxicity sequence	132
4.4.3	Putative transmembrane domain.....	132
4.4.4	Tight junction modulator region	133
4.4.5	C-terminal binding domain.....	133
4.4.6	Latch binding site.....	133
4.5	UPDATED MODEL FOR THE MOLECULAR MECHANISM OF ACTION OF CPE..	134
4.5.1	Step 1 – Receptor binding and formation of the small complex	134
4.5.2	Step 2 – Oligomerization of CPE and formation of the pre-pore	135
4.5.3	Step 3 – Pore-formation by membrane insertion	135
4.6	FUTURE INVESTIGATIONS	137
4.6.1	NTCCS latch and binding site	137
4.6.2	Confirming the putative TMD of CPE	137
4.6.3	Additional dominant negative analysis.....	138
4.6.4	Solving the three-dimensional structure of CPE.....	139
4.7	FINAL SUMMATION	141
4.8	ORIGINAL KNOWLEDGE CONTRIBUTED.....	142
	BIBLIOGRAPHY	143

LIST OF TABLES

Table 1.1 Classic toxinotypes of <i>C. perfringens</i>	3
Table 1.2 Some members of the β -PFT family of toxins.....	38
Table 2.1 Bacterial strains used in this study.....	46
Table 2.2 DNA primers used in this study for mutagenesis or sequencing	48
Table 3.1 Summary of rCPE variant phenotypes.....	63
Table 3.2 Gross histology scores of rabbit ileal loops treated with the indicated constructs	73
Table 3.3 Binding analysis of constructs in this study.....	77
Table 3.4 Ferguson plot calculations for CPE large complexes	96

LIST OF FIGURES

Figure 1.1 Ligated rabbit ileal loops	5
Figure 1.2 Gastrointestinal diseases caused by <i>cpe</i> ⁺ <i>C. perfringens</i>	7
Figure 1.3 Map of <i>cpe</i> gene	10
Figure 1.4 Two-stage effects of CPE treatment of the mammalian small intestine	14
Figure 1.5 Cellular death pathways induced by CPE treatment	18
Figure 1.6 Membrane topology and domain structure of claudin and occludin.....	20
Figure 1.7 Model for molecular action of CPE prior to start of present study	22
Figure 1.8 Primary amino acid structure of CPE.....	27
Figure 1.9 Kyte-Doolittle hydrophobicity analysis of CPE.....	28
Figure 1.10 Secondary amino acid structure predictions of CPE.....	29
Figure 1.11 Enzymatic, chemical, and cloning fragments of CPE	30
Figure 1.12 Deletion mutagenesis of rCPE using molecular cloning	32
Figure 1.13 Random point mutagenesis of rCPE	33
Figure 1.14 Deletion mutagenesis of the C-CPE fragment of CPE	34
Figure 1.15 Three dimensional crystal structure of the <i>S. aureus</i> alpha hemolysin monomer	39
Figure 1.16 Three dimensional crystal structure of the <i>S. aureus</i> alpha hemolysin heptamer	40
Figure 1.17 Alignment of TMDs of several β -PFTs and CPE amino acids 81-110	43
Figure 3.1 Map of the N-terminal cytotoxicity region.....	60
Figure 3.2 Caco-2 morphologic damage assay	61

Figure 3.3 Assessment of pore-formation by rCPE variants	62
Figure 3.4 Competitive binding analysis of rCPE variants	64
Figure 3.5 Small complex formation by rCPE variants	65
Figure 3.6 Formation of the SDS-resistant large complexes by rCPE variants	67
Figure 3.7 Limited trypsin proteolysis of rCPE variants	68
Figure 3.8 Fluid accumulation by rCPE constructs	72
Figure 3.9 Histology of rabbit ileal loops	74
Figure 3.10 Structure-function map of CPE depicting the putative TMD	75
Figure 3.11 Constructs used to investigate membrane insertion	76
Figure 3.12 Caco-2 morphologic damage assay	78
Figure 3.13 Assessment of pore-formation by rCPE variants	79
Figure 3.14 Formation of SDS-resistant large complexes by rCPE variants	80
Figure 3.15 Comparative pronase susceptibility of large complexes formed by rCPE and TM1 ...	82
Figure 3.16 Dissociation of the large complexes formed by rCPE and TM1	84
Figure 3.17 Heat denaturation of the CPE large complex	85
Figure 3.18 Constructs used to investigate the oligomerization of CPE	88
Figure 3.19 Western blots of constructs before and after large complex formation	89
Figure 3.20 Heteromer gel shift analysis of the “~155 kDa” CPE large complex	91
Figure 3.21 Heteromer gel shift analysis of the “~200 kDa” CPE large complex	92
Figure 3.22 Effect of altering acrylamide concentration in large complex gels	94
Figure 3.23 Ferguson plot analysis of CPE	95
Figure 3.24 Ferguson plot analysis of CPE large complexes	97
Figure 3.25 Size exclusion chromatography of the CPE large complexes	99
Figure 3.26 Dominant negative effects on oligomerization by some rCPE variants	102
Figure 3.27 Dominant negative effects on pore-formation by some rCPE variants	104

Figure 4.1 Current structure-function map of CPE with predicted secondary structure.....	106
Figure 4.2 Membrane topology model of TMDs of β -PFTs.....	115
Figure 4.3 Kyte-Doolittle hydrophobicity analysis of two β -PFTs.....	116
Figure 4.4 Crystal structure of perfringolysin O	117
Figure 4.5 Small-scale fluorescence study of the putative TMD of CPE.....	120
Figure 4.6 Possible configurations of the CH1 and CH-2 complexes	127
Figure 4.7 Model for the molecular mechanism of action of CPE.....	136
Figure 4.8 Montage of various crystal morphologies formed by CPE.....	140

PREFACE

It is a sheer impossibility that this thesis dissertation could have been produced without the advice, fellowship, and encouragement of so many people. I must foremost thank God for the opportunities and blessings which I am provided on a daily basis. My faith in Jesus Christ has provided a great deal of inner strength and personal confidence during some of life's hardest times, and this relationship is one that is truly invaluable. I owe the faculty of the Department of Biological Sciences of Duquesne University thanks for my development as a student of the sciences. Despite an unremarkable undergraduate career, my attitude toward academic achievement quickly matured after being given a chance by Duquesne to earn a Master's degree. I must specifically thank my Master's thesis advisor, Dr. Peter Castric, who provided exceptional mentorship during my time at Duquesne, enabling and inspiring me to continue on for my doctorate. I would like to thank Drs. Steven Phillips and Joanne Flynn who played key advisory roles to me during my early years at the University of Pittsburgh. Also deserving thanks are members of my thesis committee consisting of Drs. Mike Cascio, Jay Carroll, Tim Mietzner and Mike Parniak, and I am especially grateful to Drs. Carroll and Parniak for their helpful personal and scientific mentorship. I also wish to thank my scientific twin brother, Dr. Derek Fisher, for his sincere fellowship both in and out of the laboratory. I also wish to acknowledge my friendship with former lab-mate Dr. Qiyi Wen. Though Dr. Wen has left this world for a better place, his light-hearted spirit and dedication to family has left an indelible mark in my heart.

I also wish to acknowledge my thesis advisor, Dr. Bruce McClane, for his contributions to my scientific development. Dr. McClane has provided me with an appropriate balance of freedom and supervision that has been vital for my achievements and growth into an independent scientist. While being the recipient of excellent training on protein biochemistry and eukaryotic cell culturing in his laboratory, I have also learned important aspects of the 'business end' of science which will no doubt be of value as I continue my scientific career.

Lastly, I have to acknowledge my family for their constant encouragement and support. My parents Jim and Becky have deeply impressed the value of education into me, and without their support (both emotional and financial), I would be unable to attain the goals I have set forth. It is my wife, Kelly, who deserves my deepest gratitude. Even though the road leading to my academic endeavors can be seemingly endless, Kelly's unwavering support and encouragement has been an irreplaceable aspect of my drive to continue forward. I am truly blessed by God to have her as my loving wife, the mother of my son, and my best friend.

1.0 INTRODUCTION

Bacterial toxins have had a significant negative impact on their eukaryotic hosts throughout evolution, and unfortunately humans are no exception. In order to mitigate the effects of these toxic proteins, we must first understand, at the molecular level, how toxins execute their activities to cause disease. This thesis dissertation describes a detailed examination of the mechanism of action of the *Clostridium perfringens* enterotoxin using analysis which correlates its structural attributes to its molecular activities. Findings from this work regarding the functional domains and oligomeric state of the enterotoxin have contributed extensively to the understanding of the molecular events occurring between this protein and the host cell. It is the ultimate hope that this work will advance both basic and applied research approaches to further appreciate the activities and potential remedies for this dynamic toxin.

1.1 *Clostridium perfringens*

1.1.1 General bacteriology

The Gram-positive bacterium *Clostridium perfringens* is a notorious human and veterinary pathogen, and is most appreciated for its tremendous toxin-producing capability (168). As a member of the *Clostridium* genus, *C. perfringens* is a spore-forming anaerobe with a rod-shaped cellular morphology and a pilus-based motility (219). First isolated as *Bacterium welchii* by the American physician William Henry Welch in 1892, *C. perfringens* is thought to have been responsible for the deaths of hundreds of thousands of soldiers suffering from wound-induced

gas gangrene in World War I (183). *C. perfringens* is believed to be the most wide-spread bacterial pathogen in nature (120), as it can be found in water, soil sediments, and also part of the normal intestinal flora of humans and other animals. Its genetic manipulability, fast growth rate, and relative tolerance to oxygen has enabled *C. perfringens* to be a genetic model organism for the entire *Clostridium* genus (167).

1.1.2 Genomic analysis of *C. perfringens*

As typical of the Firmicutes, *C. perfringens* maintains an exceptionally low G+C content of ~28% (149, 183). The genomes of several *C. perfringens* strains have recently been sequenced, revealing an average ~3.0 Mbp genome size between the 3 strains (149, 183). A considerable amount of variation exists not only between the three completely sequenced *C. perfringens* strains, but also between many other *C. perfringens* human and animal disease isolates (149). These genomic differences cluster to over 300 different genomic islands and can encode genes involved with metabolism, capsule synthesis, toxin production, and mobile genetic elements. This finding undoubtedly reflects the phenotypic diversity required for the wide array of human and veterinary diseases which this bacterium can cause. In addition to its chromosome, *C. perfringens* can harbor several large plasmids, many of which contain toxins and other virulence factors vital for the establishment and maintenance of infections (90, 141, 168).

1.1.3 *C. perfringens* toxins and associated diseases

The *Clostridium* genus has evolved an extreme expertise for producing many highly potent toxins. The tetanus toxin from *Clostridium tetani* is responsible for one of the most dramatic and devastating diseases worldwide (5), while the botulinum toxin produced by *Clostridium botulinum* has been acknowledged as the most poisonous substance ever identified (54). In

this regard, *C. perfringens* itself contains a potent arsenal of up to 14 different protein toxins (168). Since any one *C. perfringens* isolate produces only a small repertoire of these toxins, a classic typing scheme is commonly used to categorize *C. perfringens* isolates based on the presence of four “major lethal” toxins (Table 1.1).

Table 1.1 Classic toxinotypes of *C. perfringens*

Toxinotype	Toxins produced:			
	alpha toxin	beta toxin	epsilon toxin	iota toxin
A	+	-	-	-
B	+	+	+	-
C	+	+	-	-
D	+	-	+	-
E	+	-	-	+

1.1.3.1 Typing toxins of *C. perfringens*

The *C. perfringens* alpha toxin is carried by all types and has hemolytic, phospholipase C, sphingomyelinase, and lethal activities (172). This toxin has been shown to be the primary mediator of gas gangrene caused by *C. perfringens* (7). *C. perfringens* types B and C can produce beta toxin, a pore-forming toxin (150) shown to be the primary lethal toxin in a mouse intravascular injection model (43). Type C isolates of *C. perfringens* are a cause of necrotic enteritis in humans, the symptoms of which beta toxin is thought to be the principal mediator (43, 193). Epsilon toxin, produced by type B and D isolates of *C. perfringens*, is another pore-forming toxin (144, 159, 160) which localizes to nasal, brain, and kidney tissues once absorbed into the blood stream (205). Though epsilon toxin has not been experimentally shown to affect humans, its extreme potency (trumped only by the previously-mentioned tetanus and botulinum toxins) has led to its classification by the Centers for Disease Control as a Class B Select Toxin. Type E isolates of *C. perfringens* express the iota toxin, a classic binary toxin with ADP-

ribosyltransferase activity (163). Though iota toxin has homology both in structure and function to several other bacterial binary toxins affecting humans (*Clostridium difficile* transferase, *C. botulinum* C2 toxin, and *Salmonella enterica* SpvB toxin; (104)), type E *C. perfringens* isolates have only been associated with veterinary enteritises (193).

1.1.3.2 Non-typing toxins of *C. perfringens*

C. perfringens also produces several other toxins not used in the typing scheme. Theta toxin, or perfringolysin O, is a member of the cholesterol-dependent cytolysin family of pore-forming toxins, and is reported to act in synergy with alpha toxin in a mouse model of myonecrosis (7). The beta2 toxin can be produced by all *C. perfringens* types (17) and has been associated with both veterinary enteric disease (9, 194) and with some human non-foodborne diarrheas (44). Several other non-typing toxins have been identified but are incompletely characterized with regard to their pathogenic contribution, including proteases (lambda and kappa toxins), glycolytic enzymes (nanI, nanH, nagH, mu toxin), and a collagenase (colA) (168).

In addition to the multitude of aforementioned toxins, the *C. perfringens* enterotoxin, or CPE, could be currently considered the most medically significant *C. perfringens* toxin. As will be illustrated below, CPE is responsible for the symptoms of *C. perfringens* type A food poisoning, as well as non-foodborne gastrointestinal illnesses in humans.

1.2 *C. perfringens* ENTEROTOXIN

1.2.1 *C. perfringens* type A food poisoning and the discovery of CPE

C. perfringens has been linked with food poisoning since the 1940's and 1950's, and institutions such as military bases and hospitals in both the U.S.A. and Europe were frequent sites of reported *C. perfringens* food poisoning outbreaks (24, 25, 91, 128). While attempts have been made to construct mouse, monkey, lamb, chicken, and even pigeon models for the food poisoning caused by this bacterium (74, 153, 211, 212, 224, 239), a rabbit ileal loop model (Fig. 1.1) established by Duncan and colleagues in 1968 remains, nearly 40 years later, as the standard *in vivo* assay for *C. perfringens* type A enterotoxicity (33). A human volunteer study later verified this rabbit ileal loop model, since enteropathogenic cultures of *C. perfringens* which could elicit fluid accumulation in rabbit ileal loops were able to cause diarrhea 61% of the time when administered orally to human volunteers (199).



Figure 1.1 Ligated rabbit ileal loops. Arrows indicate individual loops treated for 3 h with 50 μ g of CPE (photograph courtesy of Francisco Uzal, CAHFS Laboratory).

Evidence that *C. perfringens* food poisoning may be caused by a factor released or secreted from the bacterial cell first came from a key study demonstrating fluid accumulation in rabbit ileal loops after treatment with cell-free extracts of *C. perfringens* (31). Early characterization studies of crude preparations of enterotoxic *C. perfringens* suggested the enterotoxic factor was a single protein of approximately 35,000 Da (73, 196). Purified CPE (127) was later shown to be the primary enterotoxic factor for the experimental disease in many animal enteric models (reviewed in (122)), and diarrhea could be experimentally induced in healthy human volunteers after ingestion of highly purified CPE (189). Confirming this notion was the finding that *C. perfringens* strains containing a knock-out mutation of the gene encoding CPE could not elicit fluid accumulation or histopathologic damage like their isogenic parent strains (175). Currently, CPE-producing isolates of *C. perfringens* are ranked as the second and third most common cause of foodborne illness in the U.K. and U.S.A, respectively (155). In addition, *C. perfringens* type A food poisoning (Fig. 1.2A) has been estimated to have a \$187 million/year effect on the economy (adjusted for today's dollars) (209).

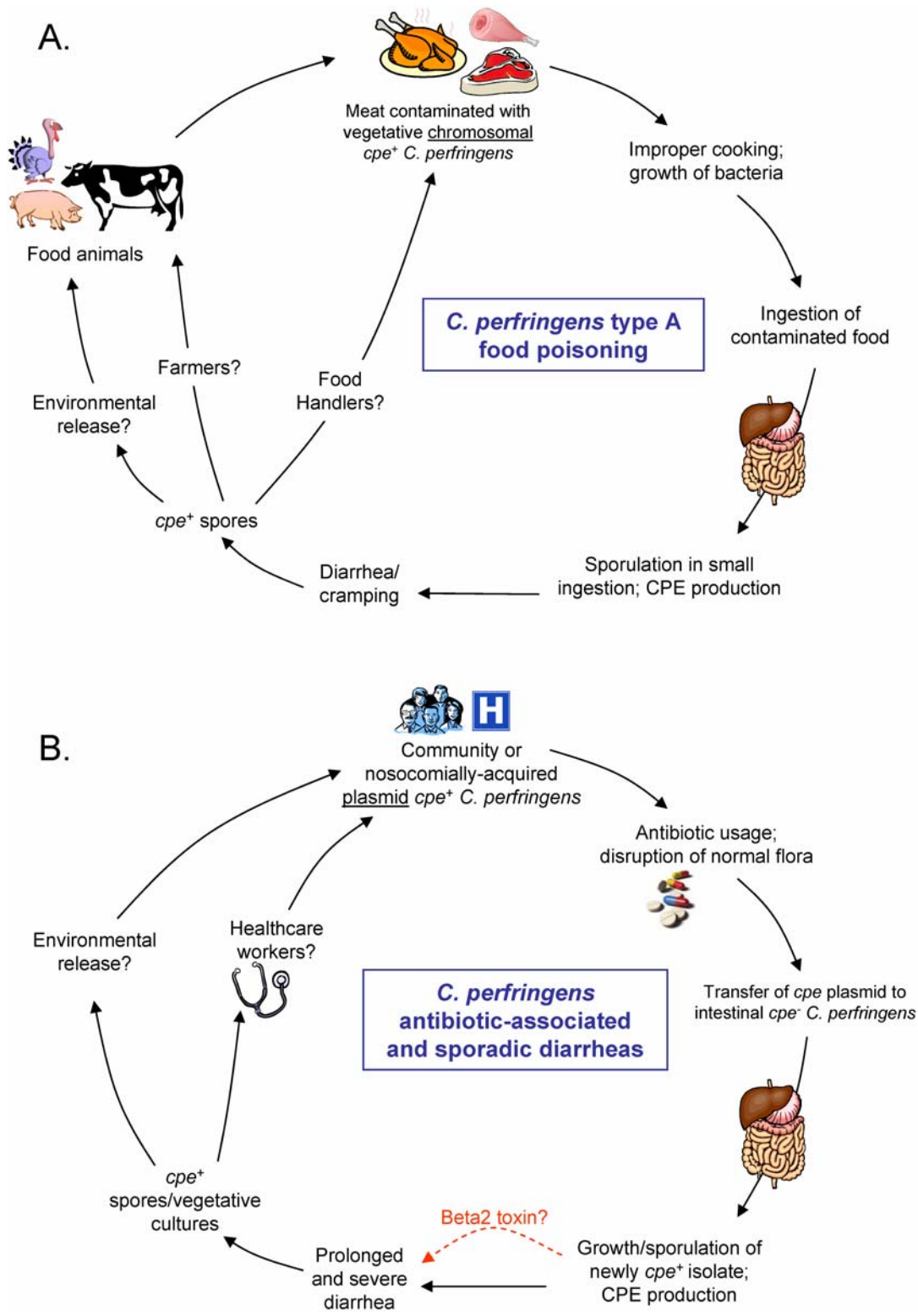


Figure 1.2 Gastrointestinal diseases caused by *cpe*⁺ *C. perfringens*. A, Model for the cycle of *C. perfringens* type A food poisoning. B, Model for the cycle of non-foodborne diarrheas caused by *cpe*⁺ *C. perfringens*.

1.2.2 Association of CPE with non-foodborne diarrheas

While *C. perfringens* (and later, CPE) has been implicated in foodborne (FB) disease for over five decades, only within the last 20 years have CPE-producing strains of *C. perfringens* been recognized as a legitimate source of non-foodborne (NFB) diarrheas (18). One such illness, antibiotic-associated diarrhea (AAD), has predominantly thought to be caused by a *C. perfringens* relative, *C. difficile*. However, a study in 1984 (14) described the detection of CPE in the stools of 11 patients receiving antibiotics who were suffering from prolonged and severe diarrhea (symptoms distinct from the rather short-lived diarrhea associated with *C. perfringens* type A food poisoning). Not only was *C. perfringens* also isolated from these stools samples, but *C. difficile* was absent, indicating that CPE-producing *C. perfringens* isolates could be responsible for these AAD infections (12, 14). A more recent comparative analysis determined that CPE-positive *C. perfringens* accounted for 21% of the known AAD pathogens in an over 700 sample AAD survey (6). In addition to contributing to diarrheas associated with antibiotic use, CPE-producing *C. perfringens* isolates have also been implicated in sporadic diarrhea (SD) episodes, particularly in the elderly population (18). While detection rates of CPE-positive *C. perfringens* in cases of SD range from 18% (148) to 6.8% (15), it is clear that enterotoxigenic type A isolates of *C. perfringens* appear to be an emerging etiology for SD as well as AAD (Fig. 1.2B).

1.2.3 Beta2 toxin: an AAD/SD accessory toxin?

As mentioned above, the symptoms witnessed in AAD and SD have been reported to be more prolonged and severe than seen in cases of *C. perfringens* type A food poisoning (18). While the basis for this difference is not entirely clear, one possible explanation could be the action of an additional toxin. The beta2 toxin, mentioned above, is frequently found associated with *cpe*⁺ *C. perfringens* isolates which cause AAD/SD (>75% of tested isolates) and infrequently with *cpe*⁺

C. perfringens food poisoning isolates (<15% of tested isolates) (44). In addition, beta2 toxin itself has been associated with many serious veterinary enteric diseases, including in horses, piglets, and cattle (17, 37, 51, 53, 103). Although there are currently no reports of human disease where beta2 toxin was identified as the single causative agent, purified beta2 toxin has been shown to be cytotoxic for Caco-2 cells (44), a human colon carcinoma cell line (described in detail below). Collectively these findings suggest that beta2 toxin, because of its genetic associations with CPE and its own cytotoxic/enterotoxic activities, could contribute in an accessory fashion to CPE and be responsible for the more intense gastrointestinal symptoms seen during AAD/SD (Fig. 1.2B; (42)).

1.2.4 CPE genetics

1.2.4.1 Gene structure and transcriptional regulation of *cpe*

The gene for CPE (*cpe*) is roughly 1.3 kbp in length and encodes a 319 amino acid protein with a molecular mass of 35,346 Da (29). The *cpe* gene contains no significant DNA or amino acid homology to any other bacterial toxins. However, it does have 27% identity and 46% similarity at the amino acid level to the non-toxic hemagglutinin components of the type C botulinum toxin (45). Remarkable sequence conservation of the *cpe* gene exists within *C. perfringens*, including *cpe* genes from both FB and NFB isolates (26).

Early investigations of regulation of the enterotoxin established that, unlike the other *C. perfringens* toxins, CPE is produced only by sporulating cells (31, 32). When induced to sporulate, *cpe*⁺ *C. perfringens* isolates produce massive amounts of the enterotoxin which accumulates in a large inclusion body inside the mother cell (101, 102). Both the quantitative and temporal characteristics of *cpe* expression can be explained by the presence of three sporulation-associated promoters (two SigE-like and one SigK-like) upstream from the *cpe* ORF

(Fig. 1.3; (238)). In addition, the distal SigE-like promoter of *cpe* is thought to be directly regulated by the SpoOA, an very early regulator of sporulation in both the *Bacillus* and *Clostridium* genera (81). Termination of *cpe* transcription is thought to be Rho-independent, mediated instead by a putative stem loop structure preceding an oligo-T tract located downstream of the stop codon (Fig. 1.3; (29)). Although *cpe* is most commonly only carried by type A *C. perfringens* isolates, CPE can be produced by natively *cpe*⁻ type A, B, and C isolates transformed with a *cpe*-containing shuttle plasmid (28). Also, *cpe* expression has been detected in sporulating cultures of natively *cpe*⁺ type B, C, and D isolates of *C. perfringens* (40, 42, 177). CPE can be produced (although in much lower quantities than from the *cpe* promoter) in an *Escherichia coli* background (28), an indication that sporulation is not required for *cpe* expression. Production of recombinant CPE (rCPE) from highly active promoters in *E. coli* has allowed great strides to be taken in structure-function analysis of CPE, as will be illustrated below.

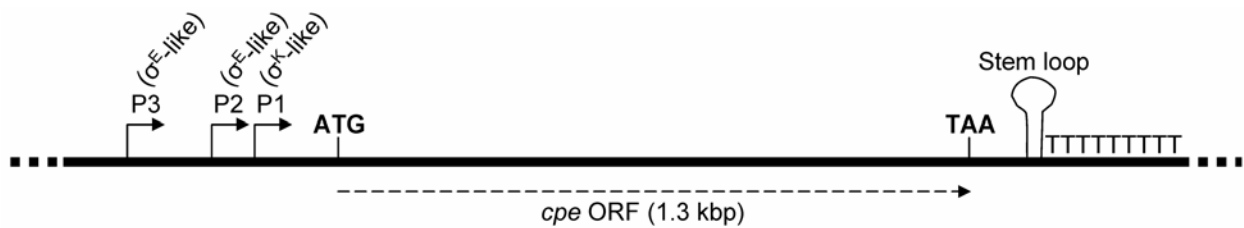


Figure 1.3 Map of the *cpe* gene depicting its three sporulation-regulated promoters and 3' transcription termination elements.

1.2.4.2 Genetic locus of *cpe*

Despite the stringent sequence conservation in *cpe* sequence between FB and NFB isolates of *C. perfringens* (26), the genetic context of *cpe* in these two distinct etiologies is very different. Genetic analysis of NFB *cpe*⁺ *C. perfringens* isolates identified an episomal location of *cpe*, while FB enterotoxic *C. perfringens* isolates were found to harbor their *cpe* genes on the chromosome (27). In both loci however, *cpe* is flanked by mobile genetic elements suggesting that plasmid *cpe* *C. perfringens* isolates have acquired this toxin gene via horizontal gene transfer from chromosomal *cpe* *C. perfringens* isolates (140). The differences in *cpe* locus organization between chromosomal and plasmid *cpe* *C. perfringens* isolates has enabled development of a multiplex PCR assay that can be used to rapidly identify whether an enterotoxic *C. perfringens* isolate is of FB or NFB origin (142, 225). Complete sequencing of two *cpe* plasmids has identified that these ~70-75 kbp plasmids carry genes for the conjugative transposon Tn916, suggesting a possible mechanism of plasmid transfer (141).

1.2.4.3 Molecular Koch's postulates and *cpe*

Many lines of evidence presented in the above sections support the role of CPE in *C. perfringens* type A food poisoning. In addition, CPE⁺ *C. perfringens* can cause NFB diarrheas such as AAD and SD, though the exact contribution of CPE in these diseases remains to be completely evaluated. Robust confirmation of CPE's role in both FB and NFB gastrointestinal illnesses came from molecular Koch's postulates analysis of both plasmid and chromosomal *cpe* isolates (175). Knockout mutations in both chromosomal and plasmid *cpe* genes were generated by homologous recombination and assayed for enterotoxicity in the rabbit ileal loop model. Sporulating culture lysates from either the chromosomal or plasmid *cpe* knockout mutants were unable to induce fluid accumulation or the typical histopathology associated with

CPE treatment (villus blunting, epithelial desquamation, etc.). When these same chromosomal and plasmid knockout mutants were complemented in *trans* with a plasmid copy of *cpe*, the enterotoxic phenotype was completely restored (175). This careful analysis conclusively showed that CPE is necessary for *C. perfringens* type A gastrointestinal diseases.

1.3 MECHANISM OF ACTION OF CPE

CPE mediates its toxicity through several distinct levels of action, ranging from the early molecular events occurring at cell membranes, to the cytotoxic effects leading to cell death, and finally culminating in enteropathology resulting in diarrhea and cramping. Detailed below is a description of the enteric, cellular, and molecular facets of the mechanism of action of CPE.

1.3.1 The enterotoxic consequences of CPE delivery in the small intestine

The symptoms of *C. perfringens* type A food poisoning, diarrhea and cramping, begin within 8-18 h after consumption of a food source contaminated with vegetative cultures of a *cpe*⁺ isolate of *C. perfringens* (Fig. 1.2A; (122)). A relatively large dose of bacteria (10^7 - 10^8) is required to initiate *C. perfringens* type A food poisoning (98) since most of the bacteria perish in the acidity of the stomach. *C. perfringens* cells surviving this challenge continue to the small intestine where the presence of bile salts is thought to cause the bacteria to sporulate (76). As described above, the multiple sporulation-regulated *cpe* promoters (Fig. 1.3) allow for large amounts of CPE to be produced by the sporulating bacteria. Instead of being secreted like other *C.*

perfringens toxins, CPE is released into the intestinal lumen by lysis of the mother cell at the end stages of sporulation.

On the other hand, the details of CPE production in cases of AAD/SD is not so clear. Since the *cpe* plasmids have been shown to be conjugative (16), and since *C. perfringens* can exist commensally in the intestinal tract, one leading hypothesis is that *cpe* plasmids are transferred in the intestine from ingested *cpe*⁺ environmental *C. perfringens* isolates to *cpe*⁻ *C. perfringens* isolates already acclimated to the intestinal tract (Fig. 1.2B). A balance between colonization and sporulation of intestinal *cpe*⁺ *C. perfringens* isolates would be responsible for the more prolonged and severe symptoms experienced with AAD/SD. Also, beta2 toxin has been shown to be produced by both sporulating and vegetative *cpe*⁺ cultures (44), so the possibility of beta2 acting as an accessory toxin must be considered (42).

Regardless of the means by which CPE is produced, its presence has a devastating effect on the intestine. An early rat ileum model of enterotoxin action found that CPE treatment led to a switch from absorption to secretion of fluid, sodium, and chloride (121). In this study, histopathological changes of the intestine were also noted, including destruction of villus tips resulting in an exposed lamina propria. Similar histopathology effects have been reported in the rabbit model of CPE action at doses that were sufficient to cause fluid accumulation, making an important link between these two events (124). Scanning electron micrographs confirmed these findings by showing villus tip damage, with heavy blebbing occurring at villus tips after rabbit ileum was treated with CPE (123). Later studies (182) described the two-phase effects of CPE on the intestine: i) inhibition of the absorption of fluid and ions occurs as epithelial cells are intoxicated by CPE, and ii) death of intestinal epithelial cells leads to progressive desquamation of the epithelium culminating in a net secretion of fluid into the intestinal lumen (Fig. 1.4). Recent studies have been performed on sections of human intestine examined *ex vivo* for their electrophysiological responses to CPE. This work revealed that human ileal epithelium experiences a decrease in transepithelial resistance and water absorption after CPE-treatment,

and that these effects seemed to correlate with damage of the intestinal tissue (41). Also, the abdominal cramping that is typically associated with *C. perfringens* type A gastrointestinal disease has been attributed (by one study) to the increased myoelectric activity seen in CPE-treated small intestine (87).

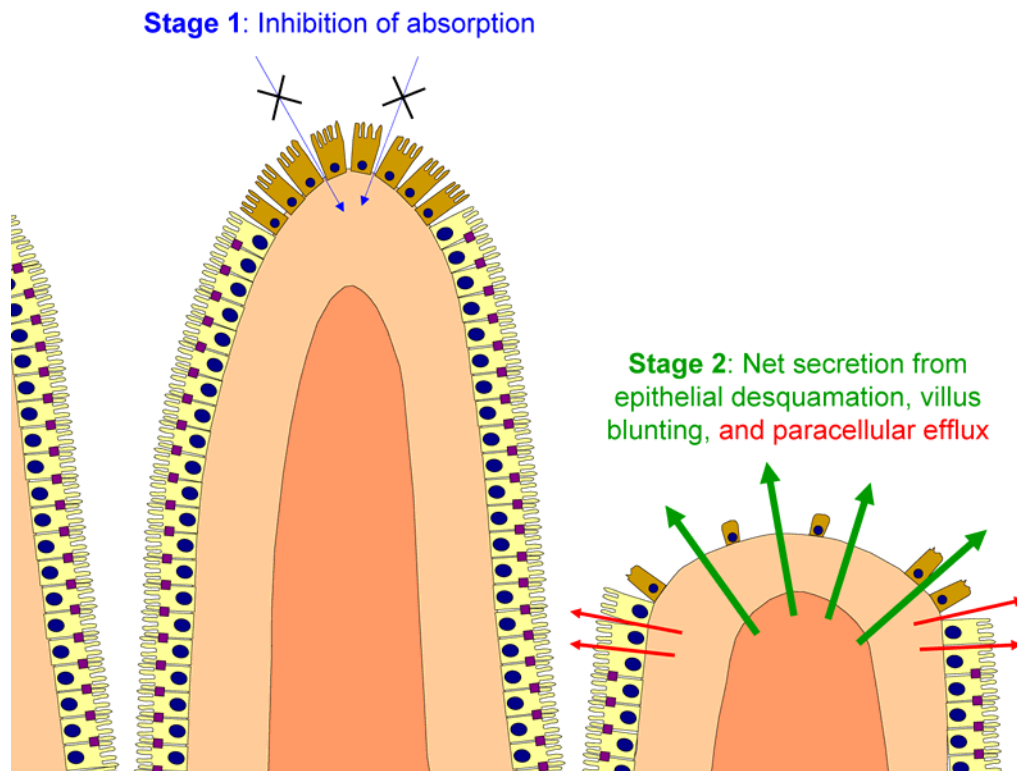


Figure 1.4 Two-stage effects of CPE treatment of the mammalian small intestine.

1.3.2 Cellular toxicity induced by CPE

Hints on how CPE acts at the cellular level came first from transmission electron microscopy studies of CPE-treated rabbit small intestine. Ultrastructural analysis showed that microvilli of the columnar epithelial cells were partially or completely missing, and that the epithelial cells at

the tips of villi showed heavy amounts of blebbing (indicative of cellular death) (123). The disruption of the brush border and loss of apical membrane explains the initial absorption inhibition effects described previously (Fig. 1.4). It was also interesting to note in that electron microscopy study that cells which had succumbed to CPE toxicity contained organelles that were normal in appearance, indicating that the toxic effect was outside-in rather than the inverse (123). Other studies showed that epithelial tissue pre-treated with protein synthesis inhibitors is not protected from fluid accumulation or tissue damage, signifying that CPE action is not dependent on the synthesis of new proteins after the toxin interacts with the cell (125).

1.3.2.1 Cell culture models of CPE cytotoxicity

The introduction of immortal cell lines to CPE research greatly aided in further analyzing CPE-mediated cytotoxicity. The green monkey kidney cell line, Vero, was the first cell line reported to be sensitive to CPE (63). CPE treatment of these cells rapidly causes dramatic changes in cellular morphology (116), including the development of blebs similar to what is seen with CPE treated epithelial cells of the rabbit intestine (126). Binding of CPE to Vero cells was shown to be a crucial first step in the cellular action of the toxin, as Vero cells selected for resistance to CPE demonstrated a 10-fold reduction in CPE binding (126). Other cell lines have been shown to be naturally sensitive to the enterotoxin, including HeLa cells (108) and MDCK cells (55).

The rapid cytotoxic response (63, 116) involving membrane blebbing (116, 123) without detectable organelle damage (126) gave clear indications that the cellular plasma membrane was the target for CPE action. Plasma membrane permeability alterations of Vero cells were discovered initially using a marker-release assay (206) with various sized radio-labeled molecular mass markers. It was shown in this work that nearly all of the ^{14}C -amino-isobutyric acid (103 Da) and most of the ^3H -uridine (244 Da) could pass freely out of Vero cells treated with CPE for 30 min. However macromolecules such as ^{51}Cr -protein complexes (3,000 Da)

and ^3H -RNA (25,000 Da) were greatly restricted in their cellular efflux after CPE treatment (115), presumably because these molecules could not fit through the CPE pore. Osmotic protection studies of Vero cells showed that sucrose could prevent the CPE-induced cytotoxic response, however poly-ethylene glycol was unable to provide similar protection (114). This work was later confirmed by determining that molecules such as Tris (120 Da) and arabinose (150 Da) could not osmotically protect Vero or HeLa cells, whereas glucuronic acid (185 Da) and N-acetylglucosamine (225 Da) conveyed a partial or complete, respectively, protective effect from CPE-induced damage (107). These observations collectively suggested that CPE treatment of cells induces the formation of a pore, through which these experimental molecules pass.

While Vero and HeLa cells provided an important initial cytotoxic model for CPE action, more physiologically-relevant insights regarding the interactions between CPE and the intestinal epithelium were gained when the human colon carcinoma cell line, Caco-2, was employed. Isolated in the 1970's from a colorectal adenocarcinoma, Caco-2 cells are like enterocytes in that they form tight junctions and can generate microvilli brush borders similar to those seen in native intestinal epithelial cells (reviewed in (133)).

The CPE response of Caco-2 cells has been examined in great detail. Initial studies involving CPE treatment of Caco-2 cells demonstrated that CPE binds and forms the SDS-sensitive 'small complex' (see following sections on molecular action of CPE) similar to Vero cells (229). CPE was found to elicit a ^{86}Rb -release response from Caco-2 cells typical of that of CPE-sensitive cells (186), and when monolayers of Caco-2 cells were grown on Transwell[®] permeable supports, these cells were 2-3-fold more sensitive when challenged with CPE basolaterally rather than apically (185). Electrophysiological analysis of Caco-2 monolayers has also been used to show that CPE can reduce the transepithelial resistance by increasing the paracellular flux of small cations such as sodium (70). When single Caco-2 cells were patch-clamped after CPE treatment, cationic currents were detected and were blockable by both zinc and barium (70).

1.3.2.2 Cellular mechanism of death

The detection of cationic currents induced by CPE treatment of Caco-2 cells is significant because of previous findings regarding the involvement of Ca^{2+} in CPE action. In the Vero and HeLa cell models of CPE action, Ca^{2+} was found to be required for the initiation of morphologic damage (108). Interestingly, however, this same study showed that binding of CPE to these cells was independent of the presence of Ca^{2+} in treatment buffers. Several other studies later showed that small molecule permeability alterations resulting from CPE action were also independent on the presence of Ca^{2+} (79, 108, 118, 203).

Rather than being involved in early molecular events at the cell membrane, such as binding and pore formation, Ca^{2+} appears to have a direct role as a second messenger, driving cell death pathways (Fig. 1.5). An investigation of the cell death pathways of CPE cytotoxicity demonstrated that treatment of Caco-2 cells with low doses (1.0 ug/ml) of CPE triggers apoptosis, since DNA damage and morphological changes were blocked by inhibition of the apoptosis-specific caspase-3 and -7 (20). Conversely, high doses (10.0 ug/ml) of CPE seemed to induce oncosis because the cytotoxic response to CPE was blocked using oncosis-specific inhibitors glycine and YVAD-CHO (20). It was later determined that the degree of Ca^{2+} influx is responsible for driving the CPE-treated cell to either apoptosis or oncosis, both of which are mediated through calpain- and calmodulin-dependent pathways (19).

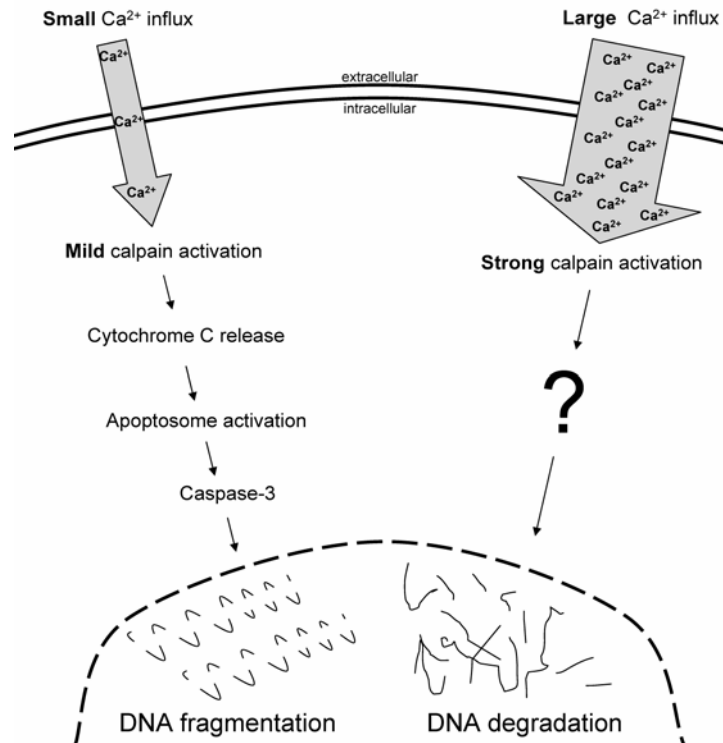


Figure 1.5 Cellular death pathways induced by CPE treatment. A small degree of Ca²⁺ influx by lower doses of CPE leads to an apoptotic response (left pathway). High doses of CPE treatment induce large amounts of Ca²⁺ influx leading to oncosis (right pathway).

1.3.3 Membranes and complexes: the molecular action of CPE

The early molecular events occurring as a result of enterotoxin treatment of sensitive cells have garnered the interest of a wide array of scientific investigators, from toxinologists to cell biologists, and even oncologists. CPE maintains some unique features in its molecular mechanism of action, however, as the present body of work proceeds it should become clear that CPE has several mechanistic and structural characteristics reminiscent of a particular family of bacterial toxins (discussed later in this dissertation).

1.3.3.1 Receptor binding

Specific binding of CPE to membranes was first recognized in 1979 as being essential for cytotoxicity (126) and remains to this day the necessary first step in molecular action of CPE. While CPE is able to bind to non-intestinal tissues such as liver and kidney (119), the physiological relevance to this capability is questionable and more likely a result of coincidental expression of CPE receptors (detailed below). One interesting feature of CPE binding to the membrane surface of cells is that it is reported to be irreversible, even resistant to dissociation with chaotropic salts (119). Since the association and dissociation rates of CPE with membranes are so different, it has been put forth in the literature that CPE undergoes a conformational change after receptor binding, thus not permitting escape of the toxin from the membrane after binding (122).

Using a Vero cell expression library created in natively CPE-resistant L929 mouse cells, Katahira *et al.* discovered a functional receptor for CPE which they entitled “CPE-R” (88). L929 cells induced to express CPE-R bound high levels of the toxin and exhibited extensive morphologic damage (blebbing, cellular detachment) after CPE treatment (88). Another functional receptor, androgen withdrawal apoptosis protein (RVP1), was later defined through analysis of human and mouse cDNAs homologous to the Vero CPE-R protein (89). These CPE receptors were then determined to be part of a large multi-gene family of tetraspan integral membrane proteins, named claudins, found to be associated with tight junctions (Fig. 1.6A; (146)).

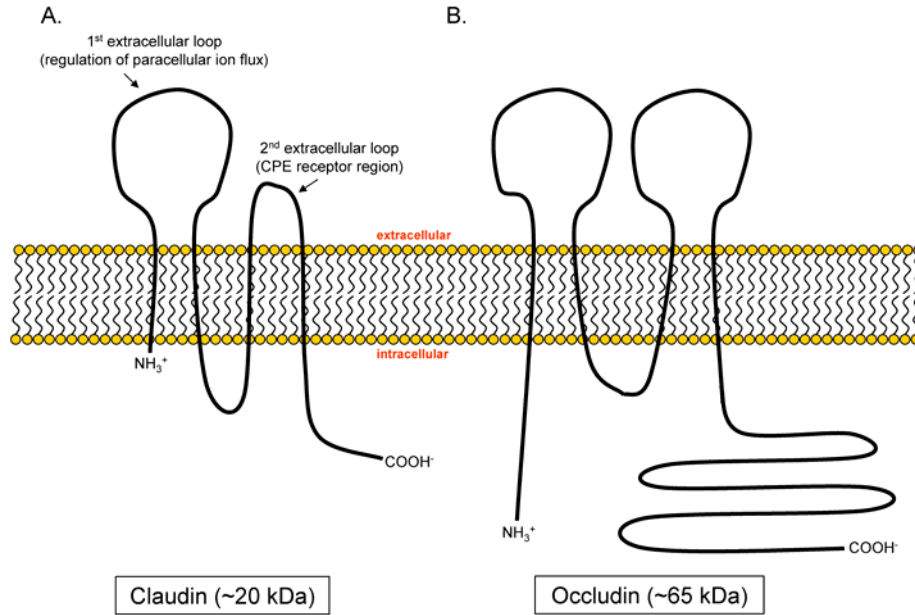


Figure 1.6 Cartoon model of the membrane topology and domain structure of claudin (A) and occludin (B).

While the involvement of claudins in the structure and function of tight junctions is an incredibly active area of research (reviewed in (50, 216)), additional work on characterizing CPE:claudin interactions continues to put forth interesting findings regarding the molecular level CPE action. Among the 24 claudins currently identified, six claudins (claudin-3 (RVP1), -4 (CPE-R), -6, -7, -8 and -14) have been shown to be capable of CPE binding (47). Conversely, four claudins (claudin-1, -2, -5, and -10) were identified in that same study to lack the ability to serve as a CPE receptor. The second extracellular loop of claudins (Fig. 1.6A) has been determined to be the region responsible for CPE binding, as chimeric claudins constructed from claudin-1 and claudin-3 only could interact with CPE when the second extracellular loop of claudin-3 was present (47).

The discovery of claudins as a cellular receptor for CPE is highly consistent with the location of the enterotoxin in natural disease. While tight junctions are known for their 'fence' function of defining the apical and basolateral membrane compartments, they also provide a

'gate' function in regulating paracellular permeability across epithelia (50, 216). Since individual claudins contain differences in charged amino acid residues in the first extracellular loop (Fig. 1.6A), it is thought that the differential expression of claudins in epithelial tissue directly regulates permeability of ions and other molecules paracellularly (23, 218). Not only are the CPE receptors claudin-3, -4, -7, -8 expressed in the mammalian small intestine (46, 162), but each have been shown to be localized along the length of intestinal villi (as opposed to the crypts) suggesting they would be fully accessible to CPE during infection. Thus, it appears that CPE has been perfectly selected to bind receptors which it is likely to encounter in its passage through the intestinal tract.

1.3.3.2 Small complex formation by CPE

When CPE initially binds to membranes containing functional CPE receptors, the toxin is localized in an SDS-sensitive complex of roughly ~90 kDa in size (Fig 1.7; (229)). Referred to in the literature (and hereafter) as the 'small complex', this association of proteins has been shown to contain a ~50 kDa protein by CPE co-immunoprecipitation studies of CPE-treated Vero and Caco-2 cells (229). The CPE small complex appears to not insert into membranes, since CPE in this complex is not protected from digestion by soluble proteases (228). In addition, rabbit polyclonal antibodies against CPE could readily react with CPE in the small complex, indicating this complex is surfaced-exposed at this stage (94).

One interpretation of the observation of the small complex is that it simply represents CPE bound to its receptor. However, since some claudins (20-27 kDa) have been clearly shown to serve as functional receptors (47, 88, 89), whether the ~50 kDa protein (229) is a multimer of claudin (or some another protein altogether) is unknown at this time. Evidence providing support for the ~50 kDa protein being a claudin multimer has come from recent results demonstrating that both receptor and non-receptor claudins can be located in the small complex

(166). Since claudin self-association and multimerization has been previously reported (49, 106, 139, 176, 217), the idea of the unknown ~50 kDa protein being comprised of two or more claudins (receptor and non-receptor) is particularly attractive.

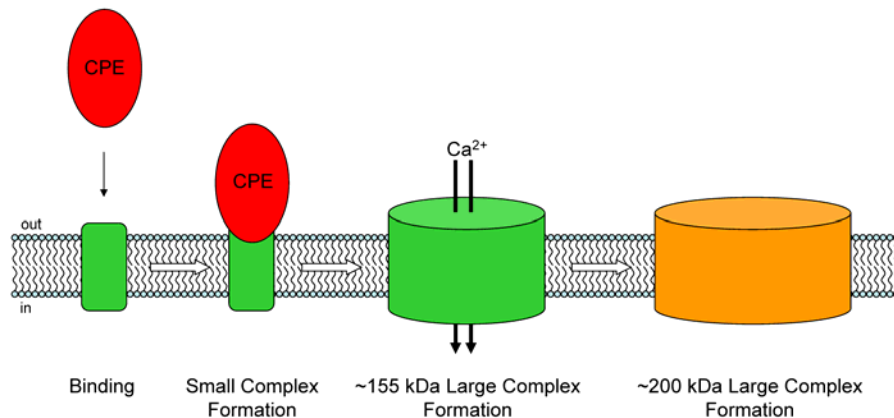


Figure 1.7 Model for the molecular action of CPE prior to start of the present study. CPE binds to transmembrane cellular receptor proteins (claudins) to form the small complex. At physiological conditions, CPE rapidly forms a large complex of ~155 kDa which is concomitant with membrane permeability changes of the cell. A second large complex of ~200 kDa can also be formed by CPE and contains the tight junction protein occludin.

1.3.3.3 Large complex formation by CPE

After receptor binding and formation of the small complex, CPE associates with additional proteins to form an SDS-resistant complex of high molecular mass (Fig. 1.7). This was first discovered when SDS-PAGE gels showed that the formation of high molecular mass radioactive material correlated with increasing treatment times of rabbit brush border membranes (BBMs) with ¹²⁵I-CPE (118). A follow-up study using size exclusion chromatography initially assessed the molecular mass of this CPE complex to be ~160,000 kDa, and a CPE-affinity chromatography column precipitated an ~70 kDa protein in similarly treated BBMs (232). It was

presented in this preliminary work that one molecule of CPE, one ~50 kDa protein (described above (229)), and one ~70 kDa protein combined to form the ~160,000 kDa large complex which was resistant to SDS (232).

The significance of the formation of large complex was established when it was found to precisely correlate with membrane permeability alterations of cells (117), suggesting that this complex functions as a pore (or a subunit thereof). It was also determined that the large complex only is formed under physiological temperatures; Vero cells treated with CPE at 4°C only formed large complex after being warmed to 37°C (117). Unlike the SDS-sensitive small complex, the SDS-resistant CPE large complex rapidly gains resistance to pronase when associated with membranes (228). Since extraction of membranes leaves CPE sensitive to pronase, this implies that CPE acquires pronase resistance by insertion into the membrane, an concept consistent with the pore-forming action of CPE (108, 114, 116). Despite its insertion into membranes, part of the CPE large complex must remain surface exposed, as anti-CPE polyclonal antibodies can react with CPE in the large complex (94).

When Caco-2 cells were utilized in CPE action studies and characterized for their response to CPE, not one, but two SDS-resistant large complexes were detected after CPE treatment of isolated Caco-2 cells (186). The first complex was reported to have a molecular mass of ~155 kDa and is believed to be the same large complex seen when BBMs and Vero cells are treated with CPE at 37°C (118, 232). The second large complex is of higher molecular mass (~200 kDa) and was shown by immunoprecipitation, electroelution, and Western blotting analyses to contain the tight junction protein, occludin (186). Although this ~65 kDa protein was initially thought to be the major structural constituent of tight junctions, the identification and functional characterization of claudins quickly usurped the importance of occludin in tight junction physiology. Interestingly, CPE treatment of Caco-2 monolayers causes removal of occludin from the tight junction via internalization (185). While it is currently unclear what role occludin plays in both tight junction composition or CPE-mediated cytotoxicity, rat fibroblast

transfectants expressing occludin (but no claudins) could not bind CPE and were not sensitive to the toxin (186). This result indicates that CPE does not interact directly with occludin (at least initially), and though likely, it remains to be shown that association of occludin with these CPE large complexes is mediated through claudin.

The specific involvement of claudins within the CPE large complexes has been recently evaluated (166). Preliminary work demonstrating the association of CPE with claudin showed that when mouse L929 cells expressing claudin-4 were treated with the enterotoxin, high molecular mass material was formed that apparently contained claudin-4 (88). Recent work has conclusively demonstrated that claudins are located in the small and both large complexes formed by CPE-treated Caco-2 cells (166). One of the more interesting findings from this study is that claudin-1, previously determined to lack the ability to bind CPE (47), is also physically-associated with CPE in each of the complexes (166). Since claudin-1 cannot directly interact with CPE, its presence must be a result of claudin:claudin reactions. The association of multiple claudins with these complexes will be revisited later in this dissertation.

1.3.3.4 Exploiting CPE:claudin interactions: clinical and therapeutic applications

As mentioned above, the discovery that CPE specifically interacts with claudin has piqued the interest of not only those who study bacterial toxins, but also cell and cancer biologists. Within the past five years, alterations in claudin expression have been detected in over ten different cancers, including breast, prostate, and ovarian cancers (reviewed in (95)). Since claudin-3 and claudin-4 are overexpressed in many tumors (including some resistant to current chemotherapeutics (174, 197)), a novel CPE-based therapeutic has been pursued by several investigators. One study demonstrating the tremendous potential for a CPE-based cancer therapy approach gave intraperitoneal injections of CPE to treat ovarian tumors explanted on the backs of severe combined immune deficiency mice (135). All mice receiving these

injections had a significant inhibition of the growth of their explanted tumors with excellent survival rates.

Other investigators have taken advantage of the remarkable effect of CPE on claudin-expressing cells. A binding, but non-cytotoxic recombinant fragment of CPE (C-CPE; see CPE structure-function section below) has been shown to remove claudin-4 from tight junctions, while leaving claudin-1, a non-receptor claudin, unaffected (195). Tight junction functionality of C-CPE-treated cells was also investigated in this study, showing that transepithelial resistance dramatically decreased when C-CPE was added to MDCK cell monolayers. Several follow-up studies have shown that C-CPE treatment of rat intestinal loops enhances the absorption of dextrans, and structure-function studies of this claudin-modulating fragment are actively ongoing ((34, 35, 69, 96, 105, 204); described in detail below). While the botulinum toxin has established an incredible precedent for the application of bacterial toxin activity for clinical benefit (reviewed in (21)), CPE maintains impressive potential for both direct treatment of cancers and for enhancing small molecule absorption through paracellular permeability modulation.

1.4 CORRELATING CPE STRUCTURE WITH ACTIVITY

1.4.1 CPE biochemistry

As mentioned above, CPE is a single polypeptide of 319 amino acids (Fig. 1.8; (29)). Though determined to be 35,346 Da in molecular mass, CPE undergoes anomalous aggregation in the presence of detergents, most notably with SDS (36, 188). An isoelectric point near 4.3 indicates that CPE is a highly negatively-charged molecule with a net charge of approximately -9 at neutral pH. CPE on average has normal hydrophobicity (Fig 1.9), however one significantly hydrophobic section appears to exist between residues 80-110. Serine, leucine, asparagine, and isoleucine are among the most abundant amino acids within CPE's primary amino acid structure. Biological activity of CPE can be abolished after only 5 min at 60°C (151), and incubation in solutions with pH values of 1.0, 3.0, 5.0, and 12.0 can also readily inactivate the toxin (31).

```

      10      20      30      40
.....|.....|.....|.....|.....|.....|
MLSNNLNPMVFNAKEVFLISEDLKTPINITNSNSNLSDG

      50      60      70      80
.....|.....|.....|.....|.....|.....|
LYVIDDKGDGWILGEPSVVSSQILNPNETGTFSQSLTKSKE

      90     100     110     120
.....|.....|.....|.....|.....|.....|
VSINVNFSVGFTSEFIQASVEYGFGITIGEQNTIERSVST

      130     140     150     160
.....|.....|.....|.....|.....|.....|
TAGPNEYVYYKVYATYRKYQAIRISHGNI SDSGSIYKLTG

      170     180     190     200
.....|.....|.....|.....|.....|.....|
IWLMKTSADSLGNIDQGS LIETGERCVLTPSTDIEKEIL

      210     220     230     240
.....|.....|.....|.....|.....|.....|
DLAAATERLNLT DALNSNPAGNLYDWRSSNSYPWTQKLNL

      250     260     270     280
.....|.....|.....|.....|.....|.....|
HLTITATGQKYRILASKIVDFNIYSNNFN NLVKLEQSLGD

      290     300     310
.....|.....|.....|.....|.....|.....|
GVKDHYVDISLDAGQYVLVMKANSSYSGNYPYSILFQKF

```

Figure 1.8 Primary amino acid structure of CPE. While a detailed discussion of the functional regions can be found below, residues in blue box represent the N-terminal cytotoxicity domain, residues in yellow box represent the putative TMD, and residues in the red box represent the C-terminal binding domain.

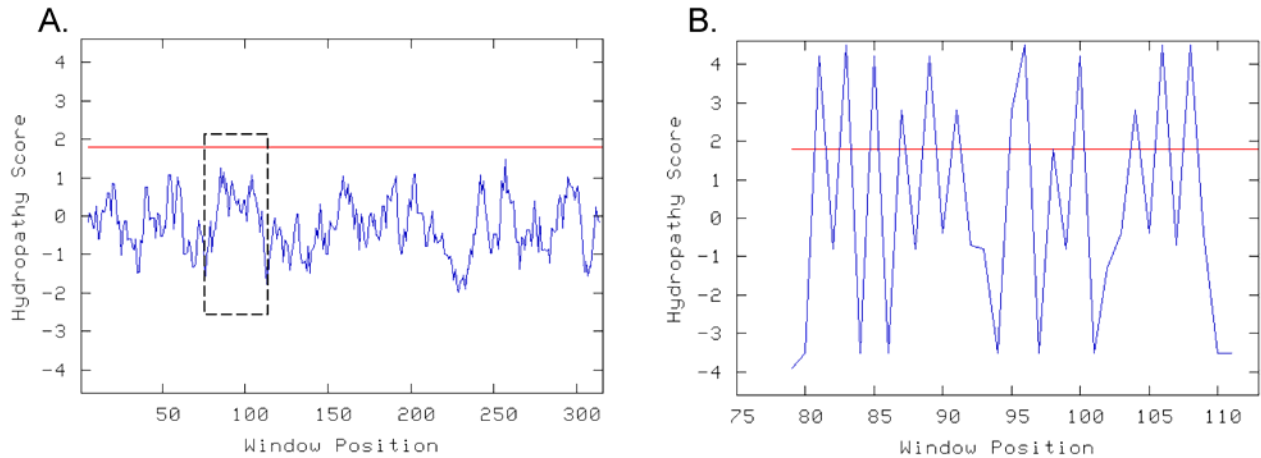


Figure 1.9 Kyte-Doolittle hydrophobicity analysis of CPE (97). A, Hydrophobicity plot using all 319 amino acids of CPE shows overall average hydrophobicity with the exception of a region between roughly amino acids 80-110 (dashed box). B, In addition to overall increased hydrophobicity, amino acids in this 80-110 region contain striking pattern of alternating hydrophobicity.

Two circular dichroism studies examining the secondary structure of CPE observed very high beta sheet composition (60-80%) and low alpha helical content at physiological conditions (58, 173). Both studies also noted a shift in secondary structure from sheet to helix at pH extremes or in the presence of SDS. Current secondary structure prediction analysis is somewhat consistent with these early studies in that ~85% of the residues are in a beta sheet or loop structure and only ~15% in a helix (Fig. 1.10; (170)). Additional correlations between elements of CPE's predicted secondary structure and its structure-function relationships will be presented later in this dissertation.

of CPE caused a 2-3 fold increase in ^{86}Rb release from these cells, but not an increase in receptor binding (Fig. 1.11; (67)). Limited digestion of CPE with another intestinal protease, chymotrypsin, also resulted in an ~3-fold increase of cytotoxicity toward Vero cells (Fig. 1.11; (59)). The removal of these 25 or 36 amino acids from the N-terminus of CPE (164, 165) by treatment with trypsin or chymotrypsin (respectively) is believed to represent an activation step for the enterotoxin, since it is likely to encounter these enzymes while initiating disease in the small intestine.

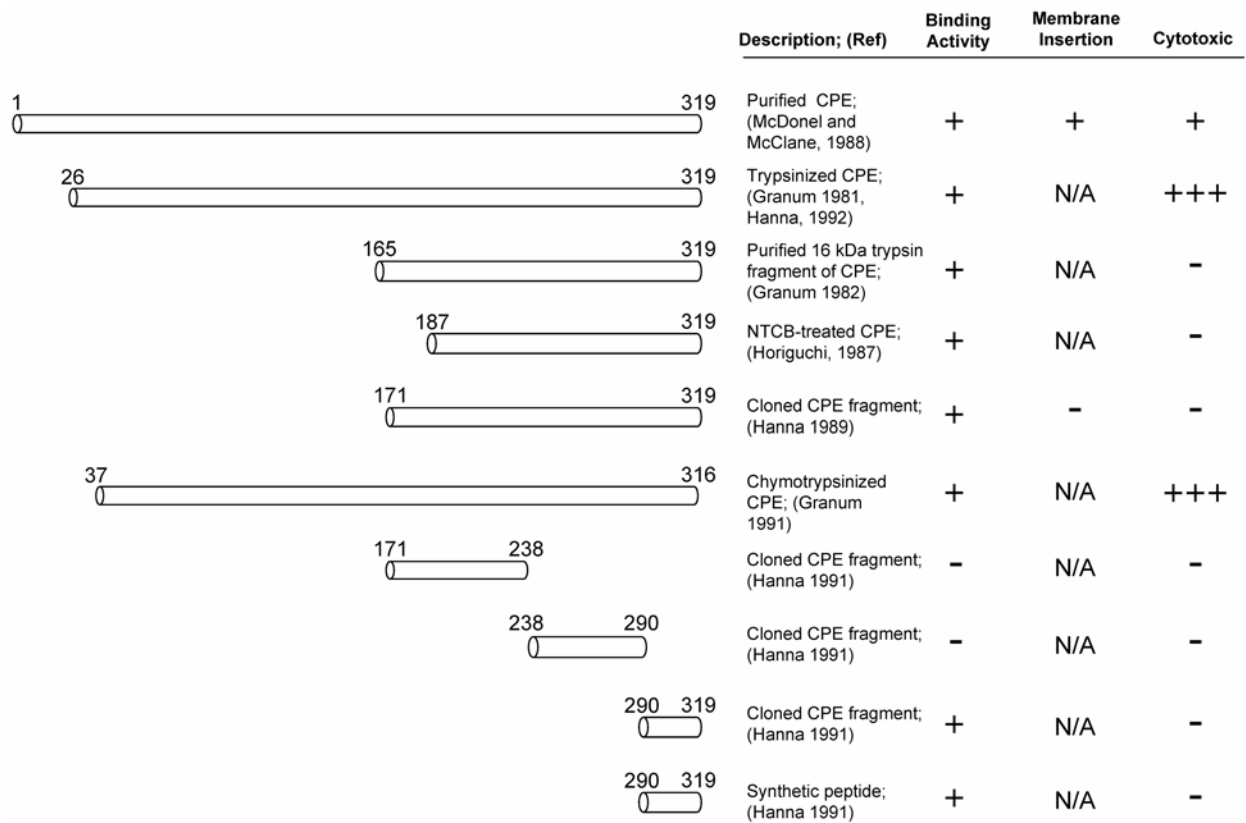


Figure 1.11 Enzymatic, chemical, and cloning fragments of CPE and their respective CPE activities.

A deletion mutagenesis study of rCPE confirmed the idea that some amino acids at the N-terminus are inhibitory since rCPE constructs lacking 36 or even 44 amino acids from the N-terminus were ~2-fold more active than full length rCPE or native CPE (Fig. 1.12; (93)). This same study also showed that rCPE (containing a 42 amino acid (His)₆ tag fused to the N-terminus) was less active than native CPE in the Vero ⁸⁶Rb release assay. These observations collectively suggest that amino acid sequences up to residue 44 at the N-terminus (whether existing natively or recombinantly engineered) seem to have an inhibitory effect on cytotoxicity, but not binding. While the exact molecular basis for this effect is not currently known, results presented later in this dissertation provide a possible role for the N-terminus in the molecular mechanism of action of CPE.

1.4.2.2 N-terminal cytotoxicity region

While the several investigations mentioned above have shown the inhibitory nature of some amino acids at the N-terminus of CPE, removal of extensive portions of the N-terminal half of the toxin has a deleterious effect on cytotoxicity. A purified 16 kDa trypsin fragment of CPE (containing roughly amino acids 165-319) maintained binding activity but was not cytotoxic (Fig. 1.11; (57)). Similar effects were seen when 2-nitro-5-thiocyanobenzoic acid was used to cleave CPE after its sole cysteine residue at position 186 (Fig. 1.11), as this purified C-terminal fragment of CPE could bind but was inactive (78). Molecular cloning of amino acids 171-319 of CPE confirmed these results, as *E. coli* lysates expressing this recombinant construct could compete for CPE binding but were unable to elicit a cytotoxic response (Fig. 1.11; (68)). It was also shown in this study that the 171-319 fragment of CPE could not insert into membrane like CPE, thus assigning a potential functional role for the missing 170 N-terminal amino acids (Fig. 1.11).

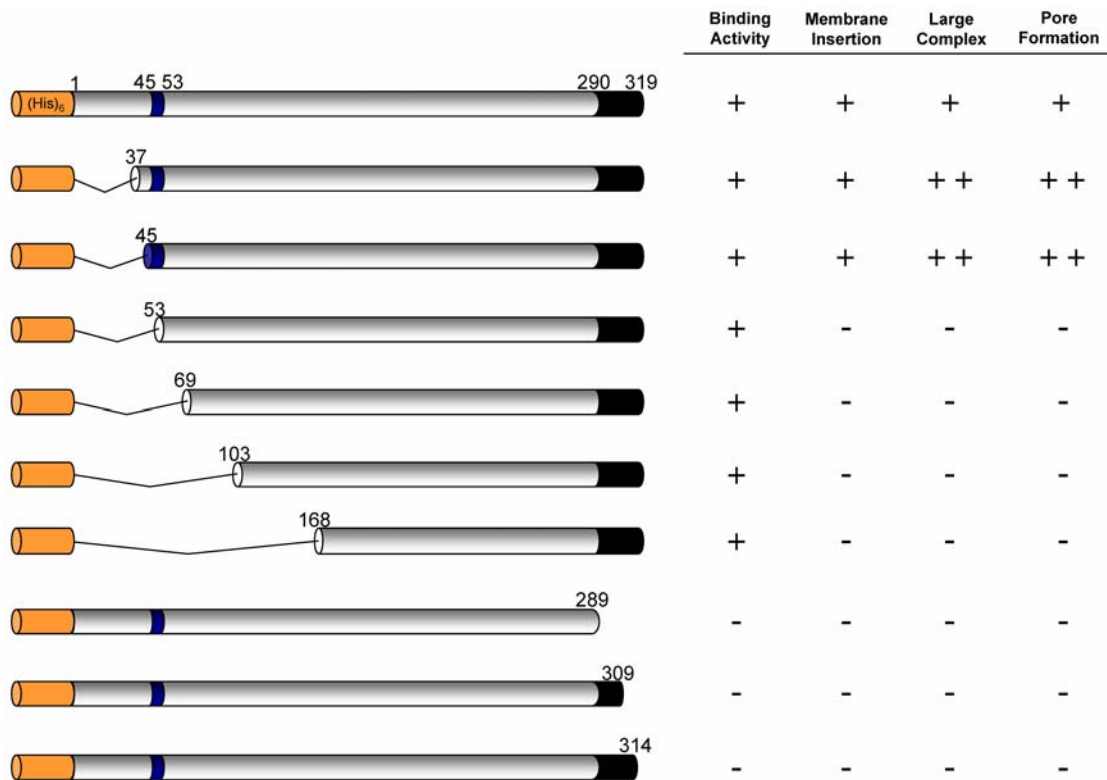


Figure 1.12 Deletion mutagenesis of rCPE using molecular cloning (93).

The aforementioned deletion mutagenesis study of rCPE more systematically truncated the N-terminus of CPE in efforts to define a region required for cytotoxicity. It was found in this work that while deletion of 36 or 44 residues from the N-terminus appeared to activate the toxin, removal of 52 amino acids completely ablated large complex formation and cytotoxicity without affecting receptor binding (Fig. 1.12; (93)). Also, deletion of 68, 102, or 167 residues from the N-terminus paralleled the binding-competent but non-cytotoxic phenotype of rCPE₅₃₋₃₁₉ (Fig. 1.12). This result identified a specific region between D45 and G53 which is required for the formation of large complex and eliciting cytotoxicity. Random mutagenesis of full length rCPE in an *E. coli* mutator strain generated several attenuated mutants, but two contained single point mutations near this N-terminal cytotoxicity region (Fig. 1.13; (92)). The negative charge introduced with a G49D mutation in CPE was sufficient to eliminate large complex formation and

cytotoxicity, but did not affect binding or small complex formation. A similar effect was seen when the S59L mutation was introduced, though this mutation lies outside of the N-terminal cytotoxicity region defined by deletion mutagenesis (Figs. 1.12 & 1.13).

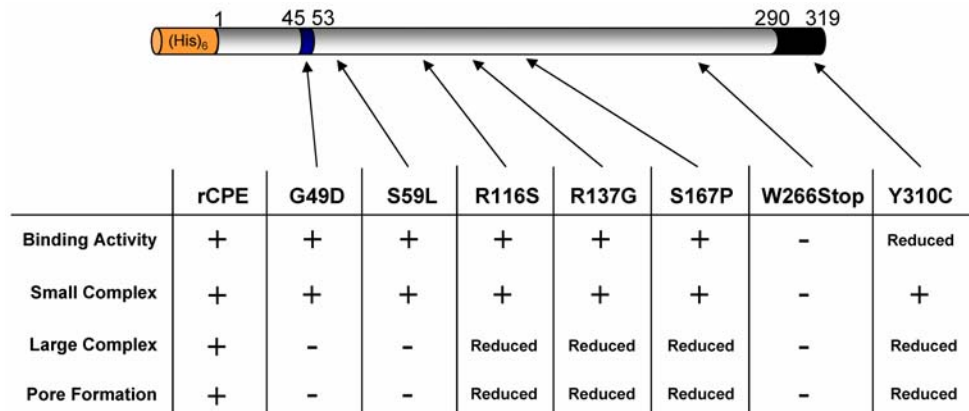


Figure 1.13 Random point mutants of rCPE deficient for one or more CPE activity (92).

1.4.2.3 C-terminal binding domain

It was discovered early on in investigations of CPE that the C-terminal half of the protein contained the receptor binding activity. As mentioned above, C-terminal fragments of CPE generated by enzymatic digestion (57), chemical cleavage (78), or molecular cloning (68) were completely deficient in cytotoxicity. Each of these fragments, however, could competitively inhibit binding of native CPE and protect cells from CPE-induced cytotoxicity (Fig 1.11). While chymotrypsinization of CPE was shown to remove 36 N-terminal residues and enhance cytotoxicity, treatment with this enzyme also removed 3 amino acids from the C-terminus without functional consequence. Another study determined that an even smaller C-terminal fragment (amino acids 290-319) could compete with CPE for receptor binding, and a synthetic peptide corresponding to these same amino acids functioned similarly (Fig. 1.11; (66)).

Interestingly, rabbit polyclonal antibodies derived against this 30 amino acid peptide could neutralize CPE activity (136), giving promise for a potential protective vaccine against CPE-induced gastrointestinal disease.

Deletion mutagenesis of the C-terminus of CPE (93) confirmed the above findings when it was shown that removal of the 30 C-terminal amino acids completely eliminated binding activity (Fig. 1.12). Interestingly, deletion of only 5 or 10 amino acids had the same effect, suggesting that residues at the extreme C-terminus of CPE make up the essential components of the C-terminal binding domain. Combined with the chymotrypsin cleavage results described above (59), these results suggest that L315 or F316 may be crucial for binding activity.

The observation that the C-CPE fragment of rCPE (amino acids 184-319; Fig. 1.14) can remove claudins from tight junctions (195) has prompted several investigators to more carefully examine N- and C-terminal residues of this fragment and their contributions to tight junction modulation. C-CPE has been demonstrated to enhance the intestinal absorption of small molecules by binding to claudins and disrupting the barrier function of tight junctions (34, 35, 105, 195, 204). A C-CPE fragment missing residues 184-219 is able to bind to claudins, however this fragment variant cannot modulate tight junction permeability (Fig. 1.14; (105)). This effect apparently suggests that disruption of tight junctions is mediated by N-terminal sequences in this C-terminal fragment of CPE. Removal of 30 or 16 amino acids from the C-terminus of C-CPE (Fig. 1.14) completely attenuates claudin binding activity (204), consistent with previous reports of the involvement of these residues in CPE binding (65-67, 93).

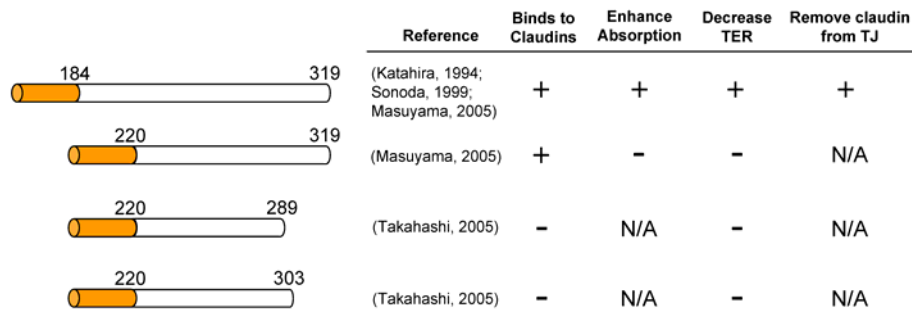


Figure 1.14 Deletion mutagenesis of the C-CPE fragment of CPE

The aforementioned random mutagenesis study of rCPE generated a Y310C point mutant which was reduced in binding activity compared with wild type CPE (Fig. 1.13; (92)). This finding motivated some workers to investigate the role of three tyrosine residues at the C-terminus of C-CPE. While some reduction in claudin binding and tight junction modulation was seen when the single Y310A and Y312A mutations were introduced, a Y306A mutation seemed to be most severe (69). Double mutations were also most detrimental when a Y306A mutation was included, and a triple mutant of Y106A/Y310A/Y312A completely inhibited the ability of this variant C-CPE construct to interact with claudins (69). When non-alanine substitutions were introduced at Y106 of C-CPE, replacing this residue with aromatic residues (tryptophan and phenylalanine) did not inhibit claudin binding or tight junction modulation as a lysine at this position did (34). While it is still unclear precisely how these residues interact with the second extracellular loop of claudin (47), the fragmentation and mutagenesis studies carried out to date have helped define essential components of the C-terminal binding domain of CPE.

1.5 THE β -BARREL PORE-FORMING TOXINS

As mentioned above, CPE contains significant DNA and amino acid homology with only one other known protein (a non-toxic hemagglutinin component of the botulinum toxin, (45)). In addition, CPE is not homologous to any toxins, bacterial or otherwise. Despite this, CPE has several structural and functional attributes similar to a particular family of bacterial pore-forming toxins. While these comparisons will be discussed in detail later, it is prudent to briefly review the mechanisms of action and structural characteristics of this well-studied group of toxins.

1.5.1 Membrane-damaging proteins

The cellular plasma membrane is a target for the action of several toxic proteins produced by prokaryotes and eukaryotes alike, and membrane attack is even an important constituent of the innate immune system (complement). Bacterial membrane-active toxins can be broken down into three groups, i.) small peptides with surfactant-like activity, ii.) toxins which enzymatically cleave components of the phospholipid bilayer, and iii.) toxins which insert into the membrane to form water-filled pores or channels (2). The latter category of pore-forming toxins (PFTs) can further be classified into toxins which use either α helices or β -barrels to penetrate the membrane. Many Gram-positive bacteria (including *C. perfringens*) produce toxins in this second category, and thus the β -barrel pore-forming toxins (β -PFTs) are the subject of the review provided below.

1.5.2 β -PFTs: from water soluble proteins to membrane-penetrating pores

While many investigators examine the β -PFT family from a bacterial pathogenesis standpoint, β -PFTs have been also heavily studied based purely on their unique biochemical activities. Over 30 different β -PFTs have been identified in both Gram-positive and Gram-negative bacteria (Table 1.2; (3)). Two divisions exist within the β -PFT family, the small-pore β -PFTs and the cholesterol-dependent cytolysins. While the small-pore β -PFTs form smaller oligomeric pores containing 5-8 toxin protomers (Table 1.2), the cholesterol-dependent cytolysin pores are very large oligomers of up to 50 protomers. Though variations in their mechanisms exist, these toxins form membrane pores by performing the following steps (2). First, localization to the cell membrane occurs by binding to either glycosyl-phosphatidyl-anchored proteins, cholesterol, or integral membrane proteins. Second, membrane-bound protomers undergo significant conformational changes and/or proteolytic cleavage to form an oligomeric pre-pore. Last, additional changes in protomer tertiary structure allow the cooperative insertion of one or more beta-sheet hairpins from each monomer to form a membrane-penetrating beta-barrel.

Table 1.2 Some members of the β -PFT family of toxins

β -PFT	Amino acids*	Molecular mass (Da)*	Stoichiometry of Oligomer	Internal Pore Diameter (nm)	References
<i>Vibrio cholerae</i> cytolysin	583	64,864	pentamer	1.2-1.6	(83, 234, 240)
<i>Clostridium perfringens</i> beta toxin	309	34,000	heptamer	1.2	(82, 150, 179)
<i>Staphylococcus aureus</i> alpha hemolysin	267	33,200	heptamer	1.4	(61, 192)
<i>Aeromonas hydrophilia</i> aerolysin	470	52,000	heptamer	1.7	(62, 145, 157, 213, 230)
<i>Bacillus anthracis</i> protective antigen	735	83,000	heptamer	1.1	(99, 100, 187)
<i>Clostridium perfringens</i> epsilon toxin	296	32,500	heptamer	2	(122, 144, 160)
<i>Bacillus cereus</i> hemolysin II	412	45,600	heptamer	?	(103, 132, 134)
<i>Bacillus cereus</i> cytotoxin K	304	34,000	heptamer	0.7	(38, 71)
<i>Staphylococcus aureus</i> Panton-Valentine leukocidin (LukS/LukF)	286/301	31,000/ 34,000	octamer	1.9-2.1	(8, 137, 161, 202)
<i>Clostridium septicum</i> alpha toxin	412	46,550	?	1.5	(10, 11, 130)
<i>Vibrio vulnificus</i> vulnificolysin	481	50,851	?	~3	(235, 236)

* Indicates the amino acid count and molecular mass of the secreted monomeric toxin

1.5.2.1 Structural attributes of the β -PFTs

The β -PFTs typically have high beta sheet compositions, and the monomeric proteins generally range in size from ~300 to 500 amino acids. Many of these toxins, such as *Aeromonas hydrophilia* aerolysin, *Bacillus anthracis* protective antigen, and *C. perfringens* epsilon toxin, require proteolytic activation in order to oligomerize (62, 99, 143). The crystal structure of the *S. aureus* alpha hemolysin, solved in 1996, shed tremendous amounts of light on structure-function relationships that exist within these proteins (192). Four structural elements are apparent in the *S. aureus* alpha hemolysin monomer structure (depicted in Fig. 1.15). First, the extreme N-terminus of the protein extends out to make contact with a neighboring monomer in the heptamer. This N-terminal 'latch' domain has been shown to be important for oligomerization and serves to join monomers together in the oligomeric form (215, 222, 223).

The second structural element, the cap region, is essentially the core of the protein and consists of a nine-strand β -sandwich. Upon heptamerization, this region serves as the top of the ring-shaped pore structure, thus the 'cap' demarcation (Figs. 1.15 & 1.16). A second globular domain serves as the third structural element in this protein and is referred to as the 'rim' domain. Loops in this largely beta sheet domain make peripheral contact with the membrane and serve to anchor the oligomer. Last, the central stem domain protrudes as a beta hairpin from the globular body of the protein inserting into the membrane. This transmembrane stem domain (TMD) is the hallmark of the β -PFTs, and is comprised of amino acids of alternating hydrophobicity (Fig 1.15). Numerous examinations of the β -PFTs have established that the hydrophobic residues in these stems face and insert into the membrane, while the hydrophilic side chains face the water-filled channel formed by the oligomer (reviewed in (2)).

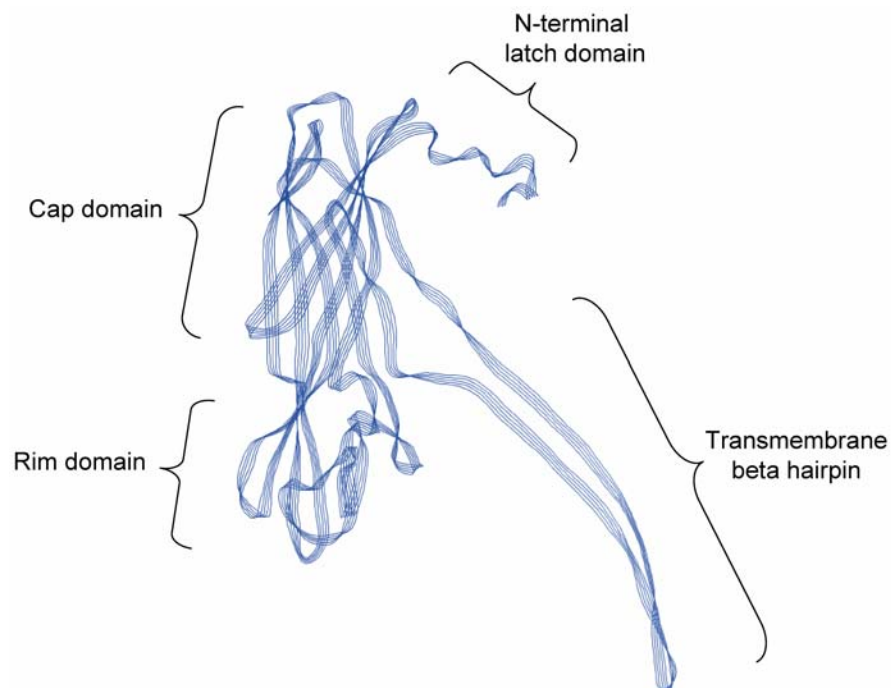


Figure 1.15 Three dimensional crystal structure of the *S. aureus* alpha hemolysin monomer (192).

The crystal structure of the *S. aureus* alpha hemolysin heptameric pore has an overall mushroom shape, with the stem spanning the phospholipid bilayer (Fig. 1.16; (192)). In total, the oligomer is 10 nm tall and 10 nm across the face of the cap. Its minimum internal diameter of 1.4 nm is typical for the β -PFTs, as most pore diameters have been measured to be between 1-3 nm (Table 1.2). The heptameric stoichiometry of *S. aureus* alpha hemolysin is shared by many of the β -PFTs, including the *C. perfringens* epsilon toxin (Table 1.2). Hexameric stoichiometries have been reported for both the *S. aureus* alpha (13, 84, 208) and gamma (152) hemolysins, however the heptameric form of each of these toxins is regarded in the literature as the functional and more physiologically-relevant oligomeric conformation. The *Vibrio cholerae* cytolysin is the lone example of a β -PFT which has a pentameric stoichiometry (240), and the *S. aureus* Panton-Valentine leukocidin the only toxin shown to be a octomer in its pore (137).

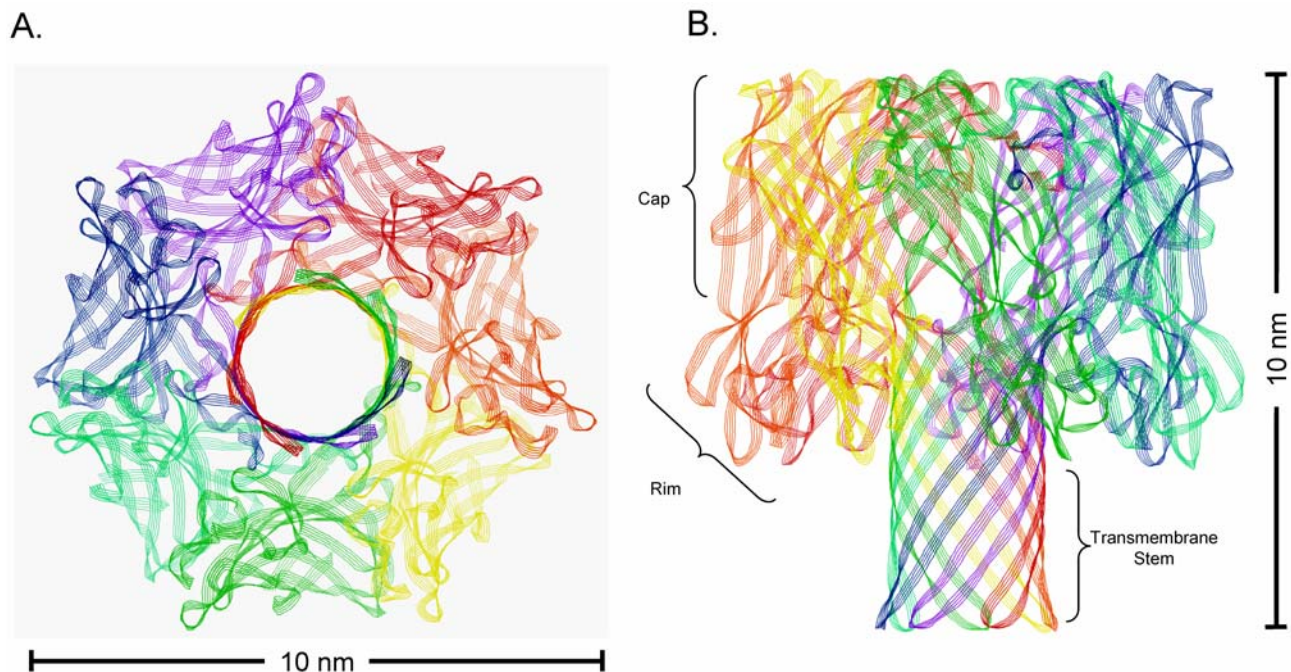


Figure 1.16 Top (A) and side (B) views of the three dimensional crystal structure of the *S. aureus* alpha hemolysin heptamer (192).

1.6 QUESTIONS ADDRESSED IN THIS THESIS

As highlighted above, investigations correlating structural elements of CPE with its various activities have provided important first steps in understanding how this toxin works. However, the many unanswered questions that remain regarding the molecular mechanism of action of CPE warrant a closer look at known and putative functional regions of the toxin. This dissertation describes a protein/membrane biochemistry based approach directed at answering three specific questions about the molecular events of CPE action. First, why is the N-terminal cytotoxicity domain essential for post-binding cytotoxic activity of CPE? Second, is there a region of CPE that is important for membrane insertion or pore formation? Third, what is the oligomeric state of CPE within large complexes? Pursuit of answers to these questions has not only furthered the knowledge of CPE action, but has also generated several unforeseen advancements in the understanding of how this toxin acts at the molecular level. Found below is a brief description of the background and rationale for each specific question asked in this study.

1.6.1 Specific question #1 – Why is the N-terminal cytotoxicity domain of CPE essential for its post-binding cytotoxic activity?

As described in detail above, fragmentation of the enterotoxin using enzymatic (57), chemical (78), or molecular cloning (68) methods demonstrated that some part of the N-terminal half of CPE is essential for cytotoxicity (Fig. 1.11). However a previous deletion mutagenesis study of CPE isolated a stretch of essential amino acids (residues D45 to G53) that, when missing, resulted in a variant unaffected in receptor binding but unable to form large complex or elicit a cytotoxic response (Fig. 1.12; (93)). A similar phenotype was noted from a G49D point mutant

of CPE generated by random mutagenesis, giving additional evidence that this region is somehow important cytotoxicity (Fig. 1.13; (92)).

While deletion mutagenesis and generation of loss-of-function variants can be an important start to defining functional regions of a protein, site-directed mutagenesis provides a much more detailed analysis of the contributions of specific amino acids in the targeted region. To this end, site-directed mutagenesis was used in the present study to make single alanine substitutions of every amino acid in the N-terminal cytotoxicity region of CPE. The resultant rCPE variants were characterized for their CPE activities, and additional non-alanine substitutions were then engineered into sites found to crucial for CPE. Also, structure-function relationships defined in *in vitro* cell culture systems were verified in an *in vivo* model of CPE action, the rabbit ileal loop model.

1.6.2 Specific question #2 – Is there a region of CPE that is important for membrane insertion or pore formation?

Previous structure-function studies of the enterotoxin have concentrated on two major functional regions, the N-terminal cytotoxicity region and the C-terminal receptor binding domain. Despite this, it is possible (if not likely) that other distinct functional regions exist within the structure of the CPE protein. For example, the enterotoxin has been shown to insert into membranes since CPE in the large complex is protected from proteolytic degradation (228). As reviewed above, members of the β -PFT family have very characteristic membrane insertion domains consisting of a beta-strand hairpin (Figs. 1.15 and 1.16) that alternates in amino acid hydrophobicity. Although CPE lacks sequence homology with this family of toxins, the high beta sheet content (58, 173) and pore-forming activity (115) of CPE suggests that it may act in a similar manner using a TMD. Secondary structure predictions only reveal one major hydrophobic patch in CPE between amino acids 80-110 (Fig. 1.9). In addition, when aligned with the TMDs of several

members of the β -PFT family, amino acids 81-106 in CPE appear to closely resemble a TMD beta hairpin (Fig. 1.17). Thus, this putative TMD of CPE serves as an ideal candidate for a region of CPE involved with membrane insertion.

To ascertain whether or not amino acids 81-106 could be important for membrane insertion, internal deletion mutagenesis was used to delete this region from rCPE. The resultant deletion variant was subsequently characterized for its CPE activity. Additional mutagenesis was performed taking into account information learned from Specific Question #1 in efforts to gain temporal insights about CPE functional regions.

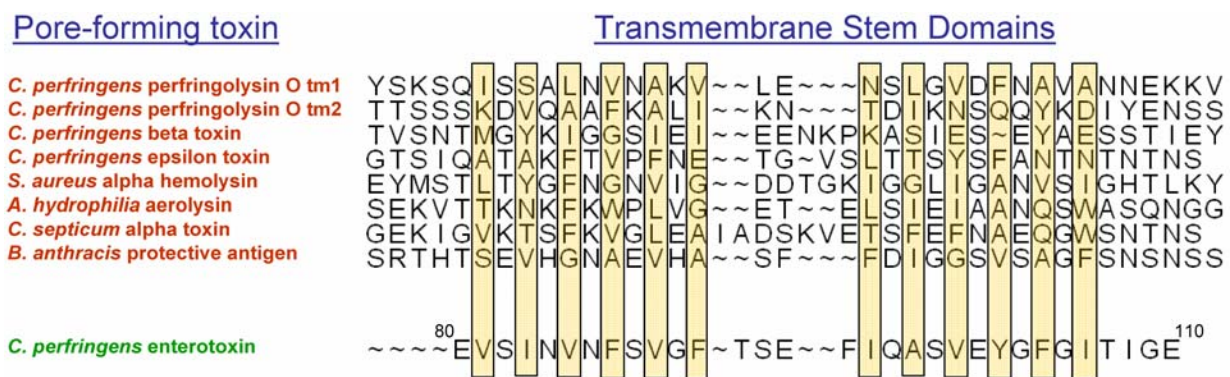


Figure 1.17 Alignment of the TMDs of several β -PFTs and CPE amino acids 80-110. In the TMDs, hydrophobic residues (boxed) alternate with hydrophilic residues to form a beta hairpin. A similar pattern can be seen between amino acids 81-106 of CPE.

1.6.3 Specific question #3 – What is the oligomeric state of CPE within the large complexes?

Many models of the CPE large complex composition have been put forth over the past two decades. The discovery that two unknown proteins (of ~50 and ~70 kDa) physically associate with CPE sparked the first model for large complex formation, where one CPE molecule (~35

kDa) and one molecule of each of the ~50 and ~70 kDa proteins associate to form an SDS-resistant large complex of ~160 kDa (232). Later, the discovery of a second SDS-resistant large complex containing occludin in CPE-treated Caco-2 cells led to the idea that the ~160 kDa large complex, plus one occludin molecule (~65 kDa), would lead to the formation of the ~200 kDa large complex (186).

Despite these findings, it has yet to be directly determined whether or not CPE is a monomer or an oligomer in these complexes. Several anecdotal lines of evidence suggest that CPE oligomerizes during cytotoxic action. First, (as illustrated in Section 1.6.2) the presence of a putative TMD (Fig. 1.17), along with other structural similarities, suggests that CPE maintains a mechanism of action akin to the β -PFT family by forming an oligomeric membrane-penetrating pore. Second, in the absence of other proteins, CPE has been shown to form ion-permeable pores in artificial membranes (72), suggesting that CPE has an inherent ability to form pores (presumably by oligomerization). Last, a previous study has shown that large complex formed by native CPE (~35 kDa) and rCPE (~40 kDa) differ in apparent molecular mass by more than the ~5 kDa which separates the two toxins alone (186). This finding is consistent with the idea that CPE is present in more than one copy in the SDS-resistant large complexes.

To directly address whether CPE is an oligomer in its two SDS-resistant large complexes, a heteromer gel shift assay was used that has defined the stoichiometries of several oligomeric pore-forming toxins (56, 143, 144, 240). Findings from these experiments prompted the reassessment of the molecular masses of complexes formed by CPE, as well as exploration of dominant negative phenotypes of several rCPE variants already in existence.

2.0 MATERIALS AND METHODS

2.1 BACTERIAL CULTURING

2.1.1 Bacterial strains, growth media, and media supplements

All plasmids used or generated in this study (Table 2.1) were harbored by the XL-1 Blue strain of *E. coli*. Solid and/or liquid Luria-Bertani media was to culture bacteria for all molecular cloning methods. Where protein production was desired, liquid SOB media was used. All plated cultures of bacteria were incubated overnight at 37°C. Liquid cultures of rCPE-expressing *E. coli* were subjected to constant shaking at 245 rpm at 37°C overnight. Ampicillin (100 µg/ml) was used when selection for *E. coli* harboring any of the Table 2.1 constructs was required. When production of rCPE (or its derivatives) was desired, culturing media was brought to 5 mM isopropyl-beta-D-thiogalactopyranoside at inoculation (unless otherwise noted). Stocks of bacterial strains were prepared by bringing 1.0 ml of the culture to 20% glycerol, then stored at -80°C.

2.2 DNA PREPARATION AND MANIPULATION

2.2.1 Site-directed mutagenesis of *cpe*

Single point mutations were introduced into the *cpe* gene of pJKFLt-1 using the QuikChange[®] site-directed mutagenesis kit (Stratagene, La Jolla, CA), as instructed by the manufacturer.

DNA oligos used for mutagenesis (Table 2.2) were synthesized by Integrated DNA Technologies (Coralville, IA). To generate the mutant plasmids, mutagenesis primers were added to a thermocycling reaction permitted *in vitro* synthesis of the plasmid DNA using the high-fidelity polymerase, *PfuTurbo*. Parental template DNA was digested away by the methylase-specific DNase, *Dpn I*, and the resultant mutated plasmid mixture was used to transform XL-1 Blue Supercompetant *E. coli* cells.

Table 2.1 Bacterial strains used in this study

Plasmid harbored	Description	Reference
pTrcHis A	Protein expression vector used for all constructs made in this study. Encodes a 42 N-terminal (His) ₆ -tag.	Invitrogen (Carlsbad, CA) (93)
pJKFLt-1	Complete <i>cpe</i> ORF cloned into pTrcHis A. With the 42 amino acid (His) ₆ -tag, produces a 40.0 kDa protein of 361 total amino acids.	(93)
pJSD45A	pJKFLt-1 with D45A single point mutation in <i>cpe</i>	This study; (190)
pJSK46A	pJKFLt-1 with K46A single point mutation in <i>cpe</i>	"
pJSG47A	pJKFLt-1 with G47A single point mutation in <i>cpe</i>	"
pJSD48A	pJKFLt-1 with D48A single point mutation in <i>cpe</i>	"
pJSG49A	pJKFLt-1 with G49A single point mutation in <i>cpe</i>	"
pJSW50A	pJKFLt-1 with W50A single point mutation in <i>cpe</i>	"
pJSI51A	pJKFLt-1 with I51A single point mutation in <i>cpe</i>	"
pJSL52A	pJKFLt-1 with L52A single point mutation in <i>cpe</i>	"
pJSG53A	pJKFLt-1 with G53A single point mutation in <i>cpe</i>	"
pJSE54A	pJKFLt-1 with E54A single point mutation in <i>cpe</i>	"
pJSD48E	pJKFLt-1 with D48E single point mutation in <i>cpe</i>	"
pJSD48N	pJKFLt-1 with D48N single point mutation in <i>cpe</i>	"
pJSW50F	pJKFLt-1 with W50F single point mutation in <i>cpe</i>	"
pJSW50Y	pJKFLt-1 with W50Y single point mutation in <i>cpe</i>	"
pJSI51L	pJKFLt-1 with I51L single point mutation in <i>cpe</i>	"
pJSI51V	pJKFLt-1 with I51V single point mutation in <i>cpe</i>	"
pJSTM1	pJKFLt-1 with deletion of amino acids 81-106 in <i>cpe</i>	This study; (191)
pJSTM1-D48A	pJSTM1 with D48A single point mutation in <i>cpe</i>	This study; (191)
pJK22	pJKFLt-1 with deletion of amino acids 1-36 in <i>cpe</i> (rCPE ₃₇₋₃₁₉)	(93)
pJK19	pJKFLt-1 with deletion of amino acids 1-167 in <i>cpe</i> (rCPE ₁₆₈₋₃₁₉)	(93)
pJKW266Stop	pJKFLt-1 with W266Stop stop mutation in <i>cpe</i>	(92)

2.2.2 Deletion mutagenesis of *cpe*

Splicing by overlap extension (80) was used to generate the internal deletion variant of CPE in this study. Regions upstream and downstream from the *cpe* sequence to be deleted were amplified by PCR, with the 3' upstream reaction primer having complementarity with the 5' downstream reaction primer. Products from these two PCR reactions were then used as the template in a third PCR reaction, adding the 5' upstream reaction and 3' downstream reaction primers after 3 cycles to allow the amplification of the entire *cpe* gene (minus the sequence to be deleted). The product from the third PCR reaction was excised from an agarose gel and purified with Freeze n' Squeeze™ Spin Columns (Bio-Rad, Hercules, CA). After simultaneous digestion with *Bam*HI and *Eco*RI, the DNA was again gel-purified before precipitation using 0.1 volumes of sodium acetate and 2.0 volumes of cold ethanol for 30 min at -20°C. The DNA was pelleted by centrifugation at 4°C for 30 min, washed once with 70% ethanol, re-centrifuged, and resuspended in the desired volume. This DNA was then ligated into a *Bam*HI and *Eco*RI-digested pTrcHis A vector, and this ligation mixture was used to transform XL-1 Supercompetent Blue *E. coli*.

2.2.3 DNA Sequencing

The presence of all mutations in the *cpe* gene of the Table 2.1 constructs were confirmed by nucleotide sequencing. Plasmids containing the mutated *cpe* gene were isolated from overnight *E. coli* cultures with the QIAGEN Plasmid Mini Kit (QIAGEN, Valencia, CA). Primers used for sequencing can be found in Table 2.2, and sequencing reactions were performed by the University of Pittsburgh Genomics and Proteomics Core Laboratories. The BioEdit DNA analysis software (64) was used to confirm the presence of the desired mutation and the absence of unintended mutations.

Table 2.2 DNA primers used in this study for mutagenesis or nucleotide sequencing

Name	Sequence (5'-3')*	Purpose; Reference
D45A-F D45A-R	GGATTATATGTAATAG <u>C</u> TAAAGGAGATGGTTGGATATTAGGGGAACCC GGGTTCCCCTAATATCCAACCATCTCCTTTA <u>G</u> CTATTACATATAATCC	D45A point mutation; (190)
K46A-F K46A-R	GGATTATATGTAATAGAT <u>GC</u> AGGAGATGGTTGGATATTAGGGGAACCC GGGTTCCCCTAATATCCAACCATCTCCT <u>GC</u> ATCTATTACATATAATCC	K46A point mutation; (190)
G47A-F G47A-R	GGATTATATGTAATAGATAAAG <u>C</u> AGATGGTTGGATATTAGGGGAACCC GGGTTCCCCTAATATCCAACCATCT <u>G</u> CCTTTATCTATTACATATAATCC	G47A point mutation; (190)
D48A-F D48A-R	GGATTATATGTAATAGATAAAGGAG <u>CT</u> GGTTGGATATTAGGGGAACCC GGGTTCCCCTAATATCCAACCA <u>G</u> CTCCTTTATCTATTACATATAATCC	D48A point mutation; (190)
G49A-F G49A-R	GATTATATGTAATAGATAAAGGAGATG <u>CT</u> TGGATATTAGGGGAAC GTTCCCCTAATATCCAAG <u>C</u> ATCTCCTTTATCTATTACATATAATC	G49A point mutation; (190)
W50A-F W50A-R	GTAATAGATAAAGGAGATGGT <u>GCG</u> ATATTAGGGGAACCCCTCAG CTGAGGGTCCCCTAATATC <u>GC</u> ACCATCTCCTTTATCTATTAC	W50A point mutation; (190)
I51A-F I51A-R	GTAATAGATAAAGGAGATGGTTGG <u>GC</u> ATTAGGGGAACCCCTCAG CTGAGGGTCCCCTAAT <u>G</u> CCCAACCATCTCCTTTATCTATTAC	I51A point mutation; (190)
L52A-F L52A-R	GATAAAGGAGATGGTTGGATAG <u>GC</u> AGGGGAACCCCTCAGTAGTTTC GAAACTACTGAGGGTCCCCT <u>G</u> CTATCCAACCATCTCCTTTATC	L52A point mutation; (190)
G53A-F G53A-R	GGAGATGGTTGGATATTAGGGG <u>C</u> AGCCCTCAGTAGTTTC GAAACTACTGAGGGTCC <u>G</u> CTAATATCCAACCATCTCC	G53A point mutation; (190)
E54A-F E54A-R	GGAGATGGTTGGATATTAGGGG <u>C</u> ACCCTCAGTAGTTTC GAAACTACTGAGGGT <u>G</u> CCCCTAATATCCAACCATCTCC	E54A point mutation; (190)
D48E-F D48E-R	GGATTATATGTAATAGATAAAGGAGAG <u>G</u> GGTTGGATATTAGGGGAACCC GGGTTCCCCTAATATCCAACCC <u>T</u> CTCCTTTATCTATTACATATAATCC	D48E point mutation; (190)
D48N-F D48N-R	TTATATGTAATAGATAAAGGA <u>A</u> ATGGTTGGATATTAGGGGAACCC GGGTTCCCCTAATATCCAACCAT <u>T</u> TCTTTATCTATTACATATAA	D48N point mutation; (190)
W50Y-F W50Y-R	GTAATAGATAAAGGAGATGGTT <u>AC</u> ATATTAGGGGAACCCCTCAG CTGAGGGTCCCCTAATAT <u>G</u> TAAACCATCTCCTTTATCTATTAC	W50Y point mutation; (190)
W50F-F W50F-R	GTAATAGATAAAGGAGATGGT <u>TTT</u> TATTAGGGGAACCCCTCAG CTGAGGGTCCCCTAATAT <u>AAA</u> ACCATCTCCTTTATCTATTAC	W50F point mutation; (190)
I51L-F I51L-R	GTAATAGATAAAGGAGATGGTTGG <u>C</u> TATTAGGGGAACCCCTCAG CTGAGGGTCCCCTAATAG <u>C</u> CCAACCATCTCCTTTATCTATTAC	I51L point mutation; (190)
I51V-F I51V-R	GTAATAGATAAAGGAGATGGTTGG <u>G</u> TATTAGGGGAACCCCTCAG CTGAGGGTCCCCTAATA <u>C</u> CCAACCATCTCCTTTATCTATTAC	I51V point mutation; (190)
TM1-A-F TM1-D-R	CGCGGATCCGCGGATGTTAATTATAATATGCTTAGTAAC CCGGAATTCTATATGGAAGGAGAAATTAATGC	TM1 deletion; (191)
TM1-B-R TM1-C-F	TTGTTCTCCTATAGTTTCTTTAGATTTAGTTAATGATTGGCTAAA ACTAAATCTAAAGAACTATAGGAGAACAAAATACAATAGAAAG	TM1 deletion; (191)
TrcSeq-1F 2-F	GGACAGCAAATCGGTCGG GGTACCTTAAGCCAATCA	Sequencing; (191)
6-R	CCGGAATTCTATATGGAAGGAGAAATTAATGC	Sequencing; (191)
PH-309-R	TGATCAATATTCCTAAGCTATCTGCAG	Sequencing; (191)
PH-310-F	GATTTAGCTGCTACAGAAAGA	Sequencing; (191)

* nucleotides incorporating mutations are bold and underlined

2.3 PROTEIN BIOCHEMISTRY AND CHROMATOGRAPHY

2.3.1 Preparation of CPE

Native CPE was purified from *C. perfringens* strain NCTC8239 as described previously (127). All recombinant CPE constructs were affinity-enriched (via their vector-encoded N-terminal (His)₆-tags from lysates of *E. coli* transformed with the indicated construct (Table 2.1). One liter of SOB media was inoculated with 20 ml of an overnight SOB culture of the desired rCPE-expressing *E. coli* strain. After vigorous shaking for 3 h at 37°C, rCPE expression was induced by adding isopropyl-beta-D-thiogalactopyranoside to 5 mM. After an additional 4 h of shaking at 37°C, the bacteria were harvested by centrifugation. Final pellets were resuspended in HiTrap binding buffer (20 mM NaH₂PO₄, 500 mM NaCl, 10 mM imidazole, pH 7.4) and then stored at -80°C overnight. After thawing the bacterial suspension, a Heat Systems Ultrasonic Sonicator (Misonix, Farmingdale, NJ) was used to lyse the bacteria. Cell debris was pelleted by centrifugation at 7,500 × g and supernatant containing the (His)₆-tagged rCPE was passed through a MILLEX[®]HV 0.45 µm PVDF Filter (Millipore, Billerica, MA). This supernatant was then loaded on a cobalt-charged HiTrap Chelating affinity column (Amersham Biosciences, Piscataway, NJ). The column was washed with HiTrap binding buffer and rCPE was then eluted with a linear imidazole gradient from 10-500 mM. Protein-containing fractions from the elution were pooled and dialyzed overnight against sterile deionized H₂O, pH 7.0. Toxins were stored in aliquots at -80°C until use.

Toxin yield was calculated by quantitative Western blotting, as described previously (190). Briefly, known amounts of native CPE were separated on a 10% acrylamide SDS-PAGE along with 10-fold serial dilutions of each the affinity-enriched rCPE to be quantitated. After Western blotting for CPE with rabbit polyclonal anti-CPE antiserum, densitometric imaging was

performed with the Gel Doc imaging system and Quantity One software (Bio-Rad) to generate a standard curve from which the concentration of the rCPE dilutions was estimated.

2.3.2 Enterokinase digestion of rCPE₃₇₋₃₁₉

For use in the heteromeric shift experiments described below, it was necessary to cleave the (His)₆-tag from the rCPE₃₇₋₃₁₉ construct. To this end, 200 µg of rCPE₃₇₋₃₁₉ was incubated with 10 units of EKMax (Invitrogen, Carlsbad, CA) overnight at 37°C. This digestion mixture was then incubated for 20 min at 4°C with the EKAway resin (Invitrogen) to remove the enterokinase from the toxin. This slurry was added to a disposable plastic gravity column, and the flow through (containing the (His)₆-tagless rCPE₃₇₋₃₁₉) was again quantitated using the Western blot method described above, before aliquotting and storage at -80°C. This EKMax-treated rCPE₃₇₋₃₁₉ will hereafter be referred to as EK-rCPE₃₇₋₃₁₉.

2.3.3 Limited trypsin proteolysis assay

For site-directed mutagenesis studies, a limited proteolysis assay was used to assess rCPE variants for gross conformational changes induced by the introduced mutation. In these assays, 400 ng aliquots of each affinity-enriched rCPE species were brought to a final volume of 100 µl with phosphate-buffered saline containing Ca²⁺ and Mg²⁺ (PBS²⁺; Mediatech, Herndon, VA). Reactions were prepared in quadruplicate and digested at 25°C for 0, 5, 15, or 30 min with 4 ng of trypsin (Sigma, St. Louis, MO). Immediately after completion of the digestion period, 100 µl of 2X Laemmli buffer w/ 5% β-mercaptoethanol (β-ME) was added to each reaction before sample boiling (5 min) to terminate the reaction. A 50 µl aliquot of each sample was then loaded onto a 10% acrylamide SDS-PAGE, followed by Western blotting using anti-CPE antibody as described above for the rCPE quantitation.

2.3.4 Size exclusion chromatography

To estimate the native molecular masses of the two CPE large complexes, a Sephacryl S400 HR (Amersham) size exclusion column (76 × 1.5 cm internal diameter) was poured and equilibrated with S400-TX buffer (50 mM sodium phosphate, 150 mM NaCl, 0.1% Triton-X 100, pH 7.2). Using the method of Whitaker (226), the column was calibrated by calculating the elution volumes of the following standards from Sigma: bovine thyroglobulin (669 kDa), horse spleen apoferritin (443 kDa), bovine liver catalase (232 kDa), and aldolase (158 kDa). Column runs were performed overnight at 4°C with a 0.5 ml/min flow rate.

When performing gel filtration of the CPE large complexes, confluent Caco-2 cells were harvested by gentle scraping, washed, and then treated (with inversion) with 10.0 µg/ml native CPE in 10 ml Hank's balanced salt solution lacking Ca²⁺ or Mg²⁺ (HBSS, Mediatech) for 20 min at 37°C. Cells were then washed once with HBSS and lysed in S400-TX containing 1% Triton X-100 for 30 min at RT with inversion. Insoluble debris was pelleted by centrifugation, and 5.0 ml of the lysate supernatant was filtered with a Millex[®]HV 0.45 µm syringe filter. This filtrate was then loaded on the calibrated Sephacryl S400 HR column and run overnight at 4°C at 0.5 ml/min, collecting 0.8 ml fractions between 200 and 250 ml of column flow-through. To assess the fractions for the presence of CPE complexes, 100 µl samples were taken from desired fractions and brought to 1X Laemmli buffer. Those samples were then separated on a 4% acrylamide SDS-PAGE and Western immunoblotted with rabbit polyclonal anti-CPE antiserum. Densitometric scanning of autorad films using the Gel Doc imaging system and the accompanying Quantity One software (Bio-Rad) was used to quantitate the amount of each complex located in each fraction. Molecular mass estimations were calculated by correlating the elution volumes of peak Western blot fractions to the standard curve generated from the aforementioned standards.

2.3.5 Ferguson plot analysis

Ferguson plots were used in this study to analyze the molecular mass of the CPE large complexes. To perform these experiments, large complex or standards were separated on 4, 5, 6, and 7% acrylamide PAGs (16 cm), each poured with a 4% acrylamide stacking gel. Samples were electrophoresed at 15 mA per gel until the dye front had reached the bottom of the gels. Lanes containing the native molecular mass standards were excised and stained with Coomassie Brilliant Blue G-250 (Bio-Rad), while lanes containing CPE-treated cell lysates were electrotransferred onto Immobilon™ -P PVDF membranes (Millipore) for 60 min at 1.0 A with Gershoni's transfer buffer (52). Membranes were then Western blotted with rabbit polyclonal anti-CPE antiserum to detect the CPE complexes. Molecular mass calculations were performed as described elsewhere (39, 75). Briefly, relative migrations of the standards on each percentage gel were plotted versus the gel concentration. Negative slopes from best fit lines generated for each standard were then plotted, in a separate graph, versus the known molecular masses of the standards. The line equation of the best fit line from this second plot was used to extrapolate the molecular masses of each CPE-containing complex.

2.4 CPE ACTIVITY CHARACTERIZATION

2.4.1 Morphologic Damage Assay

Caco-2 cells were cultured using minimal essential medium Eagle (Sigma) with 10% fetal bovine serum (Mediatech), 1% minimal essential medium non-essential amino acids (Sigma), 100 units/ml penicillin G (Invitrogen), 100 µg/ml streptomycin (Invitrogen), and 2 mM L-glutamine (Invitrogen). Cells were kept in 5% atmospheric CO₂ at 37°C throughout culturing. To perform the morphologic damage assays, Caco-2 cells grown to confluency in 100 mm dishes were washed once with pre-warmed Hank's balanced salt solution containing Ca²⁺ and Mg²⁺ (HBSS²⁺; Mediatech), and then treated with 2.5 µg/ml of toxin in 2 ml of HBSS²⁺. Cellular morphologic damage (nuclear condensation, cell rounding, detachment from well bottom) was assayed at the indicated time points using a Zeiss Axiovert 25 inverted microscope at 10× magnification (Zeiss, Thornwood, NY). A Canon Powershot G5 digital camera and Canon Utilities RemoteCapture software (Canon, Inc., Lake Success, NY) were used to capture images of cells at each time point, and subsequent image processing was performed with Adobe Photoshop software (Adobe Systems, Inc., San Jose, CA).

2.4.2 Competitive binding analysis

Small intestinal BBMs were isolated from female New Zealand White rabbits, as described previously (184). ¹²⁵I-CPE was prepared using IODO-GEN® Pre-Coated Iodination tubes (Pierce, Rockford, IL), with 2.5 mCi of Na¹²⁵I (specific activity - 17.0 mCi/mg, ICN) for 1 mg of native CPE. As described previously (92), BBMs (100 µg) were preincubated for 20 min in 200 µl of PBS²⁺ containing various concentrations (0.01-50 µg/ml) of each competing rCPE species.

¹²⁵I-CPE (0.5 µg) was then added to each sample for an additional 20 min at RT. After washing, ¹²⁵I-CPE bound to the BBMs was quantitated using a Cobra Quantum gamma counter. Data are expressed as percent of total binding, where total (100%) binding was determined by incubating BBMs with ¹²⁵I-CPE in the absence of any competing rCPE species. The previously described rCPE random point variant W226Stop (Table 2.1; (92)) was affinity-enriched (as above) and used as a negative control in binding experiments.

2.4.3 Small complex formation

The ability of rCPE variants to form small complex was measured as previously described (92). Briefly, BBMs (200 µg) were treated for 15 min at 4°C (to inhibit formation of CPE large complexes (117)) with 5 µg of rCPE dissolved in 500 µl of PBS²⁺. Those BBMs were then pelleted, washed, and extracted for 30 min at 4°C with 40 µl of PBS²⁺ containing 1% Triton X-100 (Sigma). After microcentrifugation, 10 µl of 5X native loading buffer (5 mM Tris-HCl, 38 mM glycine, 33% glycerol, 0.25 mg bromophenol blue) was added to the extraction supernatants. These samples were electrophoresed at 5 mA on a 6% acrylamide native PAG and small complexes were electrotransferred onto Immobilon-P PVDF membrane (Millipore) using Gershoni's transfer buffer. Western blotting to detect the CPE-containing small complex was then performed as described for affinity-enrichment quantitation.

2.4.4 Large complex formation

Large complex formation by each rCPE species was assayed as described previously (190) using confluent 100 mm dish cultures of Caco-2 cells. Briefly, cells were washed once with HBSS, gently dislodged from the plate with a cell scraper, and harvested by centrifugation. After one additional wash with HBSS, 2.5×10^6 harvested cells were resuspended in 200 µl of

HBSS. An rCPE species was then added at a final concentration of 2.5 µg/ml, and samples were incubated for 45 min at 37°C with shaking. After microcentrifugation at 4°C, pelleted cells were washed with HBSS containing the Complete[®] protease inhibitor cocktail (Roche; HBSS-PI) at 2X concentration and then finally resuspended in 45 µl of ice cold HBSS-PI. Benzonase[®] Nuclease (12.5 units; Novagen, Inc., Darmstadt, Germany) was added to each sample for 10 min at RT. Samples were brought to 1X Laemmli buffer and then loaded onto a 4% acrylamide SDS-PAG that was run overnight for ~19 h at 5 mA before electrotransfer and CPE Western immunoblotting as described above.

For Ferguson plot experiments, it was necessary to form each of the ~155 kDa and ~200 kDa large complexes in the absence of one another. To accomplish this, we utilized previous findings from our laboratory that short, apical treatment of Caco-2 cell cultures grown to confluency on Transwell[®] permeable supports (Corning, Corning, NY) results in the formation of only the “~155 kDa” large complex (185). In order to form the “~200 kDa” large complex in the absence of any “~155 kDa” large complex, a Caco-2 variant cell line was used that only produces the “~200 kDa” large CPE complex when confluent monolayers are treated for 30 min. After CPE treatment, all cells were washed once with HBSS and then lysed with HBSS containing 1% Triton X-100 for 30 min at RT with constant inversion. Insoluble material was pelleted by centrifugation, and the supernatant lysate was prepared for native PAGE by the addition of an appropriate amount of 5X native loading buffer.

2.4.5 Heteromer gel shift assay with CPE large complexes

To generate heteromeric CPE large complexes, various ratios of rCPE and EK-rCPE₃₇₋₃₁₉ were used to treat 2.5×10^6 Caco-2 cells suspended in HBSS for 20 min at 37°C with constant inversion, keeping the total toxin concentration constant at 2.5 µg/ml. Samples were electrophoresed on a 4% acrylamide SDS-PAG cast in a 20 cm Protean II gel electrophoresis

system (Bio-Rad) with current kept constant at 50 mA per gel. After the gels were Western blotted as described above, blots were scored qualitatively for the number of resolvable individual bands in all lanes. Densitometric scanning of each lane was performed using the Gel Doc imaging system and the accompanying Quantity One software (Bio-Rad).

2.4.6 ^{86}Rb release experiments

Formation of CPE pores was determined by measuring ^{86}Rb release from Caco-2 cells, as described previously (190). Briefly, confluent Caco-2 cell monolayers were pre-loaded with 4 $\mu\text{Ci}/\text{well}$ of $^{86}\text{RbCl}$ (specific activity, 6.4 mCi/mg; Perkin Elmer) for 4-5 h at 37°C. After two washes with pre-warmed HBSS²⁺, the radiolabeled cultures were treated with toxin at the indicated concentrations for 15 min at 37°C. ^{86}Rb released into the culture supernatant was collected and counted with a Cobra Quantum gamma counter (Perkin Elmer). Spontaneous release of ^{86}Rb from cells was measured by incubation of radiolabeled monolayers with HBSS²⁺ alone and maximal release was determined by treating monolayers with 1 ml each of 0.5% saponin and 1.0 M citric acid. Data from ^{86}Rb release experiments were converted and plotted as percent maximal release using the following equation: $[(\text{experimental release} - \text{spontaneous release}) / (\text{maximal release} - \text{spontaneous release})] \times 100$.

2.4.7 Pronase resistance of large complex

Experiments used to analyze the pronase susceptibility of large complexes formed by rCPE (or its variants) were adapted from a previously published procedure (228). BBMs (100 μg) were treated for 20 min at RT with 1.5 μg of rCPE or 4.5 μg of TM1 (Table 2.1) in 100 μl of PBS²⁺. The BBMs were then washed once with 100 μl of ice-cold PBS²⁺, before treatment for 5 or 60 min in 50 μl of PBS²⁺ containing the indicated concentration of pronase. BBMs were then

washed three times with ice-cold PBS²⁺ containing the Complete® protease inhibitor cocktail (Roche Applied Science, Penzberg, Germany). Final pellets were resuspended in Laemmli buffer without β -ME, and loaded on a 6% acrylamide SDS-PAG and subsequently treated as a CPE Western blot detailed above.

2.4.8 Dissociation of CPE large complex from membranes

rCPE or its variants were added to 100 μ g of BBMs at a final concentration of 2.5 μ g/ml. Large complex formation was allowed to occur at 37°C for 20 min, followed by a washing step with phosphate buffered saline without Ca²⁺ or Mg²⁺ (PBS; Mediatech) containing the Complete® protease inhibitor cocktail at 2X concentration (PBS-PI; Roche). After this wash, toxin-treated BBMs were resuspended in 200 μ l of PBS-PI and inverted gently at 4°C for the indicated time periods. At the end of this incubation, the toxin-treated BBMs were pelleted by centrifugation, and both the supernatants and pellets from this spin were separated on an SDS-containing, 4% acrylamide gel and Western immunoblotted for CPE as described above.

2.4.9 Heat denaturation of CPE large complex

rCPE or TM1 was added to 100 μ g of BBMs for 20 min at 37°C in PBS-PI. After centrifugation and washing once with 200 μ l of PBS-PI, BBMs containing large complex were extracted with Laemmli buffer containing β -ME then heated at 90°C in a dry bath for the indicated time period. After this incubation, samples were separated on a 4% acrylamide SDS-PAG and Western immunoblotted for CPE as described above.

2.5 IN VIVO ANALYSIS OF CPE ACTIVITY

2.5.1 Fluid accumulation in rabbit ileal loops

Adult male New Zealand White rabbits (Charles River) were fasted overnight and then tranquilized by an intramuscular injection of xylazine and acepromazine. Analgesia was produced with buprenorphine, and anesthesia was induced with intravenous ketamine hydrochloride and maintained with inhalatory isofluorane. A laparotomy was performed and the small intestine was exposed. Several lengths (approximately 20 mm) of ileum were isolated by ligation, avoiding interference with the blood supply and leaving an empty segment of gut between consecutive loops. Toxin preparations or Ringer's solution (control) were injected into one of each of the ileal loops. Care was taken to avoid over-distension of loops. The abdominal incision was closed by separate muscle and skin sutures and the animals were kept deeply anaesthetized. After a designated incubation period, the abdominal cavity was reopened, and intestinal loops were excised sequentially, in the same order that they had been inoculated. The volume of accumulated fluid and the length of the loops were measured and the ratio volume/length was calculated for each loop.

2.5.2 Histopathological analysis of CPE-treated ileal tissues

Selected sections from loops treated for 30 min with 300 µg/ml of rCPE or its mutants were cut and embedded. Mouse monoclonal anti-CPE antibody was used to detect the location of CPE, while an anti-mouse streptavidin peroxidase conjugate was used as the secondary antibody. Sections were counterstained with hematoxylin, then photomicrographed at total magnification of 100X.

3.0 RESULTS

3.1 FINE-MAPPING OF THE N-TERMINAL CYTOTOXICITY REGION OF CPE

3.1.1 Alanine-scanning mutagenesis

3.1.1.1 Introduction of amino acid substitutions

As detailed above, previous rCPE deletion mutagenesis studies (93) have implicated the region between residues D45 and G53 of the full length rCPE as being important for cytotoxicity. For that reason, the current study targeted this region for site-directed mutagenesis (Fig. 3.1). Because the single methyl group of alanine is small in size and only slightly non-polar, this amino acid was chosen for mutagenesis of the N-terminal cytotoxicity region of CPE since it would be least likely to induce gross conformational changes. Therefore, in order to evaluate the contribution of each individual amino acid in the N-terminal cytotoxicity region of rCPE, single alanine substitutions were introduced into residues D45 to E54 in the fully-toxic rCPE background using the QuikChange[®] Kit (see Section 2.2.1). All mutations were confirmed by nucleotide sequencing of both strands of the mutated *cpe* gene, and affinity enrichments of the resultant variants were assayed for their CPE activities.

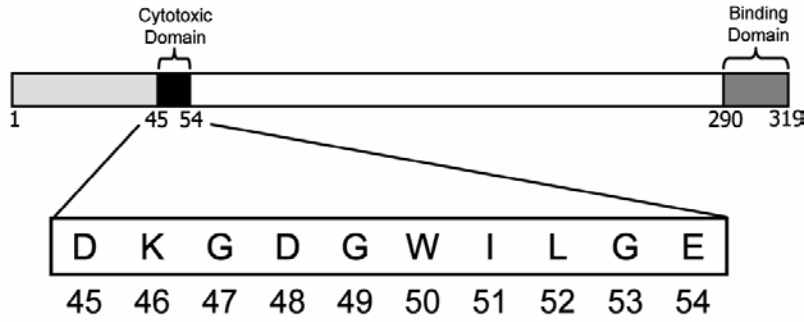


Figure 3.1 Map of the N-terminal cytotoxicity region targeted for site-directed mutagenesis in this study. Copyright © 2007, the American Society for Microbiology. All rights reserved.

3.1.1.2 Morphologic damage of Caco-2 cells by alanine variants of rCPE

Because Caco-2 cells express several CPE-binding claudins (166), they quickly develop cellular morphologic alterations (membrane blebbing, nuclear condensation, detachment from plating surface) when treated with rCPE. Thus, these cells were utilized in the present study to screen the generated rCPE alanine variants for cytotoxicity. Caco-2 monolayers treated for 1 h with rCPE developed typical changes in cell morphology (Fig. 3.2). In contrast, no detectable damage was observed in monolayers treated for 1 h with HBSS²⁺ alone or HBSS²⁺ containing the pTrcHis A mock affinity enrichment negative control. Damage to Caco-2 cell monolayers was readily apparent when all affinity-enriched, alanine-substituted rCPE variants were used except for D48A and I51A (Fig. 3.2). This observation gave early indications that these two N-terminal CPE residues are critical for cytotoxicity.

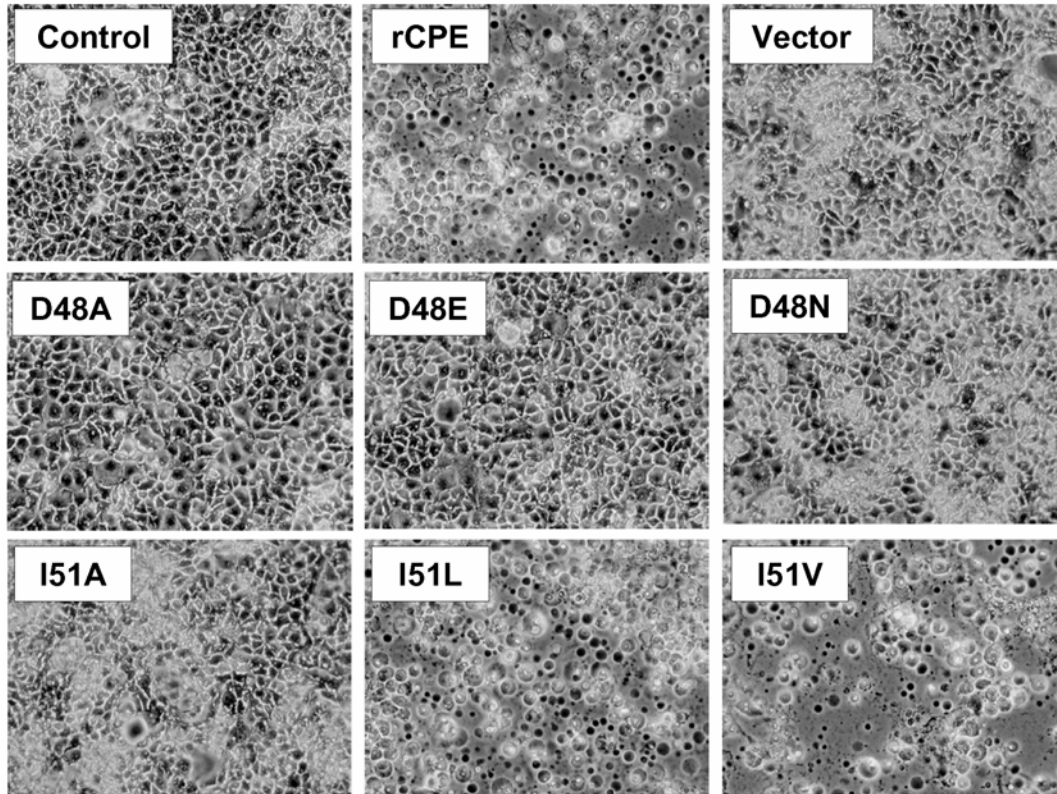


Figure 3.2 Caco-2 morphologic damage assay. Inset boxes represent toxin preparation used to treat Caco-2 monolayers for 1 h at 37°C. Final magnification of photomicrographs is 200×. Copyright © 2007, the American Society for Microbiology. All rights reserved.

3.1.1.3 Analysis of pore-formation by the alanine-substituted rCPE variants

Amino acids 45-53 in CPE have been previously demonstrated to be required for inducing the plasma membrane permeability alterations responsible for CPE-mediated cytotoxicity (93). Therefore, it was appropriate to assay our collection of single alanine variants of this region for their abilities to induce pore-formation in Caco-2 cells with ^{86}Rb -release experiments. Consistent with the morphologic damage screening results (Fig. 3.2), D48A and I51A were the only rCPE alanine variants that exhibited substantially reduced abilities to cause ^{86}Rb -release from Caco-2 cells (Fig. 3.3A, Table 3.1). Even at 50 $\mu\text{g/ml}$, D48A elicited no detectable ^{86}Rb

release from Caco-2 cells, while I51A induced only slight quantities of release (~35% of maximal release) at this very high toxin concentration (Fig. 3.3A). These findings indicate that the D48A and I51A variants are >160-fold less active than rCPE in this assay. All remaining rCPE alanine variants were able to elicit wild-type levels of ^{86}Rb release from cells (Table 3.1), consistent with the Caco-2 morphologic damage results (Fig. 3.2).

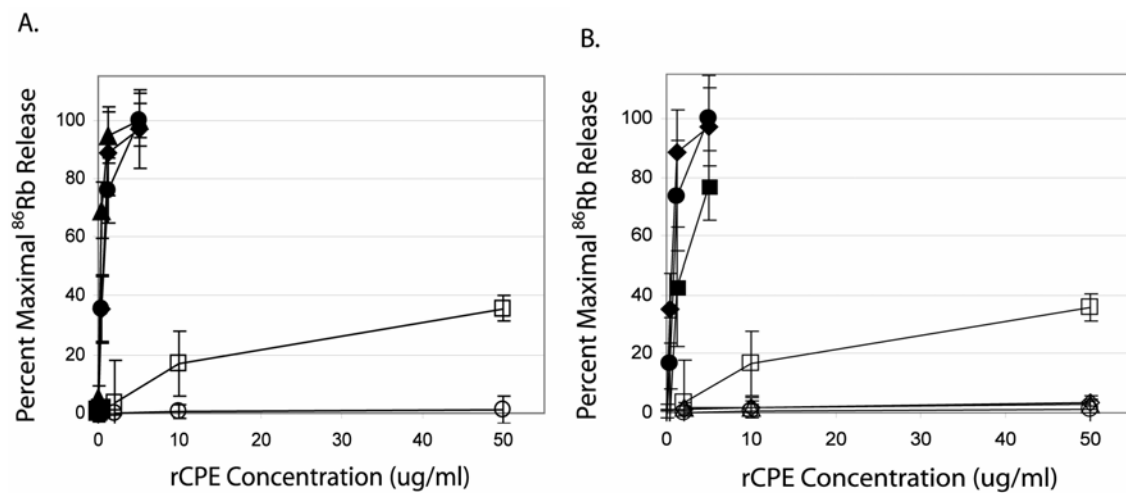


Figure 3.3 Assessment of pore-formation by rCPE variants using the ^{86}Rb -release assay. Caco-2 cells labeled with ^{86}Rb were treated with the indicated concentration of toxin. Efflux of ^{86}Rb is expressed in this figure as percent maximal ^{86}Rb release. Toxin preparations depicted in A are: rCPE (◆), D45A (▲), D48A (○), I51A (□), L52A (●). Depicted in B are ^{86}Rb -release experiments with rCPE saturation variants including: rCPE (◆), D48A (○), D48E (△), D48N (◇), I51A (□), I51L (●), I51V (■). All data points represent means of three independent experiments and error bars represent the standard deviation. Copyright © 2007, the American Society for Microbiology. All rights reserved.

Table 3.1 Summary of rCPE variant phenotypes

rCPE species	Concentration needed for 50% Maximal ⁸⁶ Rb release (µg/ml)	Concentration needed for 50% ¹²⁵ I-CPE binding inhibition (µg/ml)	Small complex formation	Large complex formation
rCPE	0.57 ± 0.19	3.69 ± 0.52	+	+
D45A	0.24 ± 0.04	1.83 ± 0.54	+	+
K46A	0.82 ± 0.07	2.89 ± 0.86	+	+
G47A	0.92 ± 0.63	5.52 ± 0.52	+	+
D48A	>50	3.31 ± 0.78	+	-
G49A	0.83 ± 0.23	2.45 ± 0.59	+	+
W50A	1.35 ± 0.64	4.13 ± 0.90	+	*
I51A	>50	2.59 ± 0.16	+	-
L52A	0.68 ± 0.21	1.45 ± 0.04	+	+
G53A	0.52 ± 0.15	3.20 ± 0.74	+	+
E54A	0.38 ± 0.19	2.47 ± 0.56	+	+
D48E	>50	1.92 ± 0.05	+	-
D48N	>50	2.21 ± 0.16	+	-
W50Y	0.65 ± 0.4	2.68 ± 0.45	+	+
W50F	0.9 ± 0.2	2.60 ± 1.41	+	+
I51L	0.9 ± 0.3	3.23 ± 0.18	+	+
I51V	1.6 ± 1.2	2.82 ± 0.57	+	+

*The W50A variant produces an atypical large complex (Fig. 3.6)

3.1.1.4 Competitive binding ability of the rCPE alanine variants

To determine why the D48A and I51A rCPE variants exhibit attenuated cytotoxicity, the ability of the rCPE alanine variants to perform early steps in CPE action was assessed. Initial interactions between CPE and claudins represent the first step in CPE action, receptor binding (reviewed in Section 1.3.3.1). Since previous structure-function analyses have mapped receptor binding activity of CPE to its C-terminal domain (Fig. 1.12; (93)), the introduction of alanine substitutions in the N-terminal amino acids 45-54 was not expected to affect binding activity. Using a well-established BBM competitive binding assay (92, 93, 117, 136, 190, 232, 233) that measures the ability of an rCPE species to inhibit binding of ¹²⁵I-labeled native CPE to BBMs, this expectation was confirmed. As can be seen in Table 3.1, all alanine-substituted rCPE variants generated in this study had similar ability as rCPE to inhibit ¹²⁵I-CPE binding to BBMs, including the attenuated variants D48A and I51A (Fig. 3.4). The previously-identified W226Stop point variant of rCPE (92) failed to inhibit ¹²⁵I-CPE binding to BBMs as expected (Fig.

3.4), further verifying the functionality of the BBM competitive binding assay. Collectively, these binding activity results support previous studies of the enterotoxin indicating that its N-terminus is not involved in binding (57, 65-68, 78, 93, 113, 136). This implies that D48 and I51 of the CPE are important for some post-binding step in CPE action.

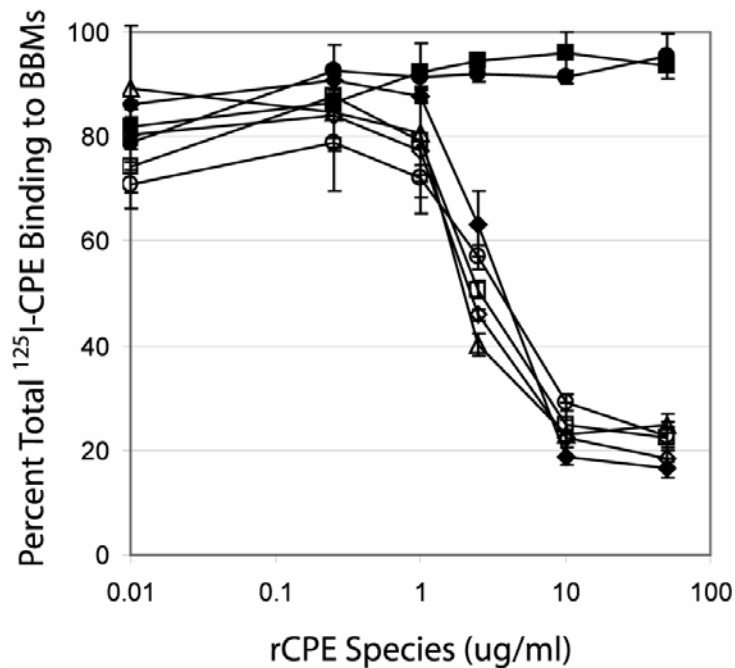


Figure 3.4 Competitive binding analysis of rCPE variants. BBMs were pre-incubated with the indicated concentrations of each rCPE species before incubating with ¹²⁵I-CPE. rCPE species depicted above are: rCPE (◆), D48A (○), D48E (△), D48N (◊), I51A (□), W226Stop (■), pTrcHis A empty vector (●). Data points represent the average of duplicate independent experiments run in triplicate, and error bars represent the standard deviation. Copyright © 2007, the American Society for Microbiology. All rights reserved.

3.1.1.5 Small complex formation by the rCPE alanine variants

Upon binding to sensitive cells, CPE can initially be localized in an SDS-sensitive complex of ~90 kDa (229, 231) that likely represents CPE bound to its receptor (reviewed in Section 1.3.3.2). It was expected, therefore, that the ability of the alanine rCPE variants to form small complex would parallel their binding activities (Fig. 3.4, Table 3.1). When each rCPE variant species generated in this study was used to treat BBMs at 4°C (to prevent formation of large complex (117)), all variants were able to form the small complex (see Fig. 3.5 for a representative experiment). Although the temperature used in these experiments is typically inhibitory for large complex formation, limited amounts of the large complex was still observed using active rCPE species (note the immunoreactive material migrating above the small complex in the rCPE lane of the blot in Fig. 3.5). Interestingly, no large complex formation was apparent in lanes containing extracts from BBMs similarly treated with the D48A or I51A variants (Fig. 3.5).

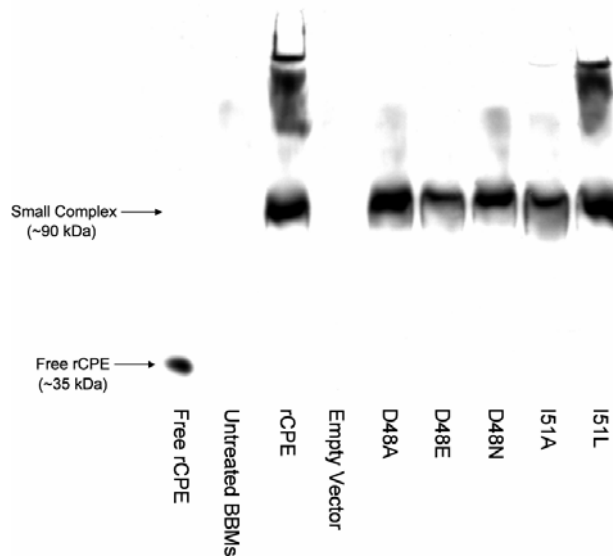


Figure 3.5 Small complex formation by rCPE variants. BBMs were treated with 2.5 µg/ml of the indicated rCPE species before washing and extraction with Triton X-100. Complexes were then separated on a 6% acrylamide native PAG and Western blotted for CPE. Copyright © 2007, the American Society for Microbiology. All rights reserved.

3.1.1.6 Large complex formation by the rCPE alanine variants

As described in detail above, CPE treatment of cells at physiological temperatures results in the formation of two large, SDS-resistant complexes in Caco-2 cells (186, 232) which are likely CPE pores (or subunits thereof). When experiments were performed to analyze the large complex forming ability of each alanine rCPE variant prepared in this study, several intriguing observations were made. The most significant result was that the completely non-cytotoxic D48A variant (Fig. 3.2 & 3.3) forms no detectable amount of SDS-resistant, high molecular mass material, while the highly attenuated I51A variant forms only small amounts of the classic ~155 and ~200 kDa CPE complexes (Fig. 3.6). These observations extend previous findings (117) that development of cytotoxicity (Fig. 3.2) and pore-formation (Fig. 3.3) correlates with (and is proportional to) the ability to form the large complexes (Fig. 3.6). Agreeing with this idea were the observations that all rCPE alanine variants eliciting ^{86}Rb -release levels comparable to rCPE (Table 3.1, Fig. 3.3A) could also form SDS-resistant, large complexes (Fig. 3.6).

The large complex phenotypes of several active rCPE alanine variants differed qualitatively and quantitatively from the classical ~155 and ~200 kDa CPE complexes formed by rCPE. For example, rCPE variants G47A and G49A produced appreciable levels of the standard ~155 and ~200 kDa CPE complexes, but each formed additional immunoreactive material even higher in molecular mass (Fig. 3.6). In contrast, W50A (which is only slightly attenuated in ^{86}Rb -release experiments (Table 3.1)), made very little ~155 kDa CPE complex despite forming some immunoreactive material of roughly similar size as the ~200 kDa large complex produced by rCPE (Fig. 3.6). Also, substantially greater amounts of immunoreactive material were present at (or near) the dye front of lanes of W50A-treated Caco-2 cells compared with rCPE-treated cells (Fig. 3.6).

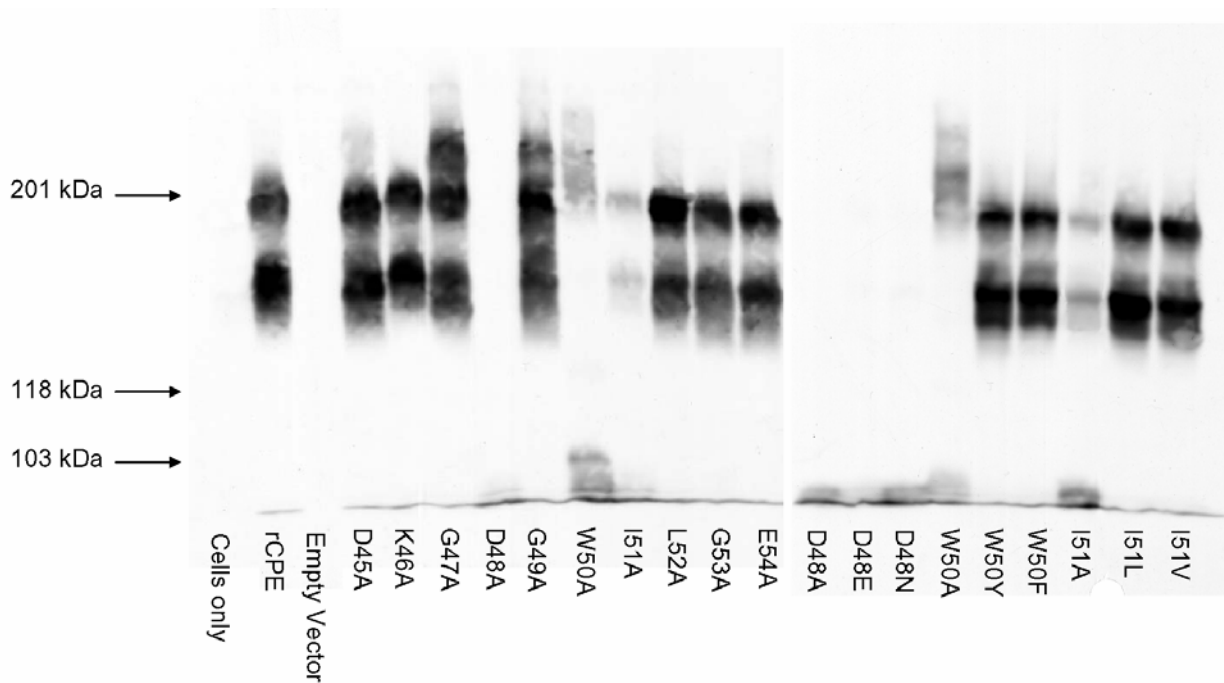


Figure 3.6 Formation of the SDS-resistant large complexes by rCPE variants. Isolated Caco-2 cells were treated with the indicated toxin for 45 min at 37°C. After washing, cells were lysed with Laemmli buffer and separated on a 4% acrylamide SDS-PAGE before Western blotting for CPE. Copyright © 2007, the American Society for Microbiology. All rights reserved.

3.1.1.7 Analysis of gross conformational changes in rCPE alanine variants

The above results indicated that the D48A and I51A rCPE variants are highly attenuated at cytotoxicity due to an impaired ability to form the large complexes. To address whether these variants lost their activity because of gross conformational changes induced by the alanine substitutions, limited trypsin proteolysis was performed. As described previously (92), the rCPE protein normally exposes only a few of the 24 trypsin digestion sites present in its primary amino acid structure. Misfolded rCPE variants have more sites exposed and thus are more sensitive to limited digestion with trypsin.

With the exception of an initial affinity-enrichment batch of W50A, all rCPE variants prepared in this study displayed similar trypsin digestion patterns as rCPE (a representative blot

is shown in Fig. 3.7). These results suggest that the attenuation of the D48A and I51A rCPE variants is specifically due to the loss of the native amino acid at D48 and I51, rather than from gross conformational changes occurring in those two rCPE variants. As mentioned, the first affinity-enrichment preparation of the W50A rCPE variant was nontoxic and displayed a trypsin digestion pattern suggestive of a substantially misfolded protein (Fig. 3.7, W50A¹). Therefore, this inactive batch of W50A served as a control, verifying the ability of the trypsin proteolysis assay to detect misfolded rCPE. Note that all subsequent affinity-enrichment preparations of W50A displayed a trypsin digestion pattern similar to that of rCPE (Fig. 3.7.; W50A²). Those later W50A preparations were also active for receptor binding, small and large complex formation, morphologic damage and ⁸⁶Rb release (Table 3.1).

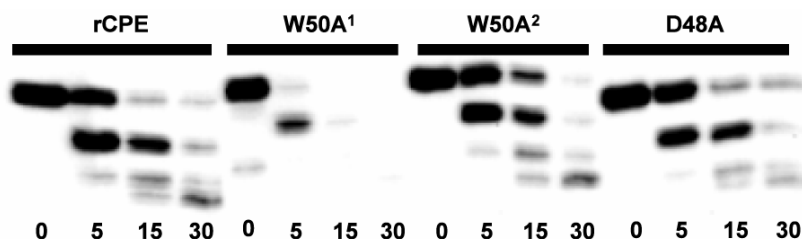


Figure 3.7 Limited trypsin proteolysis of rCPE variants. Four hundred ng of the indicated toxin preparation was digested with trypsin for the indicated time period at 37°C. Reactions were heat-terminated and then separated on a 10% acrylamide SDS-PAG and Western blotted for CPE. Copyright © 2007, the American Society for Microbiology. All rights reserved.

3.1.2 Saturation mutagenesis of residues important for CPE action

Alanine-scanning mutagenesis above identified that CPE residues D48 and I51 were important for CPE toxicity (Figs. 3.2 & 3.3). In addition, the W50 residue of CPE appears to play a

structural role for the protein, given the batch-to-batch variation in protein folding and activity observed with the W50A rCPE variant (Figs. 3.6 & 3.7). Therefore, these three CPE residues were subjected to saturation mutagenesis to evaluate which biochemical properties are important at these positions for CPE function. These additional studies involved introducing more conservative substitutions at each of the three amino acids using the QuikChange[®] kit (see Section 2.2.1) to produce the rCPE variants D48E, D48N, W50F, W50V, I51L, and I51V (Table 3.1). All saturation mutations were confirmed by nucleotide sequencing, and each saturation rCPE variant was expressed in *E. coli* for subsequent affinity-enrichment as described earlier.

3.1.2.1 Non-alanine substitutions at D48

The D48A rCPE variant was the only alanine-substituted rCPE lacking any detectable cytotoxic activity, even using extremely high concentrations (Table 3.1, Figs. 3.2, 3.3A, & 3.6). In addition, this variant exhibited no gross conformational changes (Fig. 3.7) and had wild-type binding and small complex activities (Figs. 3.4 & 3.5), indicating some property of this aspartic acid residue is specifically important for formation of the SDS-resistant, large CPE complexes. To determine whether side chain size or charge was important for toxicity at CPE amino acid 48, the rCPE variants D48E and D48N were engineered and tested for cytotoxicity. These rCPE saturation variants both failed to elicit any morphologic damage (Fig. 3.2) or ⁸⁶Rb release from Caco-2 cells even at 50 µg/ml (Fig. 3.3B), matching earlier results observed with the D48A rCPE variant. Also resembling the D48A rCPE variant, the D48E and D48N rCPE variants could bind and form the SDS-sensitive small complexes in Caco-2 cells (Figs. 3.4 & 3.5), but both variants were unable to form either of the two SDS-resistant large complexes made by rCPE (Fig. 3.6), explaining their lack of cytotoxicity in the Fig. 3.3B ⁸⁶Rb-release experiments.

3.1.2.2 Non-alanine substitutions at I51

Activity characterization studies above show that the I51A rCPE variant is highly attenuated, but maintains a small amount of cytotoxic activity (Table 3.1, Figs. 3.3A & 3.6A). Therefore, conservative mutations were engineered into rCPE at this amino acid residue to determine whether restoring the aliphatic hydrocarbon side chains at this residue would be sufficient to regain wild-type levels of toxicity. The resulting variant rCPE species, I51L and I51V, displayed the same cytotoxicity as rCPE in the Caco-2 cell morphology and ^{86}Rb release assays (Figs. 3.2 & 3.3B). Consistent with that observation, both rCPE saturation variants also had unimpaired receptor binding activity (Table 3.1), formed small complex (Fig 3.5 & Table 3.1), and formed the classic ~155 and ~200 kDa large complexes (Fig. 3.6). In addition, both I51L and I51V displayed normal trypsin digestion patterns indicating that they, like I51A, lack gross conformational changes.

3.1.2.3 Non-alanine substitutions at W50

Because the W50A variant displayed several interesting phenotypes (Figs. 3.6 & 3.7), conservative substitutions more closely resembling the tryptophan residue were engineered at CPE amino acid 50. CPE activity characterization revealed that the resulting W50Y and W50F variants were fully active. Not only did W50Y and W50F bind and form normal amounts of small complex, these rCPE variants were highly toxic toward Caco-2 cells and could form functional pores (Table 3.1). While the W50A rCPE variant formed an atypical large complex species similar in size to the ~200 kDa complex made by rCPE, the rCPE saturation variants W50Y and W50F both formed the classic ~155 and ~200 kDa large complexes (Fig. 3.6).

3.1.3 Correlation between *in vitro* cytotoxicity and *in vivo* enterotoxicity

The results described above, as well as several previous studies (65-68, 92, 93, 190), have analyzed structure-function relationships largely using *in vitro* models for CPE action. While insights gained from these works have greatly aided understanding the early molecular events of CPE action against mammalian cells, it remains unknown whether these same structure-function relationships also extend to *in vivo* gastrointestinal disease. For example, it is possible that structural elements of CPE found to be important for cytotoxicity for Caco-2 cells may be irrelevant for action at the enterotoxic level. In efforts to establish a correlation between findings made in our *in vitro* models of CPE action and an *in vivo* model of CPE gastrointestinal disease, the rabbit ileal loop model was used to test the activities of several rCPE constructs generated in the present and previous studies.

3.1.3.1 Fluid accumulation in the rabbit ileal loop model

The rCPE point variant D48A was clearly shown in the above experiments to completely lack cytotoxic activity (Figs. 3.2, 3.3, & 3.6), despite maintaining full ability to bind (Fig. 3.4) and form small complex (Fig. 3.5). In addition, a previously-described rCPE fragment containing only residues 168-319 (rCPE₁₆₈₋₃₁₉) has been shown to fully maintain binding activity but lack the ability to form large complex or be cytotoxic (93). These two constructs were affinity-enriched and assayed for their ability to elicit fluid accumulation in rabbit ileal loops. In these same experiments, native CPE and full length wild-type rCPE served as positive controls, while pTrcHis empty vector mock affinity enrichments served as a negative control.

When affinity-enriched samples of these constructs were injected into rabbit ileal loops and incubated for 6 h, a large degree of fluid accumulation was observed in loops treated with rCPE or CPE (Fig. 3.8). Histopathological scoring of rCPE or CPE-treated tissue demonstrated

severe mucosal damage involving necrosis and destruction of the superficial epithelium and lamina propria (Table 3.2 & Fig. 3.9). Villus blunting and fusion was also noted with rCPE or CPE-treated loops, along with hemorrhaging and minimal neutrophilic infiltrate. On the contrary, rabbit ileal loops treated with affinity enrichments of D48A or rCPE₁₆₈₋₃₁₉ lacked any significant fluid accumulation and resembled loops treated with the pTrcHis or Ringer's only negative controls (Fig 3.8). In addition, these rCPE variant constructs were unable to cause the histopathologic response seen with treatment with CPE or rCPE (Table 3.2 & Fig. 3.9).

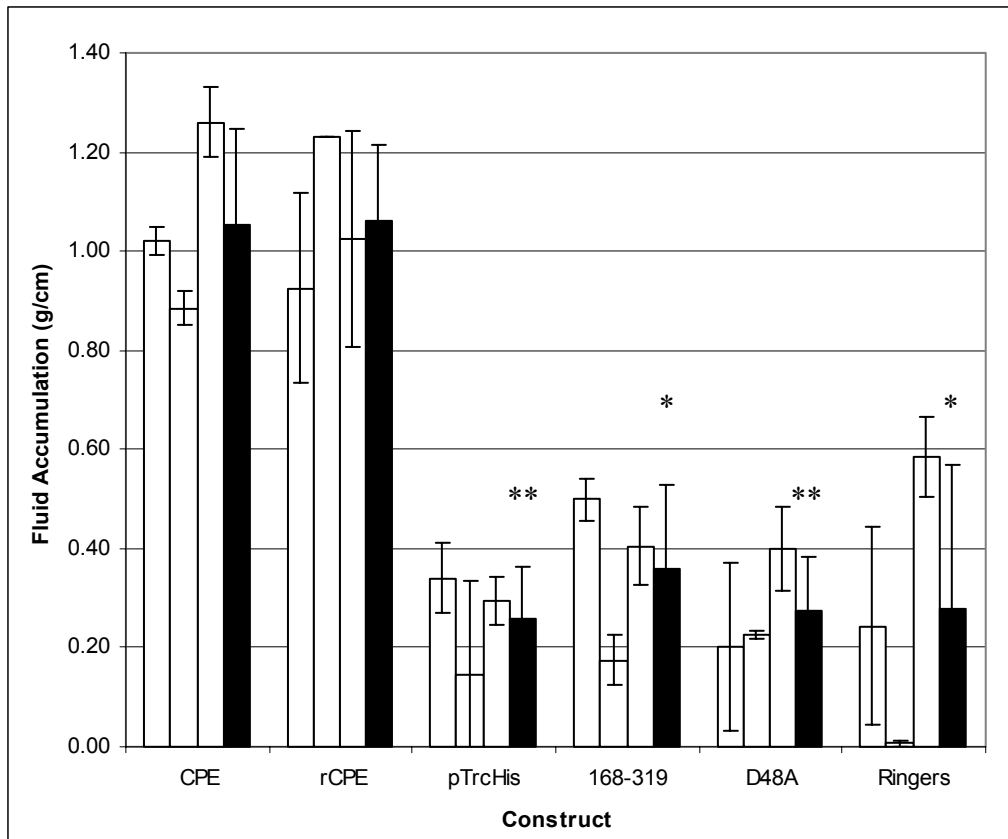


Figure 3.8 Fluid accumulation in rabbit ileal loops treated with rCPE constructs. White bars for each construct are the averages of experimental duplicates in one rabbit, while black bars for each construct represent averages of all biological replicates. * represents $p = <0.05$, ** represents $p = <0.005$.

Table 3.2 Gross histology scores of rabbit ileal loops treated with the indicated constructs.

	Desquamation of epithelium	Necrosis of epithelium	Necrosis of lamina propria	Inflammation	Dilated lymphatics	Edema	Mucus in lumen	Villus blunting	Serosal inflammation
CPE (1)	+++++	+++++	+++++	+++	++	+++	-	+++++	++
CPE (2)	+++++	+++++	+++++	+++	++	+++	-	+++++	++
rCPE (1)	+++++	+++++	+++++	+++	++	+++	-	+++++	++
rCPE (2)	+++++	+++++	+++++	+++	++	+++	-	+++++	++
pTrcHis (1)	-	-	-	-	++	-	-	-	-
pTrcHis (2)	-	-	-	-	++	-	-	-	-
168-319 (1)	-	-	-	-	++	-	-	-	-
168-319 (2)	-	-	-	-	++	-	-	-	-
D48A (1)	-	-	-	-	++	-	-	-	-
D48A (2)	-	-	-	-	++	-	-	-	-
Ringers (1)	-	-	-	-	++	-	-	-	-
Ringers (2)	-	-	-	-	++	-	-	-	-
Ringers (3)	-	-	-	-	++	-	-	-	-
Untreated loop	-	-	-	-	++	-	-	-	-

No significant histological lesions observed the following examined tissues: ileum, colon, kidney, lung, spleen, liver, heart, and brain.

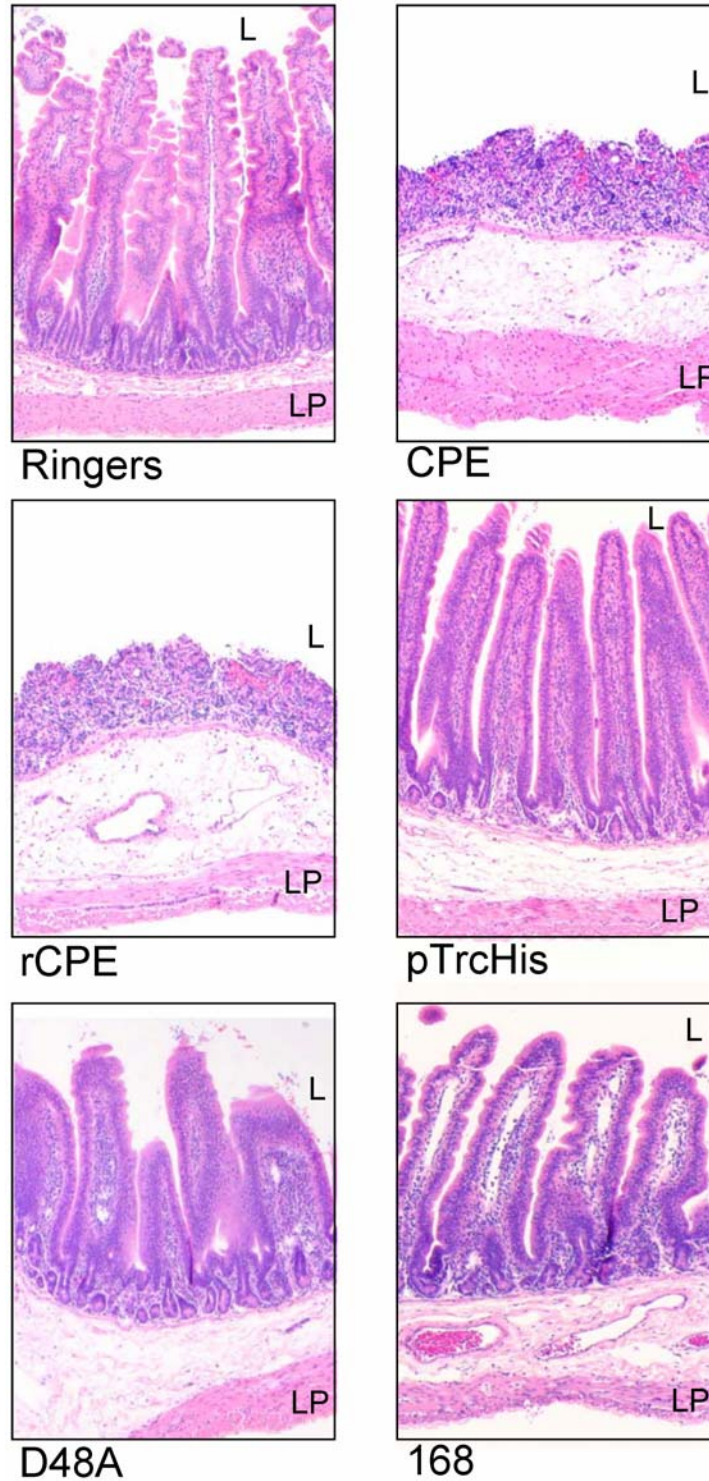


Figure 3.9 Rabbit intestinal loops were treated with 300 $\mu\text{g}/\text{ml}$ of the indicated construct (bottom of panels) for 6 h. The loops were then examined grossly and immersed for 24 h in 10% buffered formalin, pH 7.2. The tissue was processed routinely to produce 4 μm thick histological sections which were stained with hematoxylin and eosin, followed by photomicroscopy at the indicated magnification. Location of lamina propria is denoted with “LP”, while lumen of intestine is denoted with “L” in each photomicrograph. Total magnification is 40 \times .

3.2 SEARCH FOR A MEMBRANE INSERTION DOMAIN IN CPE

3.2.1 Amino acids 81-106 of CPE: a transmembrane stem domain?

As mentioned in the Introduction, CPE shares several structural similarities with pore-forming toxins of the β -PFT family including the presence of a 25 amino acid region (residues 81-106) that strikingly alternates in side chain hydrophobicity (Fig. 3.10). Because similar regions serve as the TMDs for β -PFTs (Fig 1.15-1.17; (158, 207, 214)), and since no CPE region has yet been identified that is involved with membrane penetration, these amino acids were targeted for deletion mutagenesis.

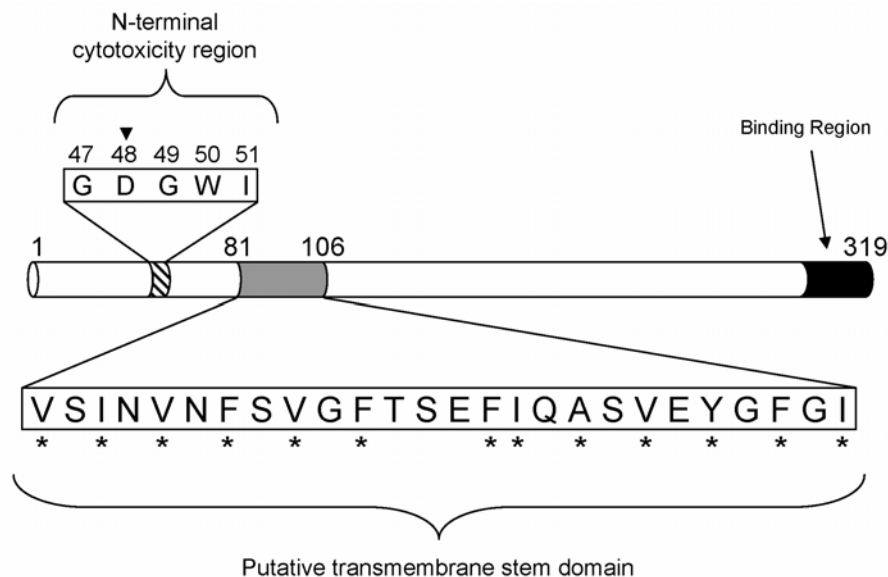


Figure 3.10 A structure-function map of CPE depicting the alternating pattern of hydrophobic (asterisk) and hydrophilic amino acids between residues 81-106. The D48 residue in the N-terminal cytotoxicity region (inverted triangle) is demonstrated in Section 3.1 to be essential for cytotoxicity. Copyright © 2007, the American Society for Microbiology. All rights reserved.

3.2.1.1 Deletion mutagenesis of the putative TMD of CPE

A complete deletion of amino acids 81-106 in CPE was generated using “splicing by overlap extension” PCR (80), which amplifies sequences upstream and downstream from the intended deletion and splices these two products together in a third reaction (see Section 2.2.2). This methodology has also been helpful with other β -PFTs to identify and characterize TMDs (22, 131, 138). The rCPE internal deletion variant generated in this study, named TM1, had a 100% deletion of the CPE 81-106 region (Fig. 3.11A). After DNA sequencing confirmed this mutation, the TM1 variant was affinity-enriched via the N-terminal (His)₆-tag contributed by the pTrcHis A vector. When enriched samples of TM1 were subjected to a CPE Western blot, the variant migrated to its expected molecular mass (Fig. 3.11B).

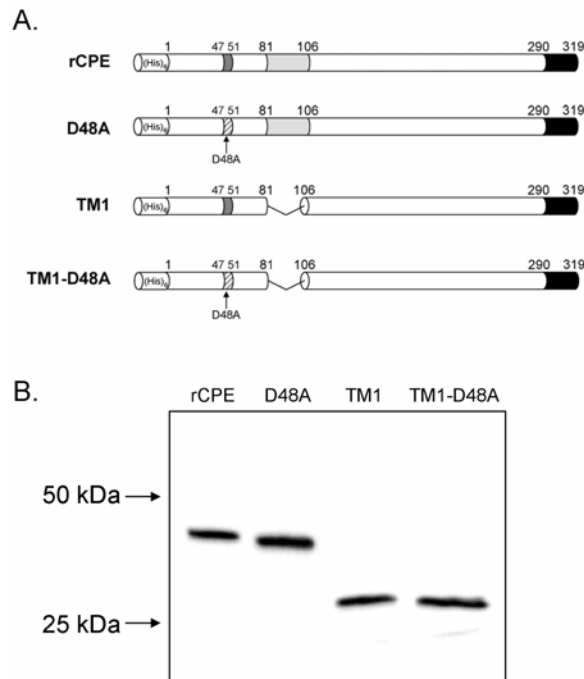


Figure 3.11 A, Constructs used in this study to investigate membrane insertion. B, Fifty ng of the indicated toxin preparations were separated on a 12% acrylamide SDS-PAGE and Western blotted for CPE. Copyright © 2007, the American Society for Microbiology. All rights reserved.

3.2.1.2 Competitive binding analysis of the TM1 deletion variant

Since the receptor binding activity of CPE has been previously mapped to the toxin's C-terminus (57, 65-68, 78, 93, 113, 136), it was expected that the rCPE variants produced in this study should be unimpaired for their binding activity. To confirm this, a competitive binding assay was performed similar to that found in Section 3.1.1.4 that measured the ability of the TM1 deletion variant to inhibit ¹²⁵I-CPE binding to BBMs. Table 3.3 contains a calculated binding inhibition index for each rCPE variant from this Section. Since TM1 had a similar binding index to rCPE, this analysis demonstrated that deletion of amino acids 81-106 does not exert a major effect on receptor binding, and that this TM1 variant can complete the first step in CPE action.

Table 3.3 Binding analysis of constructs in this study

Construct	Inhibition Index*	Standard Deviation
rCPE	330	± 80
pTrcHis A	>20,000	-
W266Stop	>20,000	-
D48A	240	± 30
TM1	410	± 120
TM1-D48A	650	± 40

*ng required to cause a 50% inhibition of ¹²⁵I-CPE specific binding

3.2.1.3 Cytotoxicity of the TM1 deletion variant

To assess whether deletion of the putative transmembrane stem region affects the ability of an rCPE variant to cause cytotoxicity, the Caco-2 morphological damage assay described in Section 3.1.1.2 was used. Treatment of Caco-2 cells with 2.5 µg/ml of rCPE for 1 h caused the development of typical CPE cytopathology, including nuclear condensation, membrane

blebbing, and cellular detachment from the plate (Fig. 3.12). No morphologic damage was observed if Caco-2 cells were treated with HBSS²⁺ alone, an affinity-enriched lysate of empty vector transformants negative control, or (consistent with previous studies (190)) the D48A point variant. Caco-2 monolayers also showed no observable morphologic damage after 1 h of treatment with 2.5 µg/ml of TM1 (Fig. 3.12). These results, along with the competitive binding data in Table 3.3, provided an initial indication that the TM1 variant is deficient in some post-binding CPE activity.

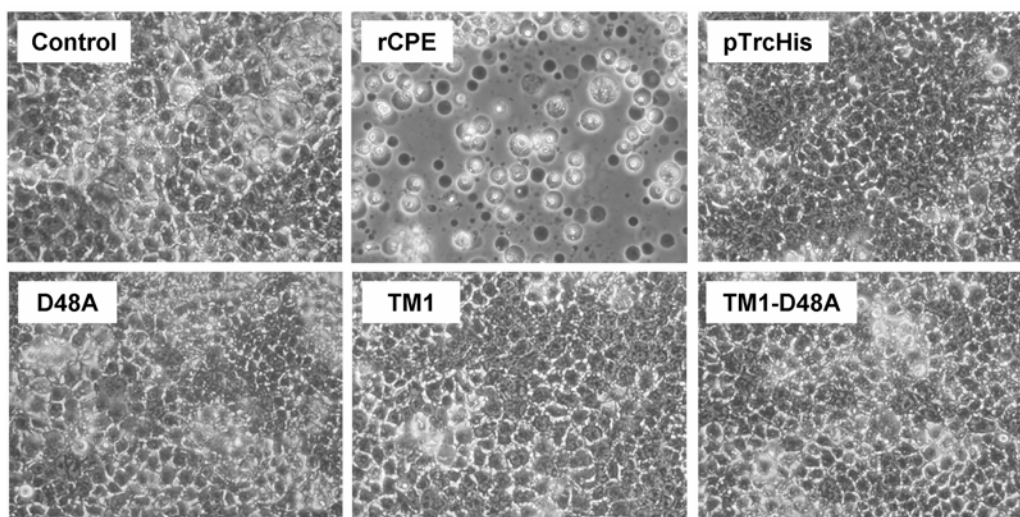


Figure 3.12 Caco-2 morphologic damage assay. Inset boxes indicate which toxin preparation used to treat Caco-2 monolayers for 1 h at 37°C. Final magnification of photomicrographs is 200×. Copyright © 2007, the American Society for Microbiology. All rights reserved.

3.2.1.4 Pore-formation of the TM1 variants

The TM1 deletion variant was next assayed for its ability to elicit ⁸⁶Rb release from Caco-2 cells via formation of a CPE pore, as performed in Section 3.1.1.3. As expected, rCPE was measured to elicit 50% maximal ⁸⁶Rb release at a concentration of ~1.0 µg/ml, while the empty

vector negative control and D48A point variant predictably did not elicit any ^{86}Rb release (Fig. 3.13). When TM1 was similarly tested, it was not able to elicit any appreciable ^{86}Rb release, even at artificially high toxin concentrations (up to 50 $\mu\text{g/ml}$). These results indicate that TM1 is non-cytotoxic to Caco-2 cells because it cannot alter plasma membrane permeability.

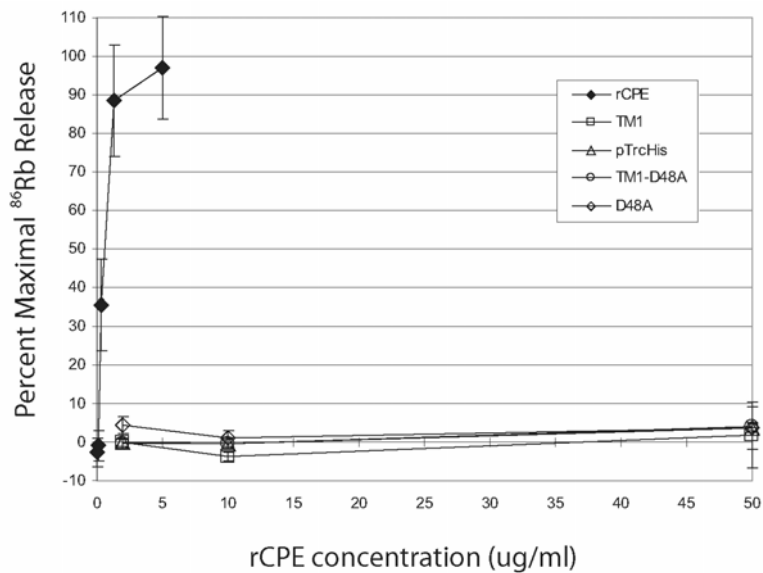


Figure 3.13 Assessment of pore-formation by rCPE variants using the ^{86}Rb -release assay. Caco-2 cells labeled with ^{86}Rb were treated with the indicated concentration of toxin. Efflux of ^{86}Rb is expressed in this figure as percent maximal ^{86}Rb release. All data points represent means of three independent experiments and error bars represent the standard deviation. Copyright © 2007, the American Society for Microbiology. All rights reserved.

3.2.1.5 Formation of SDS-resistant large complexes by the TM1 variant

The data presented above indicated that, despite maintaining receptor binding activity (Table 3.3), TM1 is deficient at inducing cytotoxicity (Figs 3.12 & 3.13). Since CPE cytotoxicity requires the formation of an ~155 kDa, SDS-resistant complex in the membranes of sensitive cells (117), we next to determined whether TM1 can form this complex. Treatment of isolated Caco-2 cells with 2.5 µg/ml of rCPE resulted in the formation of the ~155 kDa large complex, as well as a second ~200 kDa CPE complex (Fig. 3.14), as reported previously (186, 190). Also as shown in Section 3.1, the D48A variant of rCPE did not form either of the two large CPE complexes, although this rCPE variant remains membrane-associated (note the immunoreactivity at the dye front in Fig. 3.14). Interestingly, the TM1 variant was able to form the ~155 kDa large complex, despite its complete loss of cytotoxicity as depicted in earlier figures. The TM1 variant did not, however, form any detectable ~200 kDa complex.

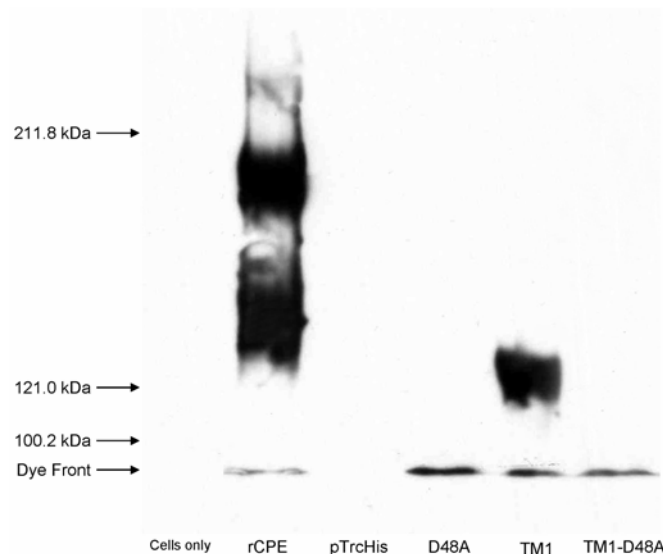


Figure 3.14 Formation of the SDS-resistant large complexes by rCPE variants. Isolated Caco-2 cells were treated with the indicated toxin for 45 min at 37°C. After washing, cells were lysed with Laemmli buffer and separated on a 4% acrylamide SDS-PAGE before Western blotting for CPE. Copyright © 2007, the American Society for Microbiology. All rights reserved.

3.2.1.6 Analysis of the TM1 pre-pore large complex

The ability of the TM1 deletion variant to form the ~155 kDa complex (Fig. 3.14) in the complete absence of cytotoxicity (Fig. 3.12) or pore-formation (Fig. 3.13) led us to investigate whether the TM1 large complex could represent a previously-unidentified pre-pore step in the mechanism of action of CPE. To this end, we examined the integrity of the TM1 large complex in membranes via resistance of the TM1 large complex to proteolytic degradation, dissociation of this complex from membranes, and heat-induced disassembly.

3.2.1.6.1 Pronase resistance of the TM1 large complex

As detailed above in Section 1.3.3.3, CPE in the large complex appears to gain pronase resistance by inserting into the membrane (228). We hypothesized, therefore, that the TM1 large complex might be trapped in a pre-pore stage because it cannot insert into membranes. To test this hypothesis, a pronase resistance assay was performed with TM1 large complex. When isolated BBMs containing ~155 kDa large complex formed by rCPE were digested with 600, 60, or 6 µg/ml of pronase for 5 or 60 min, significant amounts of rCPE large complex remained present in BBMs even after a 60 min treatment with 600 µg/ml of pronase (Fig. 3.15). In contrast, pronase treatment of membranes containing the TM1 large complex caused a nearly complete disappearance of this complex after only a 5 min treatment with 60 µg/ml of pronase. Enhancing these findings is the fact that TM1 samples in Fig. 3.15 deliberately contained ~3-fold more TM1 large complex at the start of the experiment compared to rCPE large complex. These results indicate that the ~155 kDa large complex formed by TM1 is between 10-100 fold more sensitive to pronase digestion than the ~155 kDa large complex formed by wild-type rCPE. This finding is consistent with the TM1 variant forming the ~155 kDa

large complex, but without the putative TMS, the membrane insertion step required for development of pronase resistance is blocked.

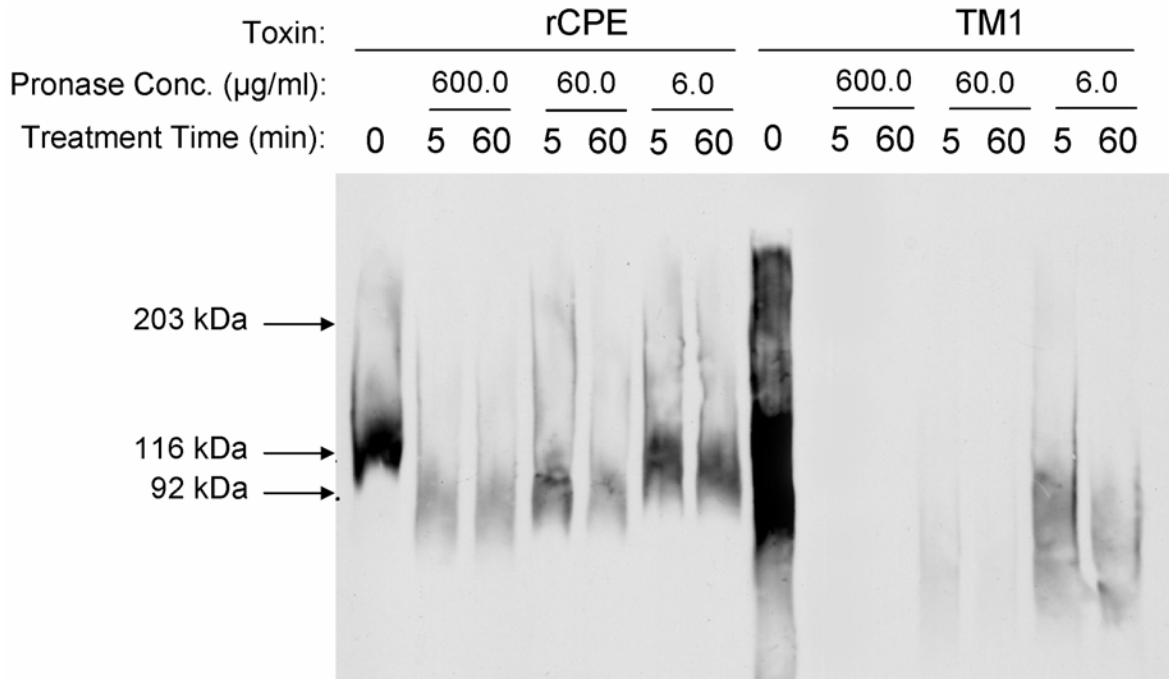


Figure 3.15 Comparative pronase susceptibility of large complexes formed by rCPE and TM1. Large complex formed by rCPE or TM1 was treated with indicated concentration of pronase for the indicated time period. Samples of these reactions were separated on a 6% acrylamide SDS-PAGE and Western blotted for CPE. Copyright © 2007, the American Society for Microbiology. All rights reserved.

3.2.1.6.2 Membrane dissociation of the TM1 large complex

Once sequestered in CPE large complexes, only limited dissociation of CPE from membranes is observed (228). If the ~155 kDa large complex made by TM1 remains trapped on the membrane surface in a pre-pore state, it might be anticipated that this TM1 variant large complex would exhibit faster dissociation from membranes compared to large complex formed by rCPE. To test this hypothesis, isolated BBMs containing the ~155 kDa large complex formed

by either rCPE or TM1 were harvested by centrifugation at the indicated time intervals, and samples from both the supernatants and pellets were Western blotted for CPE. These studies showed that the ~155 kDa large complex formed by rCPE remained largely membrane-associated even after 20 h (Fig. 3.16). In contrast, little of the ~155 kDa large complex formed by TM1 remained membrane-associated after a similar 20 h incubation. A steady kinetic increase in lower molecular mass material accompanied the loss of large complex immunoreactivity in the pellet lanes of the TM1-treated membranes (Fig. 3.16). This smaller complex may be an intermediate from the break-up of the TM1 large complex and is noticeably absent from rCPE-treated membranes.

Overnight film exposures of these blots also allowed the visualization of intact TM1 large complex that had dissociated from the membrane (Fig. 3.16, lanes marked "OE"). Very little (if any) large complex could be detected in similarly overexposed lanes containing rCPE-treated membranes. Because these reactions were performed at 4°C and constantly in the presence of a strong protease inhibitor cocktail, the TM1 large complex instability noted in Fig. 3.16 is unlikely to be the result of proteolytic activity. In support of this, we observed no differences in total protein content between rCPE-, TM1-, or control-treated BBMs after overnight dissociation experiments. Taken together, results from these experiments appear to indicate that the TM1 large complex is overall less stable and more likely to dissociate from membranes compared with large complex formed by rCPE.

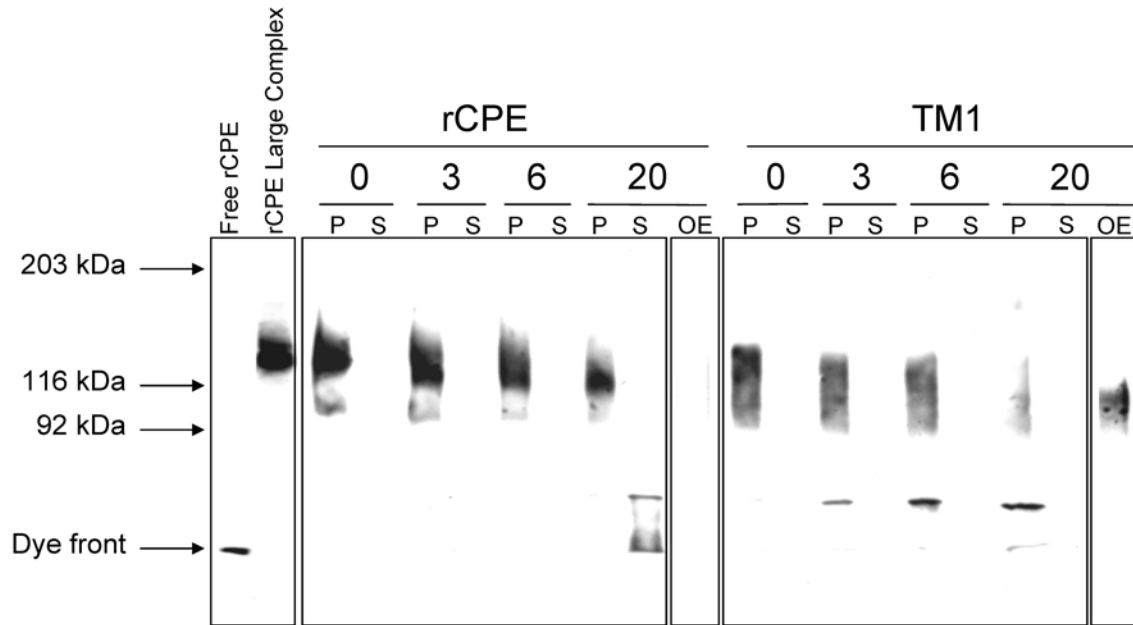


Figure 3.16 Dissociation of the large complexes formed by rCPE and TM1. BBMs were treated with 2.5 $\mu\text{g/ml}$ of the indicated toxin then were incubated at 4°C with constant inversion for the indicated time periods. Reactions were then microcentrifuged and samples of the supernatants and pellets were separated on a 6% acrylamide SDS-PAGE and Western blotted for CPE. Copyright © 2007, the American Society for Microbiology. All rights reserved.

3.2.1.6.3 Heat Denaturation of the TM1 Large Complex

Since the ~155 kDa large complex formed by TM1 appeared from Fig. 3.16 experiments to be less stable and more likely to disassemble, a heat denaturation experiment was performed to test the stability of the TM1 large complex after extraction from membranes. Heating of samples from large complex experiments prior to SDS-PAGE is typically avoided since previous studies have shown that boiling of samples promotes higher order aggregation CPE complexes (232). However, it was of interest to assess the ability of the TM1 large complex to resist disassembly as a result of heating. To perform these experiments, large complex formed by rCPE and TM1 was extracted from BBMs and then heated for 0 sec, 20 sec, 1 min, 5 min, 10 min, or 20 min (Fig. 3.17). While no obvious decrease in rCPE large complex could be seen at 1 min of heating, the TM1 large complex began to show obvious decreases after only 1 min of

heating and was undetectable as a complex past this time point (Fig. 3.17). A qualitative change of the rCPE large complex started to appear at the 5 min time point, however, this immunoreactivity remains as an intact complex in striking contrast to the presence of only free toxin in TM1 lanes at these times (Fig. 3.17). Urea was also included in similar heat denaturation experiments but had no discernable effect on the large complexes formed by either rCPE or TM1.

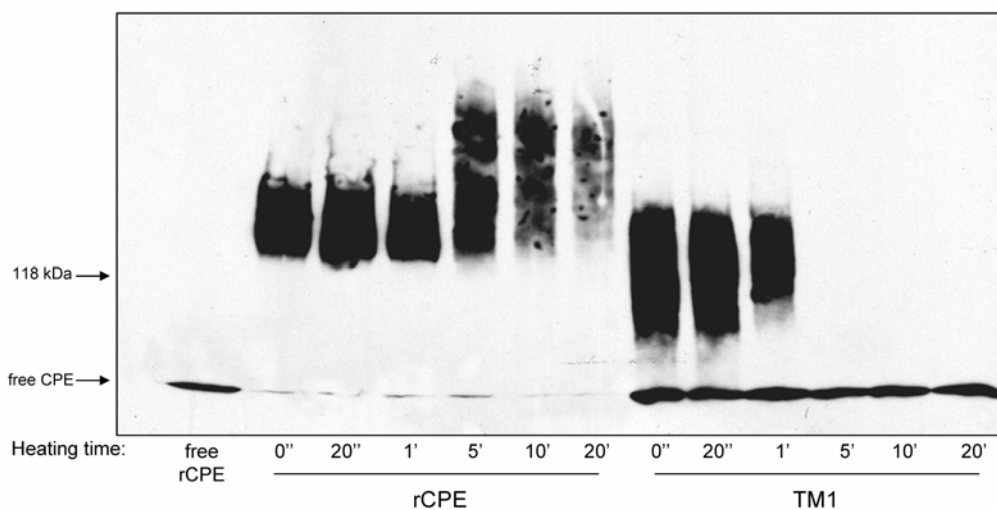


Figure 3.17 Heat denaturation of the CPE large complex. Large complex formed by rCPE and TM1 in BBMs was extracted using Laemmli buffer then heated at 90°C for the indicated time. Samples were then separated on a 4% acrylamide SDS-PAG and Western blotted for CPE. Copyright © 2007, the American Society for Microbiology. All rights reserved.

3.2.2 Temporal questions regarding functional regions of CPE

The non-cytotoxic, pre-pore phenotype of the TM1 deletion variant described above has provided evidence for the importance of amino acids 81-106 in membrane insertion/pore-formation. Still unclear, however, is whether these residues are important before or after other

functional regions of CPE. To aid in identifying the order of involvement of known functional regions of CPE, an additional variant was generated by introducing a point mutation into the TM1 deletion variant background. As demonstrated above in Section 3.1.1, D48 of CPE is a critical residue for forming large complex and cytotoxicity. While the CPE point variant D48A is functional for receptor binding (Fig. 3.4), it does not form large complex (Fig. 3.6) and is unable to alter plasma membrane permeability of Caco-2 cells (Fig. 3.3). Therefore, to determine whether the D48 residue is important before or after the involvement of the putative TMS in CPE, a D48A mutation was introduced into TM1, producing the combination variant TM1-D48A (Fig. 3.11).

3.2.2.1 Activity characterization of TM1-D48A

Both the TM1 and D48A single variants have been shown to be non-cytotoxic for Caco-2 cells, despite being unaltered in receptor binding activities (Fig. 3.4 & Table 3.3). Thus, it was not surprising that the TM1-D48A combination variant mirrored this phenotype by failing to elicit morphological damage to Caco-2 cells (Fig. 3.12) but at the same time maintaining the ability to compete with ^{125}I -CPE for binding (Table 3.3). Also like the single variants, TM1-D48A was unable to cause permeability alterations of Caco-2 cells (Fig. 3.13) indicating it is also deficient at pore-formation. A divergence in the phenotypic similarities with TM1 and D48A single variants appeared when the ability to form large complex was examined. Although the TM1 variant could form the ~155 kDa large complex, the TM1-D48A combination variant was completely deficient at formation of either of the two SDS-resistant large complexes (Fig. 3.14). Since the TM1-D48A large complex phenotype resembles the D48A phenotype, this seems to indicate that formation of the ~155 kDa large complex is directly dependent on the presence of D48, and is independent on amino acids 81-106.

3.3 INVESTIGATING THE OLIGOMERIZATION OF CPE IN THE LARGE COMPLEXES

As mentioned above in Section 1.6.3, several indirect lines of evidence imply that CPE acts as an oligomer. Briefly restated, i.) CPE contains several structural attributes similar to the oligomeric β -PFTs (high β -sheet content (58, 173) and presence of putative TMS (Section 3.2)), ii.) CPE can form functional pores in artificial membranes devoid of other proteins (72), and iii.) large complexes formed by CPE and rCPE differ in apparent molecular mass than the \sim 5 kDa which separate the two toxins alone (186). Contained within this Section is an analysis of oligomerization of CPE in the two large complexes formed by Caco-2 cells. Information gained from CPE's stoichiometry in these complexes prompted the reevaluation of their molecular masses, and additional evidence for CPE's oligomeric nature during action came from the identification of several dominant negative variants of rCPE.

3.3.1 Generation of rCPE molecular mass variants

In order to determine the stoichiometry of CPE in the large complexes, it was first necessary to have two cytotoxic rCPE variants differing significantly in molecular mass. The largest biologically-active construct that currently exists is the full length recombinant CPE (rCPE), which contains all 319 native amino acids of native CPE preceded by a 42 amino acid (His)₆-tag (total molecular mass = 40.0 kDa; Fig. 3.18; (93)). For a small rCPE construct, we used the N-terminal deletion variant, rCPE₃₇₋₃₁₉, which was generated during a previous CPE structure-function study (Figs. 1.12 & 3.18; (93)). Despite the absence of the first 36 amino acids, this rCPE variant has similar binding activity but is 2-3 fold more active than the full-length rCPE (93). To further enhance the molecular mass difference between these two rCPE variants, the 36 amino acid (His)₆-tag on rCPE₃₇₋₃₁₉ was removed with enterokinase (see Section 2.3.2). This

resulted in an rCPE variant (EK-rCPE₃₇₋₃₁₉; total molecular mass = 31.3 kDa; Fig. 3.18) that differed from rCPE by a total of 8.7 kDa.

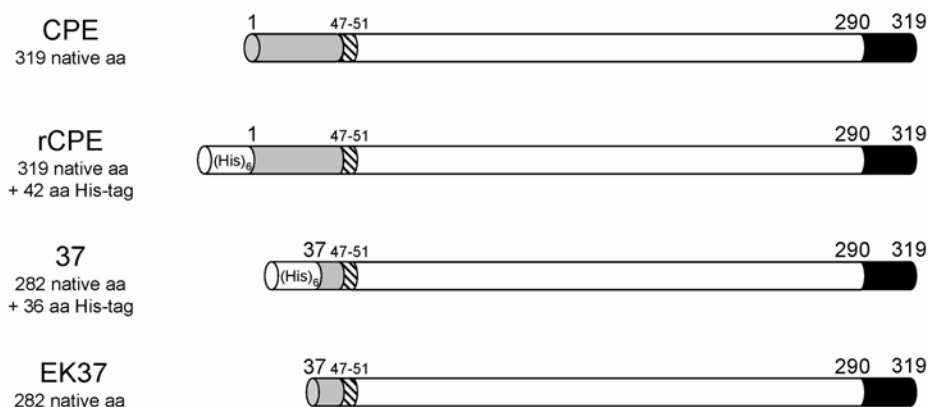


Figure 3.18 Constructs used in this study to investigate the oligomerization of CPE.

3.3.2 Characterization of large complexes made by rCPE molecular mass variants

While the difference in molecular mass between rCPE and EK-rCPE₃₇₋₃₁₉ is readily apparent on a 10% acrylamide SDS-PAGE Western blotted for CPE (Fig. 3.19A), the large complex phenotype of each of these rCPE variants is also strikingly different. When isolated Caco-2 cells were treated with either rCPE or EK-rCPE₃₇₋₃₁₉, both toxin variants formed each of the two CPE large complexes (Fig. 3.19A). The complexes formed by these variants were expected to differ in molecular mass (since the toxins alone differ by ~9 kDa), but the observed degree to which the complexes differed in migration during SDS-PAGE was noteworthy. Compared to the migration of marker proteins on these gels, the “~200 kDa” large complexes formed by the variants had an apparent molecular mass difference of ~38.4 kDa, whereas an ~34.9 kDa difference was calculated for the “~155 kDa” large complexes made by rCPE versus EK-rCPE₃₇₋

319. Since large complexes containing a single copy of each CPE variant should only differ by ~9 kDa (the mass difference between the variants alone), the sizable differences in relative migration shown in Fig. 3.19B provided early indication that CPE is present as some kind of an oligomer in these two complexes. This observation, along with the aforementioned earlier evidence implying CPE may form an oligomeric pore, provided the impetus for pursuing detailed studies of the stoichiometry of CPE in the two large complexes.

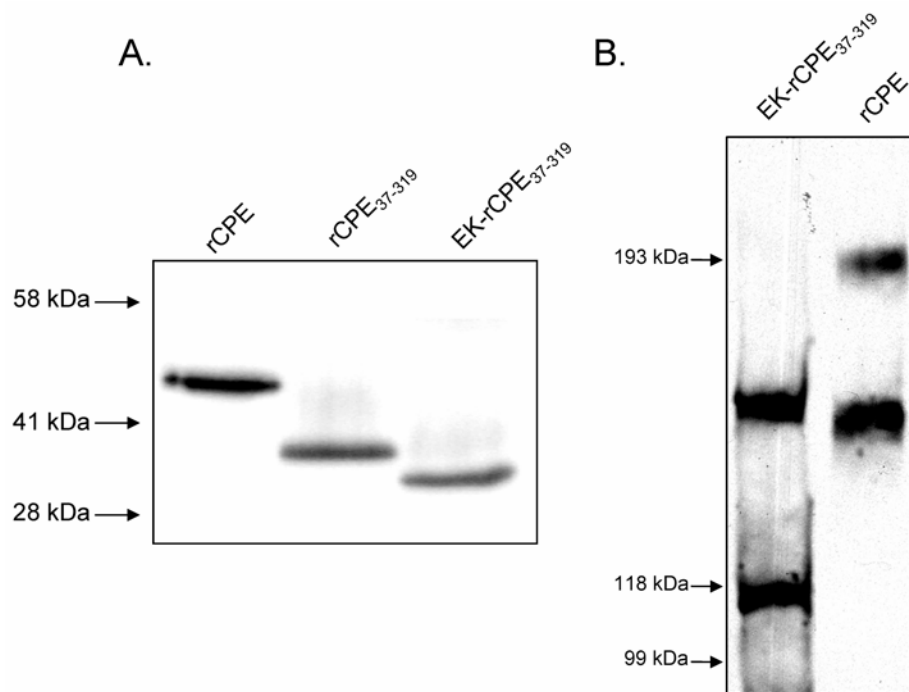


Figure 3.19 A, Fifty ng of the indicated toxin preparations were separated on a 12% acrylamide SDS-PAGE and Western blotted for CPE. B, The large complexes formed by rCPE and EK-rCPE₃₇₋₃₁₉ have drastically different relative migrations when separated on a 4% acrylamide SDS-PAGE and Western blotted for CPE.

3.3.3 Heteromeric CPE large complex gel shift analysis

In order to quantitate the number of CPE subunits present in each of the two large CPE complexes, a heteromer gel shift assay was used. This methodology involves forming heteromeric oligomers with varying ratios of two variants of the same toxin and separating these heteromers electrophoretically. By quantitating the number of different heteromers observed in these gels, the toxin stoichiometry in each oligomer can be deduced. This technique has been successfully used to demonstrate that the pore oligomers of both *S. aureus* alpha hemolysin and *C. perfringens* epsilon toxin have heptameric stoichiometries (56, 143, 144), while the pore oligomers of *V. cholerae* cytotoxin have a pentameric conformation (240). The conclusion from heteromer gel shift analysis that *S. aureus* alpha hemolysin pore is a heptamer was later confirmed when the toxin was crystallized as a heptamer (Fig. 1.16; (192)).

A similar heteromer gel shift analysis was performed with CPE by treating isolated Caco-2 cells with different ratios of rCPE and EK-rCPE₃₇₋₃₁₉ and then analyzing the heteromeric CPE complexes by Western blotting. When using conditions optimal for the formation of the “~155 kDa” large complex, seven individually resolvable complexes were observed (Fig. 3.20A), corresponding to seven different CPE oligomers containing a varying composition of rCPE and EK-rCPE₃₇₋₃₁₉ subunits. This conclusion was confirmed by performing densitometry of these lanes, where seven distinct, individual peaks can clearly be seen among the tracings (Fig. 3.20B). Since five heteromers were observed in Fig. 3.20 (along with two homomers formed by rCPE and EK-rCPE₃₇₋₃₁₉ in the absence of each other), CPE must be in six copies in the “~155 kDa” large complex to account for these results.

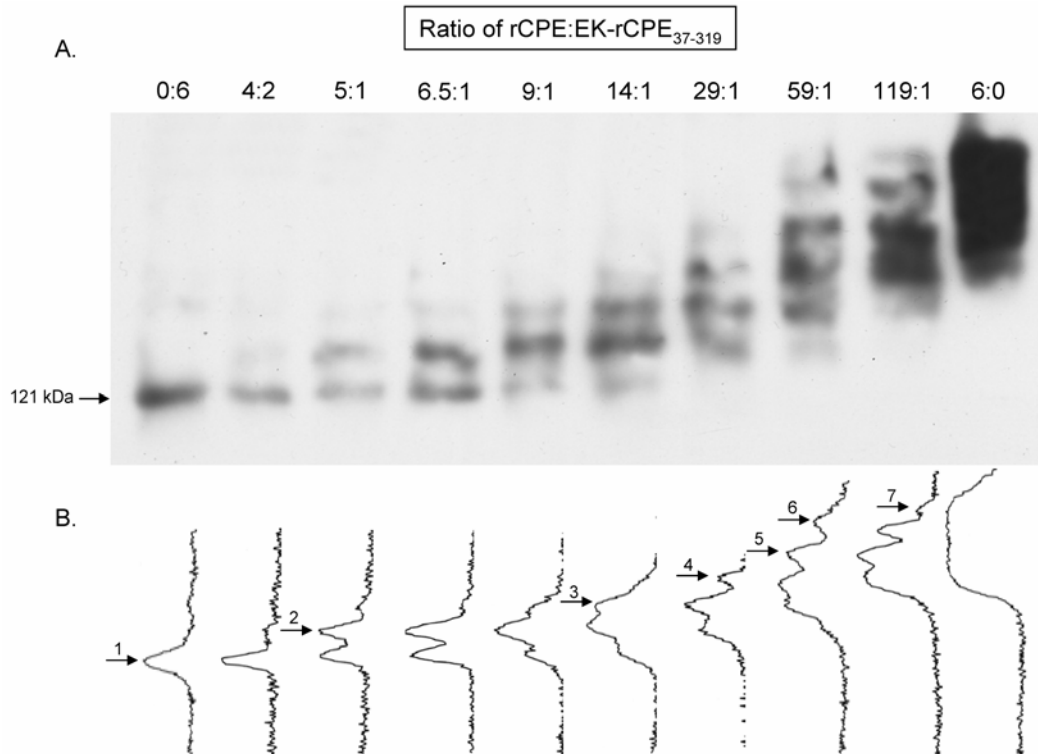


Figure 3.20 Heteromer gel shift analysis of the “~155 kDa” CPE large complex. A, treatment of Caco-2 cells with the indicated ratios of rCPE and EK-rCPE₃₇₋₃₁₉ (tops of lanes) resulted in the formation of seven different oligomeric complexes. B, Densitometric tracings of lanes from the blot in A depicting seven individual peaks.

A similar approach was then used to analyze the stoichiometry of CPE in the “~200 kDa” large CPE complex. Using heteromeric gel shift analysis with conditions optimized for the formation of this complex, seven distinct heteromeric large complex bands were resolved by Western blotting (Fig. 3.21A). Densitometric analysis was also performed on these Western blots, which confirmed the presence of seven individual peaks on these tracings (Fig. 3.21B). Taken together, these data indicate that there are also six copies of CPE in the “~200 kDa” large complex.

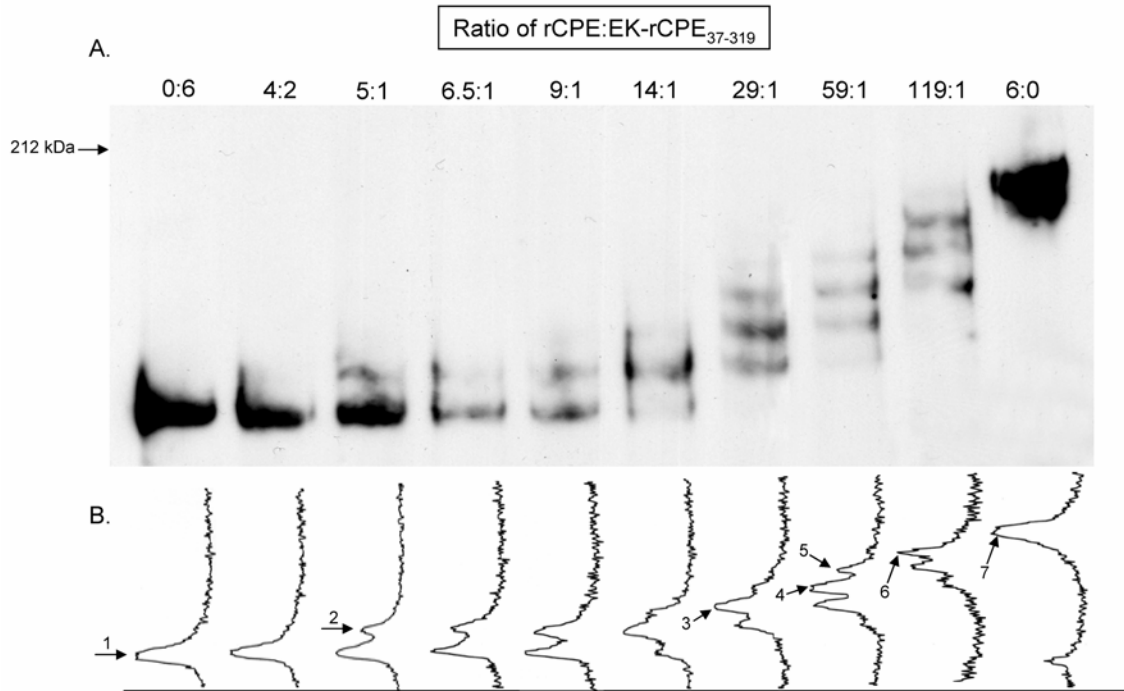


Figure 3.21 Heteromer gel shift analysis of the “~200 kDa” CPE large complex. A, treatment of Caco-2 cells with the indicated ratios of rCPE and EK-rCPE₃₇₋₃₁₉ (tops of lanes) resulted in the formation of seven different oligomeric complexes. B, Densitometric tracings of lanes from the blot in A depicting seven individual peaks.

3.3.4 Reassessment of the molecular mass of the CPE large complexes

Previous studies have suggested the presence of claudin-4 (~20 kDa) in high molecular mass, CPE-containing complexes formed in membranes of CPE-sensitive cells (88). Recent results from our laboratory have conclusively demonstrated the presence of both receptor and non-receptor claudins in the “~155 kDa” and “~200 kDa” large complexes (166). Also, we have previously shown that occludin, an ~65 kDa tight junction protein, is present in the “~200 kDa” large complex (186). The presence of these host proteins in CPE complexes (88, 166, 186), along with the heteromer gel shift results presented above indicating CPE’s hexamerization (Figs. 3.20 & 3.21), made it readily apparent that the ~155 and ~200 kDa molecular masses previously assigned to these two large CPE complexes must be underestimates. The “~155

kDa” large complex must have a molecular mass of at least ~230 kDa (six CPE molecules plus at least one claudin) while the “~200 kDa” large complex must have a molecular mass of at least ~300 kDa (six CPE molecules plus at least one molecule each of claudin and occludin). It is also possible that multiple copies of claudin and/or occludin are present in these complexes, which would even further increase their molecular masses.

Since a discrepancy clearly existed between the predicted molecular masses of the CPE large complexes and their apparent molecular masses when analyzed on SDS-containing, low percentage PAGs (186, 232), we reevaluated the molecular mass of the CPE complexes by altering the acrylamide concentration of SDS-PAGs used for the separation of the CPE large complexes. When SDS lysates of CPE-treated Caco-2 cells were separated using either a 4% or 6% PAG containing SDS, migration of the “~155” and “~200 kDa” large complexes were very different (Fig. 3.22). On the 4% gel, the “~200 kDa” large complex had a relative migration corresponding to a mass of ~180 kDa, while the same complex on the 6% gel migrated with a mass of ~215 kDa. Similarly, the “~155 kDa” large complex was observed to have a relative mass of ~140 kDa on the 4% gel, but exhibited a mass of ~160 kDa on the 6% gel. If the CPE complexes migrated through these gels solely by their molecular masses, their relative migration should not change as the acrylamide percentage of the gels was increased. Since, however, the apparent molecular mass of these complexes was dependent on the gel concentration in Fig. 3.22 experiments, we hypothesized that these complexes were migrating through the acrylamide matrix as tightly compacted, oligomeric structures that mask their actual molecular masses. In efforts to address the discrepancy between the predicted molecular masses calculations versus the apparent molecular masses on SDS-PAG, two alternative approaches were used to reevaluate the molecular masses of these large protein complexes.

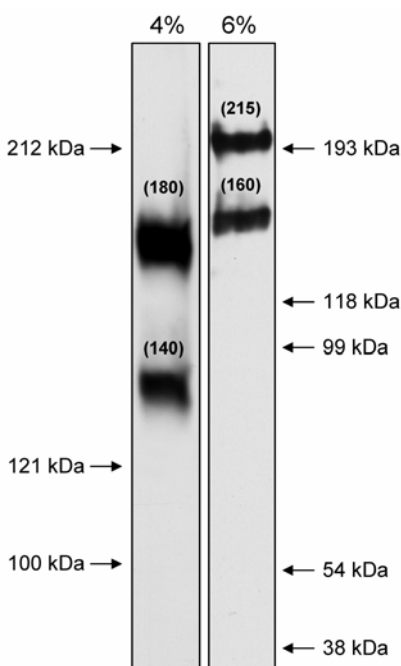


Figure 3.22 Demonstration of the effect of altering acrylamide concentration on the electrophoretic migration of CPE large complexes. Isolated Caco-2 cells were treated with CPE, lysed with Laemmli buffer, then separated on a 4% (left panel) or 6% (right panel) acrylamide SDS-PAGE before Western blotting for CPE. Numbers in parentheses above each complex represent the calculated relative molecular mass in kDa.

3.3.4.1 Ferguson plot analysis of the large CPE complexes

Based on the Fig. 3.22 findings indicating that the relative migration of CPE large complexes demonstrate a dependence on the percentage of acrylamide present in gels, Ferguson plot analysis was employed. By using this methodology, a retardation factor (R_F) is calculated from the degree by which migration of a protein (or protein complex) is retarded as a function of the acrylamide content in a series of native PAGs. By calculating R_F values from known molecular mass standards run through these same gels, a standard curve can be generated and used to calculate the molecular mass of the unknown protein or complex. Relative migrations of the native molecular mass standards from these experiments were determined after Coomassie

brilliant blue staining (Fig. 3.23A, left panel), whereas migration of CPE or CPE large complexes were measured after Western blotting with anti-CPE antibodies (Fig. 3.23A, right panel). This analysis was first performed to calculate the molecular mass of free CPE as verification of the technique. These Ferguson plots yielded a calculated molecular mass of 37.7 kDa for free CPE (Fig. 3.23B & C), which is close to CPE's actual molecular mass of 35.3 kDa.

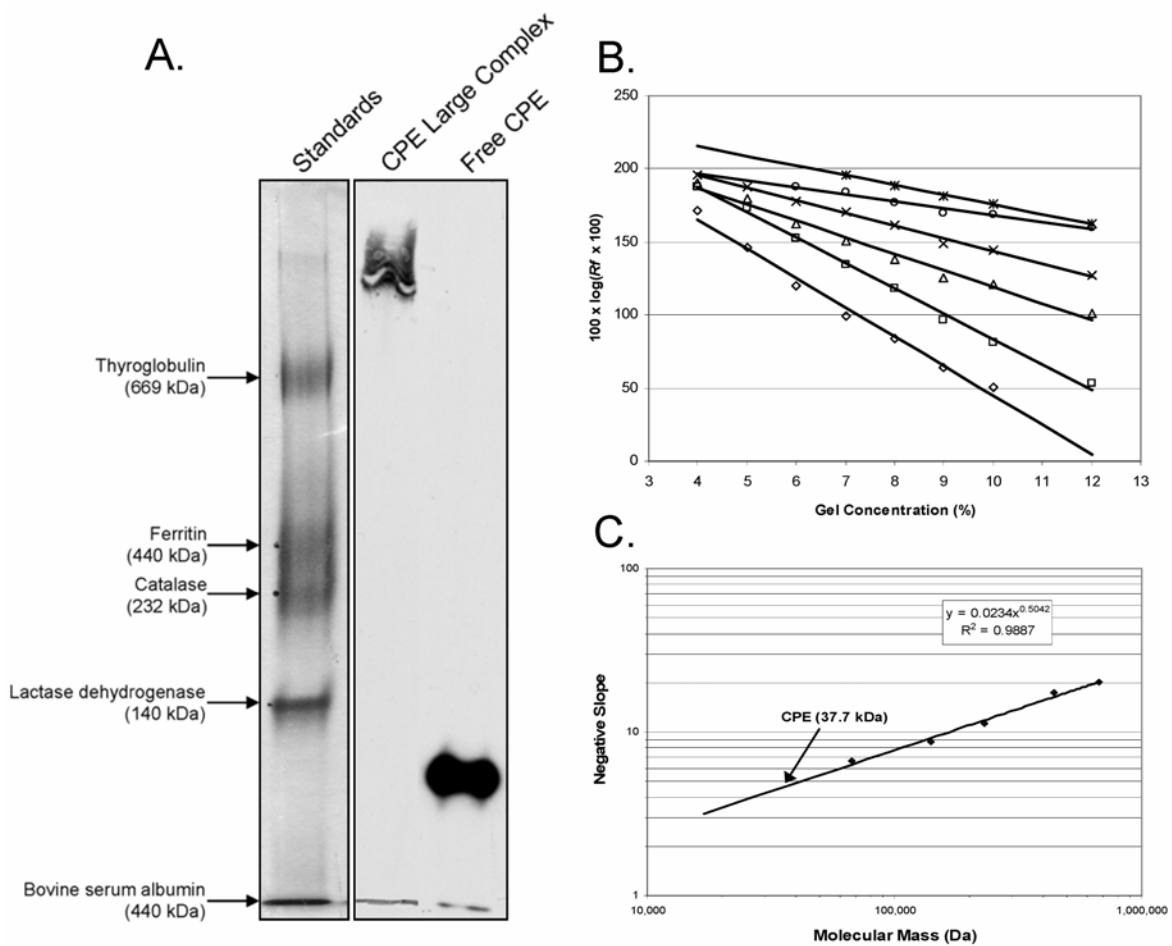


Figure 3.23 Ferguson plot analysis of CPE. A, A representative example of the native PAGs used for Ferguson analysis in this study where lanes containing standards are stained with Coomassie blue (left panel), whereas lanes containing CPE or its complexes are Western blotted (right panel). B, Molecular mass standards and free CPE were separated in a series of native PAGs in this indicated concentrations. C, Negative slopes from curves in B are plotted versus the molecular mass to estimate the molecular mass of free CPE.

The native gel conditions used in Ferguson plot analysis failed to provide adequate electrophoretic separation between the “155 kDa” or the “200 kDa” large complexes (Fig. 3.23A, right panel). Therefore, cell culturing conditions were used to form each of the complexes in the absence of the other (see Section 2.4.4). Using conditions that allowed for exclusive formation of either the “155 kDa” or the “200 kDa” large complex in Caco-2 cells (Fig. 3.24A), Triton-X 100 lysates of the large complex-containing Caco-2 cells were separated on 4, 5, 6, and 7% PAGs (note: the large CPE complexes did not enter 8, 9, 10, or 12% acrylamide separating gels, therefore these gel concentrations could not be used for this analysis). When the relative migrations of the resultant CPE complexes were calculated on the subsequent CPE Western blots, the “~155 kDa” large complex was determined to have a molecular mass of ~430 kDa, whereas the “~200 kDa” large complex displayed a molecular mass of ~550 kDa (Table 3.4, Fig. 3.24B & C).

Table 3.4 Ferguson plot calculations for CPE large complexes.

	Actual Molecular Mass (Da)	Line Equations from Fig. 7B	Calculated Molecular Mass from Fig. 7C Line Equation (Da)
Thyroglobulin	669,000	$y = -19.896x + 241.77$	654,483
Ferritin	440,000	$y = -15.52x + 245.53$	425,191
Catalase	232,000	$y = -11.85x + 232.95$	266,148
Lactase dehydrogenase	140,000	$y = -7.7891x + 222.41$	128,435
"~155 kDa" Large Complex	?	$y = -15.536x + 200.48$	425,953
"~200 kDa" Large Complex	?	$y = -17.934x + 200.98$	546,520

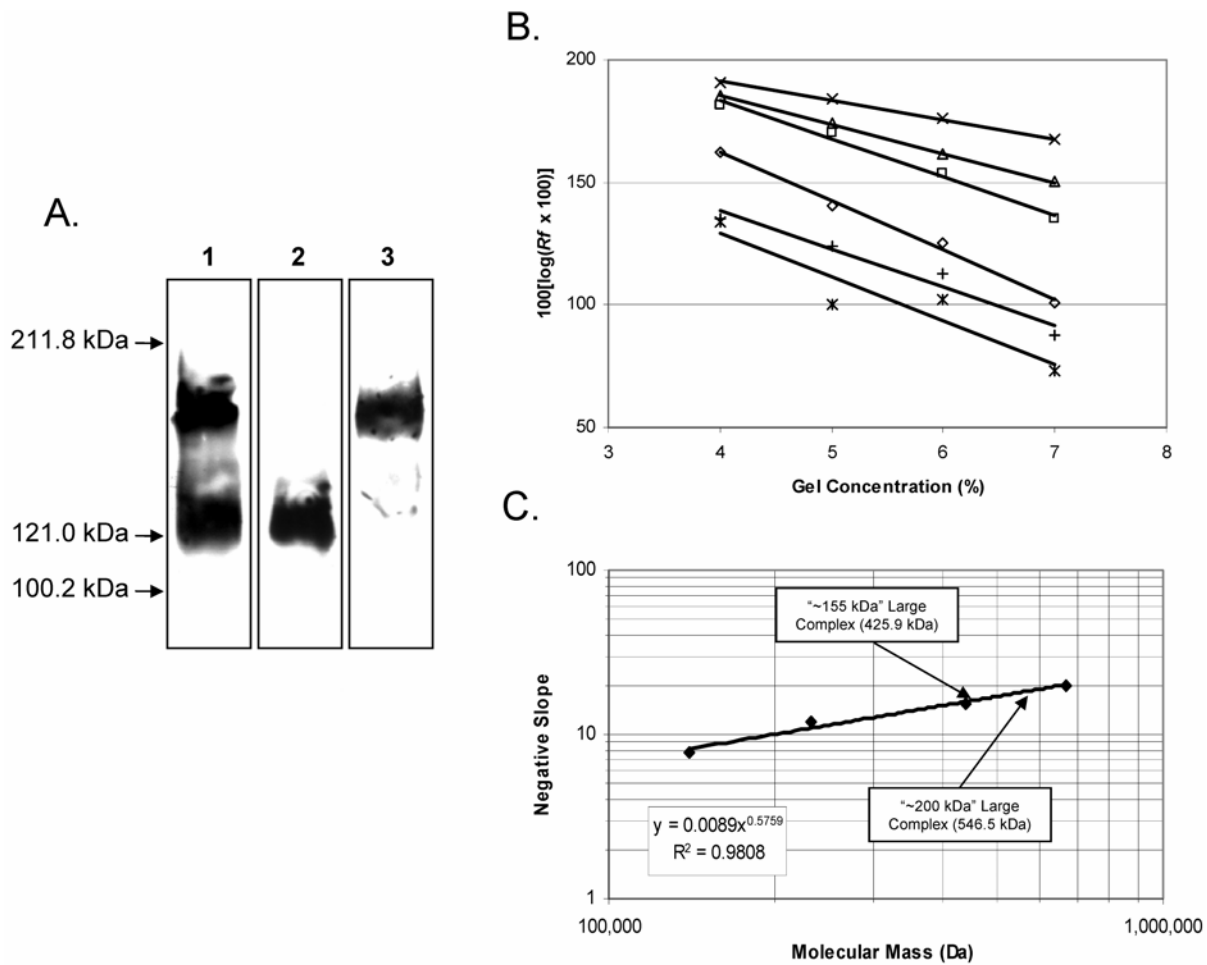


Figure 3.24 Ferguson plot analysis of CPE large complexes. A, Cell culture conditions were manipulated to achieve the formation of both of the large complexes (lane 1), only the “~155 kDa” large complex (lane 2), or only the “~200 kDa” large complex (lane 3). R_F values were calculated for these complexes along with molecular mass standards by their migrations in 4, 5, 6, and 7% acrylamide native PAGs. C, Negative slopes from curves in B are plotted versus the molecular mass to estimate the molecular masses of the CPE large complexes.

3.3.4.2 Analysis of the large CPE complexes by size exclusion chromatography

In order to confirm the Ferguson plot analysis, size exclusion chromatography of the CPE large complexes was performed. Caco-2 cells treated in suspension with CPE were lysed with 1% Triton-X 100 and loaded onto a Sephacryl-400 HR column calibrated with several molecular mass standards (Fig. 3.25A; see Section 2.3.4). Column fractions were then analyzed on a 4% acrylamide SDS-PAG and subjected to CPE Western blotting (Fig. 3.25B). Densitometric analysis of exposed Western blot films was then used to determine the relative intensities of the “~155” and “~200 kDa” large complexes in each fraction (Fig. 3.25C). The peak intensity for the “~155 kDa” large complex occurred at fraction 50, which corresponded to a molecular mass of ~500 kDa. Similar analysis of the “~200 kDa” large complex peak intensity (fraction 29) had a corresponding molecular mass of ~660 kDa (Fig. 3.25C).

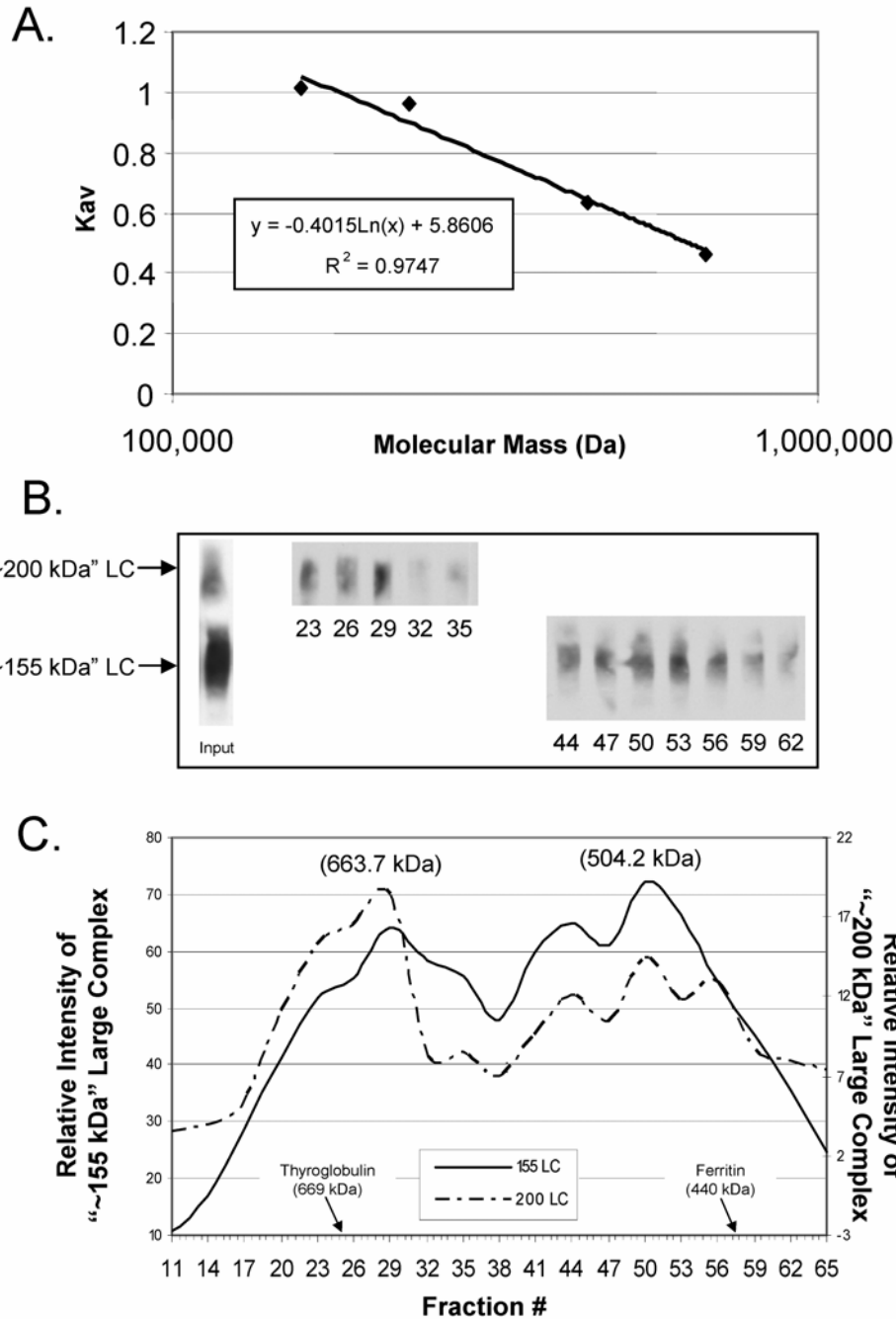


Figure 3.25 Size exclusion chromatography of the CPE large complexes. A, Molecular mass standards (see Section 2.3.4) were used to calibrate an Sephacryl-400 HR column. The K_{av} value for each standard was calculated and plotted versus their known molecular masses. B, Isolated Caco-2 cells treated with CPE were lysed with 1% Triton-X 100 and loaded on the calibrated Sephacryl-400 HR column. Samples from collected fractions were separated on a 4% acrylamide SDS-PAGE and Western blotted to detect the presence of the CPE large complexes (denoted with arrows to left of blot). C, Relative intensity of the immunoreactivity corresponding to each complex (from B) was quantitated and then plotted versus the fraction number. The solid line represents relative signal intensity of the “~155 kDa” large complex, while the dashed line depicts the “~200 kDa” large complex relative signal intensity. Shown in parentheses at the top of each signal intensity peak are molecular masses calculated using the standard curve generated in A.

3.3.5 Exploration of dominant negative phenotypes from rCPE variants

The data presented above provide robust evidence that the large complexes formed by CPE are in fact oligomers of CPE and represent the oligomeric pore that causes membrane permeability alterations of cells. Several groups studying bacterial toxins have described mutants which are capable of exerting a dominant negative effect on wild-type toxin when added in combination (178, 210, 220, 221, 237). Since many variants of rCPE have been generated both by the present and previous studies which are blocked for different stages of CPE action, it was interesting to examine the effect rCPE variants might have on rCPE oligomerization.

For example, work presented in Section 3.1 shows that the D48A point variant of rCPE is non-cytotoxic because it cannot form large complex (Fig. 3.6). Since the D48 residue appears to be essential for the formation of SDS-resistant CPE oligomers, it could easily be imagined that if D48A variant monomers were incorporated into a growing oligomer of wild-type rCPE monomers, the inability of the D48A to co-oligomerize might have a dominant negative effect by blocking the formation of a hexamer (dominant negative by 'chain termination'). In addition, dominant negative mutants of the *B. anthracis* protective antigen all have mutations that map to the TMD of these pore-forming heptamers (147). Because removal of the putative TMD of CPE results in a similar phenotype of a non-cytotoxic pre-pore oligomer (see Section 3.2), perhaps TM1 variant monomers incorporated into a wild-type rCPE oligomer could block membrane insertion of rCPE monomers (dominant negative by membrane insertion inhibition). Lastly, since the rCPE₁₆₈₋₃₁₉ fragment lacks both the N-terminal cytotoxicity region and the putative transmembrane stem domain but is binding-capable, it was of interest to determine if this fragment could also have a dominant negative effect. Each of these three variants of rCPE were evaluated for their potential inhibitory effects on rCPE action.

3.3.5.1 Dominant negative effects on CPE oligomerization

Since oligomerization of CPE precedes pore-formation, the ability of the aforementioned rCPE variants to inhibit oligomerization of rCPE was measured. To accomplish this, a standard large complex assay was performed by treating isolated Caco-2 cells with various pre-mixed ratios of variant:rCPE. After treatment, lysates of these Caco-2 cells were separated on 4% acrylamide SDS-PAGs and Western blotted for CPE. In the absence of any variant, rCPE formed the standard two SDS-resistant large complexes of ~155 and ~200 kDa in all three experiments performed (Fig. 3.26). Since the TM1 variant was previously shown to form the ~155 kDa large complex (Fig. 3.14), it was expected that all ratios of TM1:rCPE would result in the formation of some large complex as seen in Fig. 3.26. It was interesting to note a decrease in the amount of ~200 kDa large complex present as the amount of TM1 included was increased. In addition, the apparent molecular mass of the ~155 kDa large complex seems to decrease as more TM1 is added, an observation similar to Figs. 3.20 & 3.21 indicating that heteromeric large complexes are probably being formed.

The D48A and rCPE₁₆₈₋₃₁₉ variants each had a dramatic effect on the formation of large complex by rCPE. At ratios of only 1:1, a nearly complete loss of both complexes was noted in experiments where either D48A or the rCPE₁₆₈₋₃₁₉ variants were used in combination with rCPE (Fig. 3.26). Overexposed films of each of these blots could detect some of the large complexes at the 2:1 ratio, however it is clear that D48A and rCPE₁₆₈₋₃₁₉ have a powerfully dominant negative effect on rCPE oligomerization.

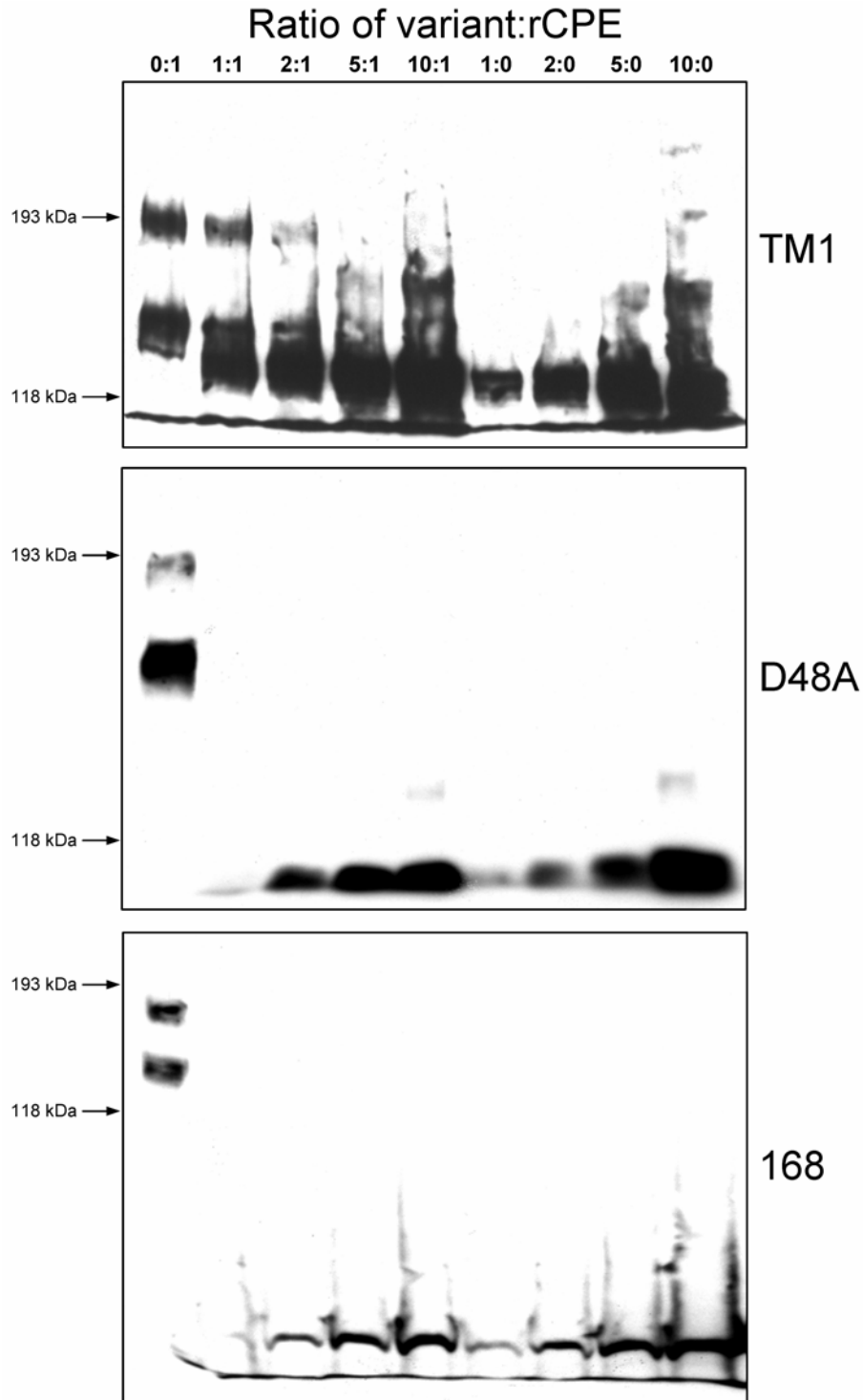


Figure 3.26 Dominant negative effects of rCPE variants on rCPE large complex formation. Isolated Caco-2 cells were treated with the indicated ratios (top of figure) of variant:rCPE, then lysed with Laemmli buffer, separated on a 4% acrylamide SDS-PAGE, then Western blotted for CPE. Values and arrows to left of blot represent migration of molecular mass markers on each blot. rCPE variant used in each experiment is indicated to the right of the blot.

3.3.5.2 Blocking of pore-formation by dominant negative variants

Since the above experiments demonstrated that some variants of rCPE could inhibit the oligomerization of rCPE, it was next appropriate to determine whether or not they also exhibited a similar effect on pore-formation. In order to evaluate inhibition of pore-formation, the standard ^{86}Rb release assay was used (as performed in Figs. 3.3 & 3.13), except that pre-mixed ratios of variant:rCPE were added to Caco-2 cell monolayers instead of a single toxin. When confluent monolayers of ^{86}Rb -labeled Caco-2 cells were treated with rCPE alone (the 0:1 ratio of all variant:rCPE data series), large amounts of ^{86}Rb were effluxed from these cells (Fig. 3.27). However, it was readily apparent that as the ratio of variant:rCPE for each variant tested was increased, the amount of ^{86}Rb released from these cells decreased. Since D48A and rCPE₁₆₈₋₃₁₉ appeared to strongly inhibit oligomerization of rCPE when added in combination (Fig. 3.26), it was expected that these variants would also have a similar inhibitory effect on pore-formation as depicted in Fig. 3.27. However, it was interesting to note the TM1 variant also could inhibit the release of ^{86}Rb from cells, though not as robustly as D48A and rCPE₁₆₈₋₃₁₉. As noted in earlier experiments (Figs. 3.3 & 3.13), neither D48A nor TM1 alone were able to elicit an ^{86}Rb response from Caco-2 cells even at the highest concentration tested (Fig. 3.27). Though not included in Fig. 3.26, the rCPE₁₆₈₋₃₁₉ has been conclusively shown to not elicit ^{86}Rb release from cells (93).

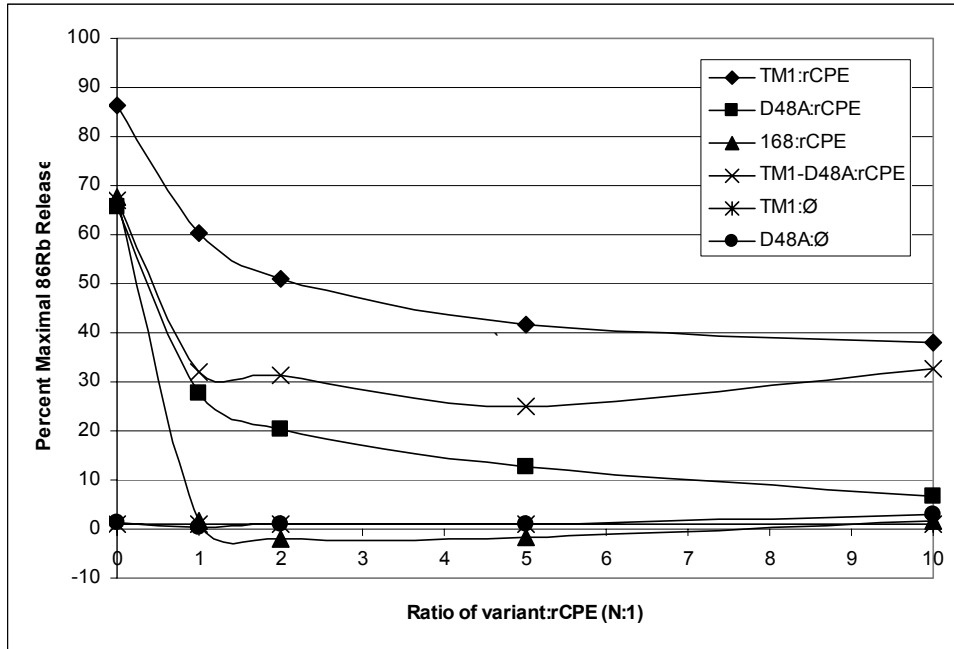


Figure 3.27 Dominant negative effects on rCPE pore formation by rCPE variants. Caco-2 cells pre-loaded with ⁸⁶Rb were treated with the indicated ratio of variant:rCPE. ⁸⁶Rb effluxed from the cells was quantitated and is expressed as percent maximal ⁸⁶Rb release.

4.0 DISCUSSION

As reviewed above, there have been several investigations into the mechanism of action of CPE which have greatly contributed to the understanding of how this toxin causes disease. However, Section 1.6 highlighted three specific and important questions that still remained prior to this thesis dissertation. First, why is the N-terminal cytotoxicity region essential for post-binding cytotoxic activity of CPE? Second, is there a region of CPE that is important for membrane insertion or pore formation? Third, what is the oligomeric state of CPE within the large complexes? The work presented above has helped to answer each of those three questions and has also generated additional unexpected insights into the molecular events leading to CPE-induced killing of enterocytes. What follows is a detailed interpretation of the results generated from this study, along with their relevancies to each specific question asked in this thesis dissertation.

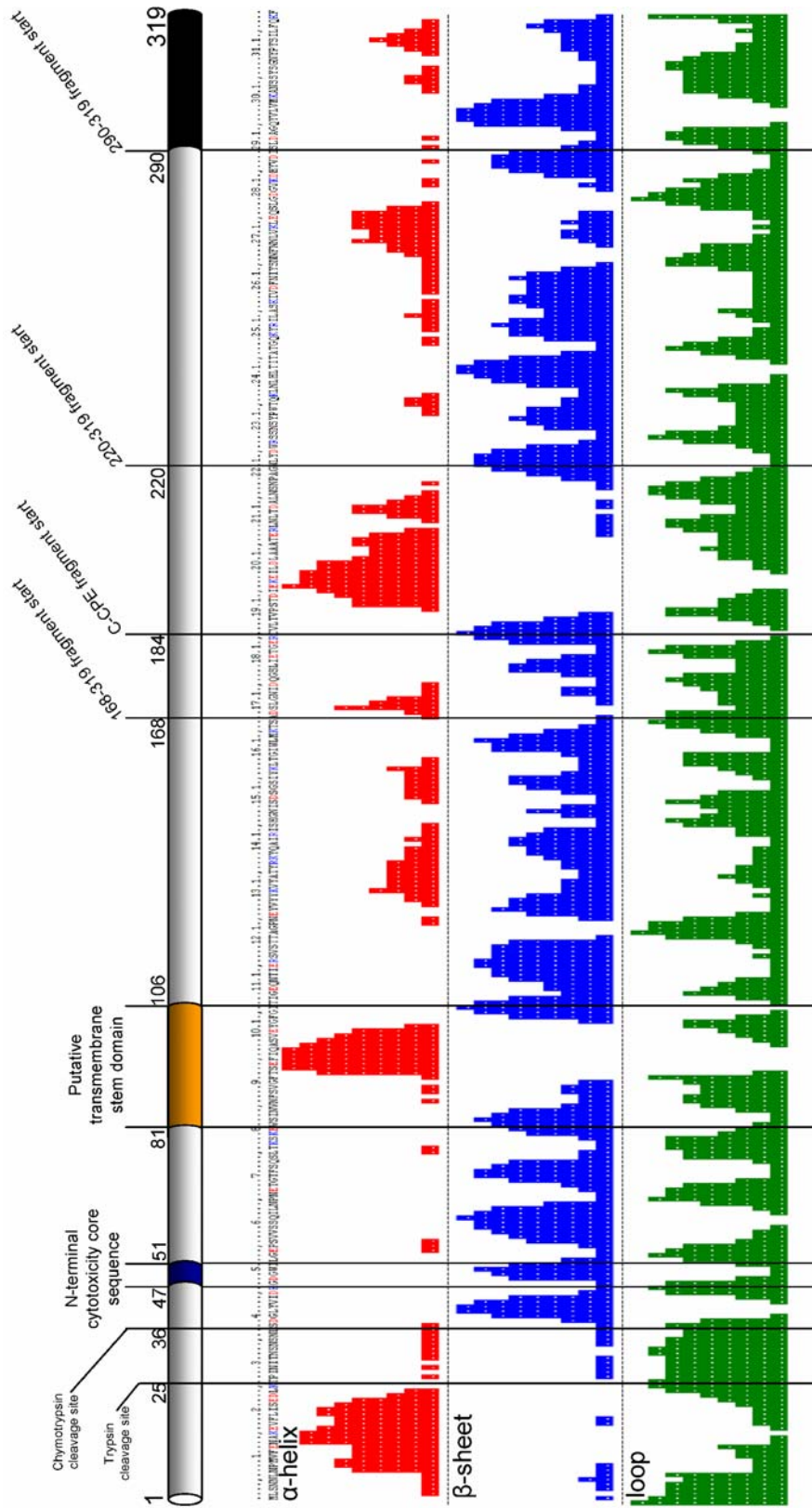


Figure 4.1 Current structure-function map of CPE (top) with a secondary structure prediction of CPE (bottom) by the PROF method (170). Highlighted above the map are locations of known and putative functional regions of CPE, as well as the N-terminals amino acids of several C-terminal fragments of CPE

4.1 WHY IS THE N-TERMINAL CYTOTOXICITY REGION ESSENTIAL FOR POST-BINDING CYTOTOXIC ACTIVITY OF CPE?

4.1.1 Explanation of mutagenesis and rCPE variant phenotypes

4.1.1.1 D48 and I51: crucial for CPE cytotoxicity

Alanine-scanning mutagenesis is a useful tool for deciphering the contribution of individual amino acids in a linear protein region. Since deletion mutagenesis performed earlier had identified that amino acids 45-53 in CPE were essential for cytotoxicity (93), this small stretch of amino acids was ideal for an alanine-scanning approach. Two alanine substitution mutants of rCPE, D48A and I51A, were found to be completely or strongly (respectively) attenuated for cytotoxicity (Figs. 3.2 & 3.3). The nontoxic phenotype of these two rCPE variants appears specifically attributable to their inability to form the large CPE complexes (Fig. 3.6) since both variants exhibited normal binding and small complex activities (Figs. 3.4 & 3.5) and neither variant appeared to have undergone gross conformational distortions (Fig. 3.7). With regard to D48, more conservative mutations were engineered that restored the side chain charge (D48E) or length (D48N). Each of these saturation variants mirrored the D48A phenotype in that they were completely deficient in large complex formation and toxicity, despite being properly folded and maintaining binding and small complex activity (Figs. 3.4 & 3.5). These observations suggest that both the negative charge and chain length supplied by the aspartic acid at amino acid 48 is essential for the formation of the CPE large complex. Regarding the alanine variant at I51 in CPE, saturation mutagenesis at this residue (variants I51L and I51V) completely restored wild-type levels of large complex formation and cytotoxicity (Figs. 3.2, 3.3, & 3.6). It was also interesting that, though highly attenuated, the I51A variant could form some residual large

complex (Fig 3.6). Taken in total, the data from the alanine and saturation mutagenesis at this residue implies that aliphatic hydrocarbon chain length is important at this position and may be roughly proportional to activity.

4.1.1.2 Glycine to alanine: loss of flexibility

Other interesting findings from the alanine-scanning studies include the distinct large complex phenotype of the G47A and G49A variants. In addition to the two standard large complexes of ~155 and ~200 kDa, both formed some immunoreactive material of even higher molecular mass than the 200 kDa large complex (Fig. 3.6). However, this odd large complex phenotype did not have any detectable effect on any other CPE activity, as levels of binding, small complex, and pore-formation were all similar to wild-type rCPE (Table 3.1). It is unclear from what this largest complex is derived since the presence or absence of occludin was not assessed in these experiments. It is interesting to note that both G47A and G49A (in the absence of any Caco-2 lysates) displayed an unusual propensity to aggregate on SDS-PAGE gels even after heating and reduction with β -ME. Therefore, it is possible that the material seen above the 200 kDa large complex in Fig. 3.6 could be simply represent anomalous aggregation. While the mutation from glycine to alanine only represents the addition of a single methyl group, this also has the effect of greatly restraining the freedom of rotation about the Φ and Ψ angles. The loss of protein flexibility in this region could be the cause of the aggregation seen in large complex experiments, however, it appears to be dependent on location since a glycine to alanine substitution at position 53 did not have a similar aggregation effect (Fig. 3.6). Since the G47 and G49 residues directly flank the D48 residue demonstrated in this study to be essential, it is possible (if not likely) that the flexibility provided by these two glycines properly frames the D48 residue for protein-protein interactions required for the formation of large complex. This

explanation would also be consistent with G53A mutation not affecting activity since it is not proximal to the D48 amino acid determined in this study to be so functionally important.

It is also interesting to consider results from a previous mutagenesis study of rCPE which isolated the point variant G49D by random mutagenesis (92). It was demonstrated in this work that the G49D variant was proficient at binding and small complex formation, however it resembled the D48 variants of the present study in that it could not form the large complexes or elicit ^{86}Rb -release from cells. Taking into account information learned from the present study, two possible explanations exist for the G49D phenotype seen earlier. First, even though the G49D variant contained the native aspartic acid at residue 48, it is apparent that rCPE can only tolerate one of these aspartic acids in this crucial stretch of amino acids. A D48A/G49D double point variant might be useful in determining if this is the case. Second, it is possible that a glycine to aspartic acid switch at position 49 may too severely constrain the Φ and Ψ angle rotation proposed here to be important for large complex formation. Perhaps the relatively conservative mutations to alanine by the G47A and G49A variant from the present study may be more easily tolerated by rCPE.

4.1.1.3 W50 is plays a structural role for CPE

As noted in the Section 3.1.1.7, our first W50A rCPE variant preparation was inactive and appeared to be improperly folded. Despite this, subsequent preparations of this variant produced active toxin lacking gross conformational changes, as measured by limited trypsin proteolysis (Fig. 3.7). However, even active W50A rCPE variant preparations formed little or no detectable ~155 kDa complex, although they did produce the atypical high molecular mass material also seen with the G47A and G49A rCPE variants (Fig. 3.6). In addition, substantially greater amounts of immunoreactive material were present at/near the dye front of large complex gel lanes loaded with extracts of W50A-treated Caco-2 cells. This finding probably represents

free W50A dissociated from large complexes (Fig. 3.6). Although it appears that the W50A rCPE variant is structurally-compromised, the large complex formed by this variant may be functional but more sensitive to the SDS used for extraction in large complex experiments. Since the W50Y and W50F saturation variants formed large complexes resembling those of wild-type rCPE (Fig. 3.6), these observations collectively suggest that an aromatic amino acid is preferred at CPE residue 50 to maintain normal structural integrity.

4.1.2 N-terminal core cytotoxicity sequence: the latch hypothesis

Considering the G47, D48, G49, W50, and I51 rCPE variant data together, it becomes notable that at least one substitution introduced at each of these five amino acid residues produced an atypical phenotype. Although the active phenotypes of G47A, G49A, and W50A differed from attenuated D48A and I51A variants, each of the three former variants displayed large complex activity distinct from rCPE (Fig. 3.6). Taken together, these observations suggest that N-terminal CPE residues G47 to I51 (Fig. 4.1) represent a minimal critical 'core' sequence important for the development of cytotoxicity. Since this sequence appears to mediate large complex formation, and since experiments in Section 3.3 have shown that these large complexes are CPE hexamers, it can be therefore deduced that this N-terminal core cytotoxicity sequence (NTCCS) is important because it facilitates oligomerization.

It is detailed above that CPE is similar in many ways to the β -PFT family of toxins (Section 1.6.2). One of these toxins, *S. aureus* alpha hemolysin, contains a latch domain at its N-terminus (Fig. 1.15) that specifically functions to link monomers together in an oligomer (156, 192, 215, 222, 223). Several aspartic acids and isoleucines are present in the latch domain of this toxin, and ionic and hydrophobic interactions have been predicted to mediate the monomer-monomer interactions necessary for oligomerization (192). The data presented in this study are consistent with the possibility that the NTCCS of CPE act in similar fashion to the *S. aureus*

alpha hemolysin latch as a region responsible for the protein:protein interactions required for oligomerization. The size and charge requirement of CPE residue 48, along with the aliphatic hydrocarbon preference at position 51, could permit ionic and/or hydrophobic interactions between the NTCCS latch and a latching site on another CPE monomer. As mentioned, the glycines at 47 and 49 flanking the critical D48 residue may provide flexibility that properly frames this latch, enabling interaction with its binding partner.

Prior to beginning this study, we noted the presence of a KGD motif at CPE amino acids 46-48 (Fig. 3.1) and hypothesized that this three amino acid sequence might explain large complex formation since RGD and KGD sequences are known protein binding motifs (4, 85, 129, 171, 198). However, the unimpaired cytotoxic activity observed for rCPE variants K46A and G47A now precludes CPE amino acids 46-48 (as a complete KGD motif) as being important for CPE action. Additionally, a GXXXG sequence also exists in the CPE N-terminal cytotoxicity region, extending from G49 to G53 (Fig. 3.1). This was interesting given that GXXXG motifs have been implicated in dimerization of the *Helicobacter pylori* vacuolating toxin (109, 110). However the GXXXG motif of the CPE N-terminal region does not appear important for toxicity, since glycine to alanine mutations did not alter the pore-forming ability of rCPE (Table 3.1), in contrast to the attenuation of oligomerization and membrane channel formation observed following some glycine to alanine mutations in VacA (110).

It is notable that none of the rCPE variants generated in the present study could form the ~155 kDa CPE complex without forming the ~200 kDa complex, or vice versa. That observation suggests the NTCCS latch is important for formation of both CPE large complexes. This leaves one of two possibilities: i) the ~155 kDa complex formation is a precursor for ~200 kDa formation, or that ii) formation of both CPE large complexes is independent but involves similar protein:protein interactions. Support for the latter possibility comes from Section 3.3 studies which have demonstrated CPE's existence as a hexamer in both the ~155 and ~200 kDa large complexes. If the NTCCS latch facilitates oligomerization, it would conceivably be required for

the formation both of these hexamers, and as a result, the formation of the ~155 and ~200 kDa large complexes would parallel each other according to this model.

4.1.3 *In vivo* validation of *in vitro* phenotypes

The rabbit ileal loop model of CPE-mediated intestinal disease has been invaluable in establishing an impressive knowledgebase about enteric CPE action (111). While the numerous technical advantages of immortal cell culture lines has no doubt accelerated the advancement of CPE structure-function relationships and CPE action, the danger of 'losing the forest for the trees' is real if efforts are not made to validate experimental findings *in vitro* with *in vivo* models. By using the two rCPE variants D48A and rCPE₁₆₈₋₃₁₉ in the rabbit ileal loop assay, we were able to demonstrate a very good correlation between our *in vitro* and *in vivo* models for CPE action. Neither of these two variants could elicit fluid accumulation or histopathological damage (Figs. 3.8 & 3.9, Table 3.2), observations consistent with the lack of cytotoxicity seen with the D48A and rCPE₁₆₈₋₃₁₉ variants seen previously (Table 3.1 and (93)). The fact that our *in vitro* and *in vivo* models parallel each other illustrates two important points. First, it is clear from this work that the cytotoxic consequences of CPE treatment are a necessary first step in the development of enteropathogenic effects caused by this toxin. Second, analysis of CPE activity with the use of Caco-2 cells is an accurate and valid model to predict the enteropathogenic phenotypes of CPE (or its variants).

It is interesting to note that the C-CPE fragment of CPE (Fig. 1.14) was found in several studies to increase intestinal absorption by removing/rearranging claudins resulting from CPE:claudin interactions (88, 105, 195, 204). Since these effects only appeared after several hours of treatment with C-CPE, it would be interesting to determine whether the D48A and/or the rCPE₁₆₈₋₃₁₉ variant could have a similar effect on rabbit ileal loops after longer treatment

times. Experiments testing the long-term effects of these rCPE variants on the tight junctions of the rabbit intestinal epithelium are currently underway.

4.2 SEARCH FOR A REGION OF CPE INVOLVED IN MEMBRANE INSERTION

4.2.1 Identification of a pre-pore large complex state

Since CPE has been definitively shown to have pore-forming activity (70, 72, 112), and since CPE in the large complex appears to insert (at least partially) into membranes (94, 228), the initial goal of the Section 2.0 studies was to define a region of CPE involved with membrane insertion. Complete deletion of amino acids 81-106 (which resembles the TMDs of the β -PFTs; Fig. 1.17) led to a novel CPE variant phenotype: formation of the ~155 kDa large complex in the absence of cytotoxicity. In addition to not being toxic for Caco-2 cells (Fig. 3.12), this TM1 deletion variant was defective in the ^{86}Rb release assay for pore-formation (Fig. 3.13). Biochemical analysis of this non-cytotoxic large complex revealed several differences from the large complex formed by wild-type rCPE. The TM1 large complex appeared to not insert into membranes (Fig. 3.15), and was more likely to both dissociate from membranes and disassemble (Fig. 3.16), especially in the presence of heat (Fig. 3.17). These observations collectively suggest that the TM1 large complex is trapped in a pre-pore state, capable of forming an SDS-resistant ~155 kDa complex on the surface of cells, yet unable to complete the final step in CPE action: membrane insertion to form a pore.

4.2.2 Possible functions of CPE amino acids 81-106

4.2.2.1 Transmembrane stem domain

While several possibilities exist to explain why amino acids 81-106 in CPE are important for pore formation, a strong case can be made for this region acting as a TMD. By simply scanning the primary amino acid structure of CPE, it was found that amino acids 81-106 have remarkable resemblance to the transmembrane β -hairpins of the β -PFTs (Fig. 1.17; (158, 207, 214)). Amino acids in these TMDs alternate in side chain hydrophobicity for ~ 12 residues, are interrupted briefly for 2-7 residues of no particular character, then the alternating pattern resumes for another ~ 12 residues (Fig. 1.17). Numerous fluorescence spectroscopy studies (reviewed (1)) in have determined that the alternating hydrophobic residues in these beta hairpins interact with the non-polar hydrocarbon chains of membrane phospholipids, whereas the hydrophilic amino acids face the water-filled channel made by the oligomeric pore. While the alignment shown in Fig. 1.17 depicts how well amino acids 81-106 of CPE adhere to this same pattern, Fig. 4.2 additionally demonstrates how easily this region in CPE fits the membrane topology model frequently used to represent TMDs of other β -PFTs.

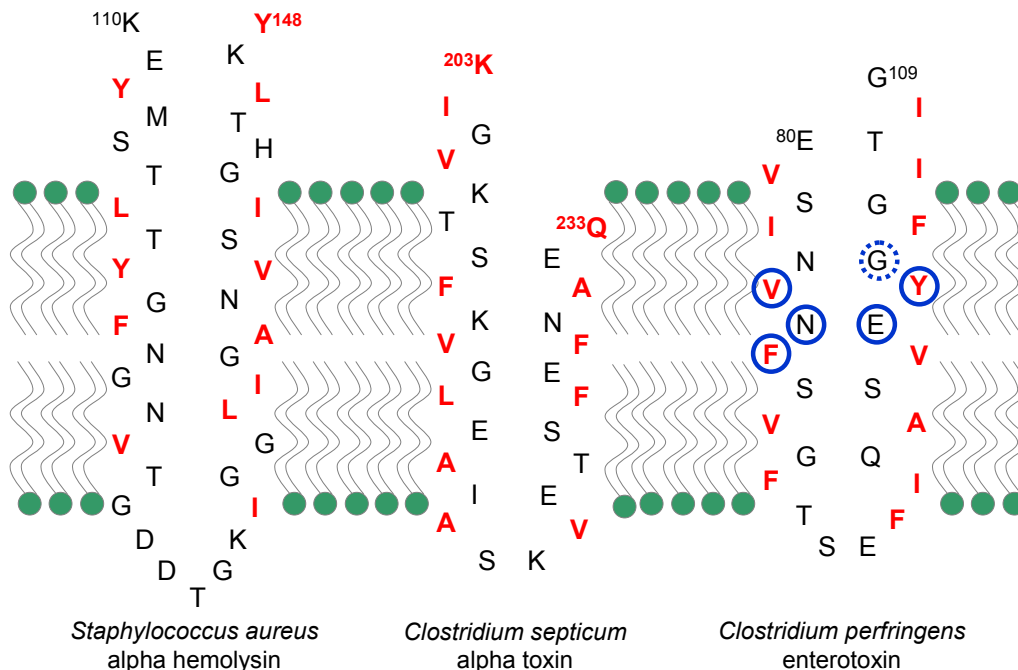


Figure 4.2 Membrane topology model of the TMDs of *S. aureus* alpha hemolysin, *C. septicum* alpha toxin, and the putative TMD of CPE. Circled in the putative TMD of CPE are residues substituted with Cys and labeled with NBD.

Additional information in support of amino acids 81-106 functioning as a TMD comes from hydrophobicity analysis of CPE. As mentioned in Section 1.4.1, amino acids 81-106 in CPE represent the only major hydrophobic patch in the protein according to Kyte-Doolittle analysis (Fig 1.9; (97)). The TMDs of β -PFTs, including those of *S. aureus* alpha hemolysin and *C. perfringens* epsilon toxin, are frequently found in distinct hydrophobic patches (Fig. 4.3). Further, secondary structure predictions of CPE are also consistent with a TMD existing between amino acids 81-106 of CPE. Several prediction methods project two beta strands between roughly V81 and T92 and again between approximately F95 and I106 (Double Prediction Method (30), Protein Sequence Analysis Server (200, 201, 227), PROF (170)). In an interesting deviation from other predictions, the PROF program actually projects a strong alpha helical structure between amino acids 90-100 flanked on each side by two shorter beta strands (Fig 4.1). While this prediction seems to argue against amino acids 81-106 forming a

transmembrane stem β -hairpin, it is important to mention that the crystal structure of monomeric perfringolysin O revealed that both of its TMDs are folded as short alpha helices (Fig. 4.4; (169)). It was subsequently demonstrated that only after oligomerization do these TMDs transition into complete beta hairpins allowing penetration of the phospholipid bilayer (181). It is entirely possible, therefore, that similar secondary structure rearrangements could take place within in CPE after to hexamerization and prior to insertion into the membrane.

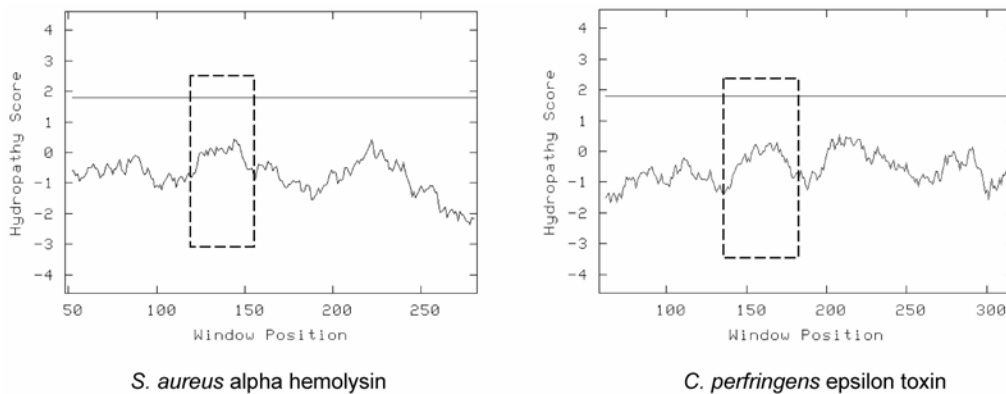


Figure 4.3 Kyte-Doolittle hydrophobicity analysis of two β -PFTs, *S. aureus* alpha hemolysin (left) and *C. perfringens* epsilon toxin (right). Dashed boxes represent location of the TMDs of these toxins.

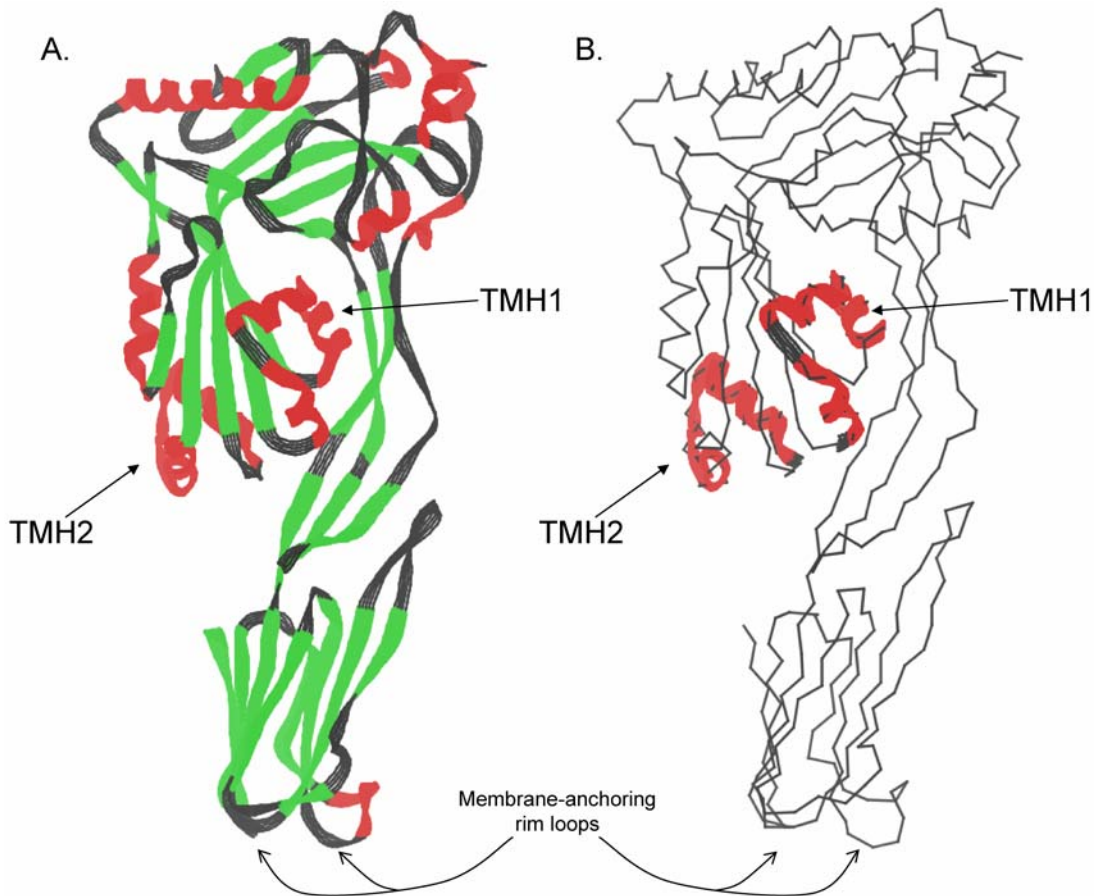


Figure 4.4 A, Ribbon rendering of the crystal structure of the *C. perfringens* perfringolysin O (169). B, Backbone carbon tracing of the same protein structure. The two TMDs and membrane-anchoring rim loops are indicated with arrows in each rendering. Images were created using the KiNG molecular modeling program.

It is prudent to note that the mere presence of a structural element does not necessitate its function as such. For example, the KGD and GXXXG motifs located in the N-terminal cytotoxicity region of CPE (Fig. 3.1) do not appear to be distinct protein-protein interaction domains in CPE, despite several examples in the literature of this being the case for both of these sequences (4, 109, 110, 171). Identification of putative functional domains must be followed by experiments testing the proposed functionality.

When the transmembrane stem domains from the *S. aureus* alpha hemolysin, *B. anthracis* protective antigen, and *C. septicum* alpha toxin were deleted in previous studies, all

resultant variant toxins were unaffected in binding activity and oligomerization, but were impaired at membrane insertion/pore-formation (22, 131, 138). In yet another similarity with this toxin family, the TM1 deletion variant of CPE maintained wild-type levels of binding activity, but formed a non-cytotoxic oligomer incapable of inserting into the membrane (Table 3.3 & 3.12-15). When these observations are combined with i.) the similar distinctive alternating amino acid pattern, ii.) the Kyte-Doolittle hydrophobicity analysis, iii.) and the secondary structure predictions, a scenario in which amino acids 81-106 in CPE acts as a TMD becomes more likely.

4.2.2.1.1 Probing the environment of residues in the putative TMD of CPE

While the indirect evidence noted above seems to implicate amino acids 81-106 in CPE action as a membrane-spanning β -hairpin, a more direct approach will be required to conclusively demonstrate transmembrane functionality from this region. As mentioned, the literature contains several examples of investigators making cysteine substitutions at proposed transmembrane residues, then using sulfhydryl labeling techniques to attach an environmentally-sensitive fluorescent dye molecule at each residue in question. Because some fluorescent dyes (such as (7-nitrobenz-2-oxa-1,3,-diazoyl)ethylenediamine, or NBD) are quenched by water, they undergo a significant increase in fluorescence intensity when inserted into the membrane. Such a shift is usually noted where hydrophobic residues have been Cys-substituted and labeled. A similar shift, however is not typically observed for Cys-substituted hydrophilic positions which face the water-filled channel. The TMDs of many β -PFTs have been identified in this manner, including perfringolysin O (180, 181) and *C. septicum* alpha toxin (131).

A small-scale version of this approach was attempted in the present study with CPE, unfortunately with only limited success. Six residues within the putative TMD of CPE (V85, N86,

F87, E101, Y102, and G103; Fig. 4.2) were each mutated to cysteines using site-directed mutagenesis in the fully-active C186A background of CPE. While the G103C mutant demonstrated substantially reduced amounts of large complex formation, the remaining five Cys-variants maintained activity similar to their C186A background construct (Fig. 4.5A). When the five active Cys-variants were labeled with NBD and tested in fluorescence intensity shift experiments, the findings were somewhat ambiguous. Of the three variants which were expected to undergo a fluorescence intensity shift (V85C, F87C, Y102C), only F87C had a significant increase when associated with membranes (Fig. 4.5B). In addition, of the two variants expected to lack a fluorescence intensity shift (E101C, N86C), N86C demonstrated an increase of fluorescence intensity after inserting into membranes (Fig. 4.5B). To summarize, two of the five residues tested displayed the predicted result, while the other three did not.

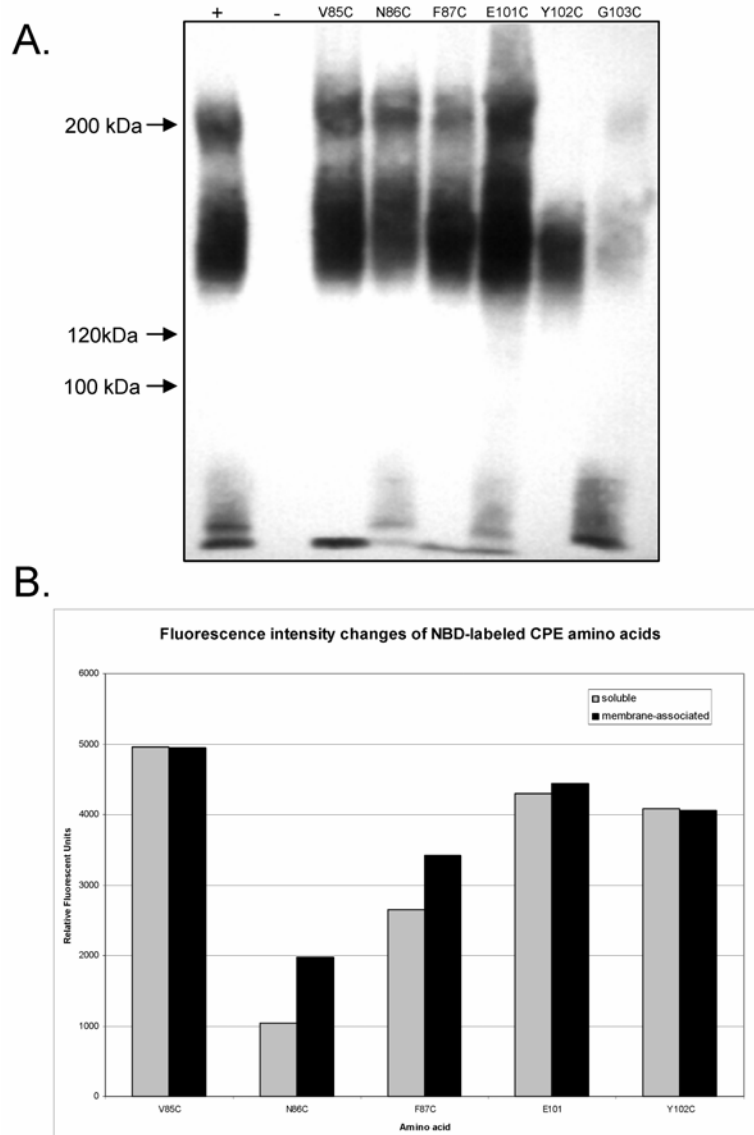


Figure 4.5 A, Large complex formation by six Cys-substitution variants in the putative TMD of rCPE. B, Relative fluorescence observed from indicated NBD-labeled Cys variants of rCPE before and after the addition of membranes.

While the data from this preliminary study are not particularly encouraging, several things must be considered before dismissing the possibility that amino acids 81-106 function as a transmembrane β -hairpin. First, it is entirely possible that this pilot study of CPE TMD insertion suffered from sampling error. Examples in the literature of fluorescence spectroscopic

studies of β -PFT TMDs define these domains by observing an alternating pattern of fluorescence intensity shifts over a span of 30+ residues, usually at hydrophobic amino acids. However, it is not uncommon for hydrophilic residues to undergo a shift, while neighboring hydrophobic residues remain quenched. For example, if the five consecutive residues of Q191, I192, S193, S194, and A195 of perfringolysin O were chosen for a pilot study similar to the one performed here for CPE, ambiguous findings would also have resulted. While Shepard *et al.* have conclusively shown with more exhaustive fluorescence methodologies that these residues in perfringolysin O are part of the first TMD, only two of the residues would have displayed the predicted fluorescence pattern while three would not have (181). A similar situation can be seen with fluorimetric analysis of the TMD of *C. septicum* alpha toxin. If only residues K211, V212, G213, L214, and E215 were examined, an equally unimpressive two of five these residues would have resulted in the predicted fluorescence intensity pattern (131). These examples make it clear that one must use caution confirming or rejecting the presence of a TMD by only assaying a few amino acids for their performance in fluorescence spectroscopy experiments.

Another possible contributor to the ambiguous results from the fluorescence study CPE's putative TMD could be the protein preparations. In nearly every experiment included in this dissertation, affinity-enrichments of rCPE (or its variants) are used. Since the sulfhydryl labeling involved in this pilot study required relatively pure protein, efforts were made to separate the Cys-variants from contaminating *E. coli* proteins. Despite these efforts, some background proteins were still observed in affinity "purifications" of these variants, and some of these contaminants were unintentionally fluorescently labeled with NBD during labeling of the CPE cysteine. Background fluorescence contributed by these labeled contaminants could have unquestionably clouded the interpretation of the data. If this fluorescence spectroscopy approach will be later revisited to examine the putative TMD of CPE, it will of utmost importance

to first establish and develop a purification protocol for the Cys-variants of rCPE which can achieve 90-95% purity before performing labeling experiments.

It would also be important to choose longer consecutive stretches of amino acids to test for insertion. In the preliminary study described above, three consecutive residues were chosen from each side of the predicted β -hairpin, representing three residues projected to insert into the membrane (V85, F87, Y102) and three residues projected to face the channel (N86, E101, G103). A better strategy for a follow up study might be to pick five to ten consecutive residues in one side of a predicted β -hairpin possibly allowing for a clearer identification of an alternating pattern of fluorescence intensity shifts.

While the alternating hydrophobic amino acids of residues 81-106 are the best candidate in CPE for TMD, there is also a second stretch of amino acids which may roughly resemble the β -PFT TMD pattern. Located between amino acids 238-265 (Fig. 1.8), the first half of the putative β -hairpin aptly alternates in hydrophobicity while the second half does not so clearly alternate. Although all of the small-pore β -PFTs only have one TMD per monomer, it is appropriate to point out that the cholesterol-dependent cytolysins all use two TMDs to penetrate the phospholipid bilayer. Whether amino acids 238-265 actually serve as the only or a second TMD awaits investigation, though it is unlikely that each CPE monomer would contribute two independent TMDs to an only hexameric CPE pore.

4.2.2.2 Rim interactions with the membrane

Besides a TMD, another possible function for amino acids 81-106 of CPE could be a role in mediating some protein:membrane interactions other than direct membrane penetration. Several pore-forming toxins are thought to contain regions in their rim domains (*S. aureus* alpha hemolysin Figs. 1.15 and 1.16) which interact peripherally with the plasma membrane. In addition, perfringolysin O contains several small loops at the bottom of its domain 4 (Fig. 4.4)

that have been shown to only shallowly insert into the membrane and participate in membrane-anchoring of the oligomer (77, 169). Several hydrophobic residues are located in these small loops of PFO, similar to the many hydrophobic residues found between amino acids 81-106 of CPE (Fig. 1.9). Additionally the preliminary fluorescence studies described above appear (at face value) to be consistent with this idea, since two consecutive residues (F87 and N86) did undergo a fluorescence intensity shift when membranes were added (Fig. 4.5B). Therefore, the large complex formed by the TM1 variant could be deficient at the membrane anchoring necessary for subsequent insertion of CPE into the membrane.

4.2.2.3 Protein-protein interactions

A final possibility for the function of amino acids 81-106 is that this CPE region mediates critical protein:protein interactions between CPE monomers or between CPE and other proteins required for membrane insertion/pore formation. Data presented in Section 3.2.1.6 appear to be consistent with this interpretation since it is clear that the ~155 kDa large complex formed by TM1 is structurally-compromised. Loss of crucial contact points between CPE monomers and/or other proteins could result in the increased rate of membrane dissociation (Fig. 3.20) compared to rCPE large complex. Also, the kinetic increase in a lower molecular mass complex in these dissociation experiments (Fig. 3.16), along with the sensitivity to heat denaturation (Fig. 3.17) both could lend support to the idea of the TM1 large complex lacking some important structural associations as a result of the deletion of amino acids 81-106.

4.2.3 Order of involvement of CPE functional regions

Introduction of a D48A mutation into the TM1 background helped assign a temporal order to the contributions of known CPE functional regions for cytotoxicity. Interestingly, the TM1-D48A

combination mutant paralleled the attenuated phenotype of the TM1 variant except that it could not form the ~155 kDa large complex (Fig. 3.14). This result indicates that the D48 residue in CPE's NTCCS acts prior to the involvement of the amino acids 81-106 in CPE, which is in agreement with a model for CPE action where NTCCS-mediated oligomerization precedes membrane insertion by the putative TMD. It also demonstrates that the NTCCS is not directly involved in membrane penetration or pore formation since the TM1 variant (containing a native D48), formed the ~155 kDa large complex, but could not insert into the membrane or form a pore (Figs. 3.13-15).

4.3 EXAMINATION OF THE OLIGOMERIC STATE OF CPE IN THE LARGE COMPLEXES

Identification of an ~155 kDa, SDS-resistant complex early in CPE investigations led to a preliminary model (232) where one CPE protein, one unidentified ~50 kDa protein, and one unidentified ~70 kDa protein interacted to form a complex critical for CPE action (117). Later studies identified a second, “~200 kDa” large complex in Caco-2 cells and demonstrated that it contained the tight junction protein occludin (186). As detailed above, claudins have been identified as receptors for CPE (47, 88), and it has been demonstrated only recently that claudins are present within these same large complexes (166). However, the question of CPE oligomerization within the CPE large complexes has never been vigorously evaluated, despite several pieces of indirect evidence supporting this possibility as described earlier. The work in Section 3.3, therefore, directly evaluated whether CPE is an oligomer in the two large complexes and then determined the CPE stoichiometry in each complex.

4.3.1 Determination the stoichiometry of CPE in the large complexes

Heteromer gel shift analysis has previously been used to identify the toxin stoichiometries of several β -PFTs (56, 137, 143, 144, 240). Using this same approach, we demonstrated that CPE exists as a hexamer in both the “~155 kDa” (Fig. 3.20) and “~200 kDa” (Fig. 3.21) large complexes formed by Caco-2 cells. This result seems to align CPE with the β -PFTs which form pores containing pentameric (*V. cholerae* cytolysin (240)), heptameric (*S. aureus* alpha hemolysin (56, 192)), or octomeric (*S. aureus* Panton-Valentine leukocidin (86, 137)) toxin stoichiometries. Interestingly, CPE appears to be the first pore-forming toxin in this family confirmed to form functional hexamers. The hexamerization of *C. perfringens* beta toxin has been previously reported but was not described as being functional (unlike the heptamer also formed by this toxin) (150). In addition, Nguyen *et al.* observed a hexameric conformation of the *S. aureus* gamma hemolysin using a FRET microscopy technique (152), however it was stated in this work that this same FRET data was also consistent with a heptameric conformation. The precise subunit stoichiometry of the bicomponent leucocidins is an area of ongoing research in the field.

A hexameric CPE oligomer is also consistent with previously reported sizes of the pore formed by CPE. Osmotic stabilizer studies have demonstrated the CPE pore to be very permeable to molecules of ~100 Da early in CPE treatment of cells (114, 118), while other work showed that only molecules over ~200 Da were able to osmotically protect cells from CPE toxicity (107). The CPE pore size estimation of 0.5 to 1.0 nm (70) is similar to the sizes seen with the small-pore β -PFTs (Table 1.2), including the 1.2-1.6 nm *V. cholerae* cytolysin pentameric pore (83), the 1.4 nm (minimum diameter) *S. aureus* alpha hemolysin heptameric pore (192), and the 1.7 nm *A. hydrophilia* aerolysin heptameric pore (157, 213). The CPE pore appears to be quite different in stoichiometry and internal diameter from the pores formed by

cholesterol-dependent cytolysin family members (such as perfringolysin O), which form large 24-48 nm pores with up to 50 toxin subunits to each oligomer (158).

4.3.2 Molecular mass and composition of the “~155 kDa” large complex

Determining that six copies of CPE are present in the “~155 kDa” large complex was in conflict with previous molecular mass estimates of this complex (186, 232). To address this discrepancy, we reevaluated the molecular mass of the “~155 kDa” large complex by Ferguson plot analysis and size exclusion chromatography. Results from these two methods gave a molecular mass range of ~430-500 kDa for the “~155 kDa” large complex. Since six copies of CPE equal a molecular mass of only ~210 kDa (Fig. 4.6), this finding strongly supports the presence of eukaryotic proteins in this complex. Consistent with this idea, it has recently been demonstrated that both receptor and non-receptor claudins can be present in the two large complexes formed by CPE in Caco-2 cells (166).

If one assumes the simplest possible stoichiometry for this “~155 kDa” large complex (six CPE molecules each bound to one claudin receptor), this configuration would result in a molecular mass of ~330 kDa (Fig. 4.6). However, since the “~155 kDa” large complex was estimated in this study to have a molecular mass range of ~430-500 kDa, a scenario where multiple claudins associate with each CPE subunit becomes more probable. The demonstration that non-receptor claudins can localize with the large complexes (166) suggests that additional claudins not directly bound to CPE become localized with the CPE complexes via claudin-claudin interactions. Several studies have shown that these tight junction proteins can self-associate both within and in between adjacent cells (49, 106, 176, 217), so it is highly likely that CPE binding and oligomerizing with the initial receptor claudin would likely itself already be bound to another (or multiple) ‘carrier’ claudin(s). This could serve as an explanation as to how non-receptor claudins can be found in these complexes. Moreover, the association of two

claudins for each CPE molecule in the “~155 kDa” large complex would yield a projected molecular mass of ~450 kDa which is well within the range of estimates reported in the present study (Fig. 4.6).

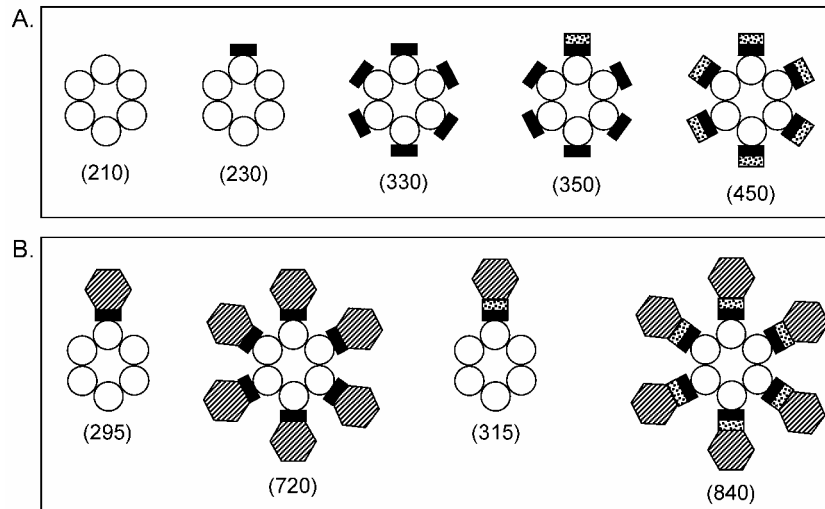


Figure 4.6 Possible configurations for the CH-1 (depicted in A) or CH-2 (depicted in B) complexes. CPE is represented as white circles, receptor claudins (black rectangles), carrier claudins (speckled rectangles), and occludin (hatched hexagons). Predicted molecular masses (in kDa) of these configurations are located below each in parentheses.

4.3.3 Molecular mass and composition of the “~200 kDa” large complex

The more recently discovered “~200 kDa” large complex is distinguishable from its “~155 kDa” counterpart because it contains occludin, a protein proposed to interact with claudin in tight junctions (48, 154). Occludin is physically present in the “~200 kDa” large complex based upon Western blot, electroelution, and co-immunoprecipitation analyses, yet naturally CPE-resistant fibroblasts transfected with occludin cDNA do not gain the ability to bind the toxin or become CPE-sensitive (186). Collectively, these observations suggests that CPE does not directly

interact with occludin (at least initially) and that the presence of occludin in the “~200 kDa” large complex may be a result of still incompletely characterized occludin:claudin interactions.

Reevaluation of the size of this complex by gel filtration estimated a molecular mass of ~660 kDa (Fig. 3.25), whereas Ferguson plot studies calculated a molecular mass of ~550 kDa for this complex (Fig. 3.24). If, similar to the “~155 kDa” large complex above, the “~200 kDa” large complex consisted of six CPE molecules and 12 claudins, it would have a molecular mass of ~515 kDa after the addition of one occludin molecule (Fig. 4.6), within range of our size estimations for this complex. Association of additional occludins would place this hypothetical conformation even closer to the mass estimations presented here within (Fig. 4.6).

4.3.4 Nomenclature change

Since results from this study have shown that the “~155 kDa” and “~200 kDa” large complexes have actual molecular masses much greater than those by which they were previously identified, it is necessary to propose a new nomenclature unrelated to molecular mass. Such a change is particularly important since the present mass estimations of these large complexes are still not very precise. We propose that the “~155 kDa” and “~200 kDa” large complexes hereafter be referred to as CPE Hexamer 1 (CH-1) and CPE Hexamer 2 (CH-2), respectively. These designations are not only more accurate descriptions, but should avoid any future need to change the nomenclature as the exact size and composition of the complexes become more precisely determined. In addition, the number value after the ‘CPE Hexamer’ can easily be extended to accommodate any forthcoming discoveries of new complexes (i.e., “CH-3”).

4.3.5 Dominant negative variants of rCPE

4.3.5.1 Inhibition by blocking membrane insertion

Additional confirmation of CPE's oligomeric state came from the finding that several variants of rCPE from present or previous studies have an inhibitory effect on the action of rCPE when added in combination. It was expected that all ratios of TM1:rCPE would form CH-1, since TM1 has been shown in Section 3.2 studies to be proficient for the formation of CH-1 but not CH-2 (Fig. 3.14). Nonetheless, it was interesting to see the amount of CH-2 formed by rCPE decrease as the TM1:rCPE ratio increased (Fig. 3.26). Since the amount of rCPE in all of these lanes remains constant, this finding seems to support a scenario where an abundance of growing TM1 oligomers incorporate rCPE and exert a dominant negative effect on the formation of CH-2. As seen in Fig. 3.14, this result may be indicating that formation of CH-2 requires membrane insertion, a step for which a heteromer consisting mostly of TM1 variants may be deficient.

Since the TM1 deletion variant of rCPE is able to form the CH-1, it was not surprising that this variant had an inhibitory effect on rCPE when added in combination in ^{86}Rb release experiments. A 5:1 ratio of TM1:rCPE was required to maximize this effect, giving implications that several copies of TM1 must be incorporated into a mostly rCPE oligomer in order to block pore formation. Studies examining the dominant negative effects of TMD mutants of *B. anthracis* protective antigen have demonstrated a similar effects but at much lower variant:wild-type ratios (147, 178). It is important to point out, though, that while the ^{86}Rb release experiments directly measure pore formation by CPE, the dominant negative variants of protective antigen in these studies are blocked for translocation of unfolded peptides through the protective antigen pore and subsequent toxic activity of that translocated peptide (147, 178). The dominant negative protective antigen system is probably very sensitive to small distortions

of pore conformation, whereas one might imagine that a rCPE oligomer with only 1 or 2 copies of TM1 might still partially insert the plasma membrane causing leakage (albeit less efficient) of ^{86}Rb from cells in this experiment.

4.3.5.1 Inhibition by chain termination

It was very interesting to find that both the D48A point variant of rCPE (generated by Section 3.1 studies) and the rCPE₁₆₈₋₃₁₉ fragment (93) were also both dominant negative. Both of these variants dramatically decreased ^{86}Rb release of Caco-2 cells even at a ratio of only 1:1 (Fig 3.27), and each variant completely inhibited the formation of both CH-1 and CH-2 at the same ratio (Fig 3.26). These effects, particularly in the ^{86}Rb release experiments, seemed to be even more severe than the TM1's dominant negative phenotype. The potent dominant negative phenotypes of D48A and rCPE₁₆₈₋₃₁₉ were especially interesting because both variants alone clearly lack the ability to form CH-1 or CH-2, as seen in Fig. 3.26. One possible explanation for this result is that these variants are inhibitory by chain termination. Described in detail above and in Section 3.1, the NTCCS in CPE is proposed to mediate the protein-protein interactions required for oligomerization. According to this proposal, this region of CPE would need to interact with second CPE region to complete this 'latching' step. While the D48A would not be able to provide a functional latch for oligomerization, it is possible that D48A can *receive* a latch from a wild-type rCPE monomer alone or one in a growing oligomer. Since the D48A mutation precludes this variant from extending the oligomer, rCPE would be perilously trapped in an partial oligomer and thus inactivated.

Valuable insights regarding the location of a potential latch 'binding site' can be gained from similar phenotype of the rCPE₁₆₈₋₃₁₉ fragment of CPE. Since the large complex experiments in Fig. 3.26 indicate that rCPE₁₆₈₋₃₁₉ is also dominant negative by chain termination, this implies that the latch binding site would exist between amino acids 168-319 of CPE. This

finding greatly narrows the search for the this additional functional region in CPE to less than half of the protein. While genetic and biochemical approaches will be required to define a region in this CPE fragment functioning as a latch binding site, it is interesting to recount results from a recent study of the C-CPE fragment of CPE (Figs. 1.14 & 4.1). It was determined that when amino acids 184-220 were deleted from C-CPE, this smaller fragment could bind claudin but was unable to modulate tight junctions and increase intestinal absorption (105). This result seems to assign some functionality to residues 184-220, and represents a reasonable starting point in the search for the latch binding site.

4.4 UPDATING STRUCTURE-FUNCTION RELATIONSHIPS OF CPE

Given the contributions of the present study, it is appropriate at this time to consolidate all known and putative functional regions of CPE to date. While the absence of a crystal structure adds great difficulty in analyzing precise structure-function relationships, several interesting insights can be gained by aligning an updated structure-function map of CPE with a prediction of secondary structure elements of the protein, as depicted in Fig. 4.1. Therefore, what follows is a synopsis of the current functional regions CPE, along with consideration given to elements of its predicted secondary structure (170).

4.4.1 N-terminal activation region

As described in Section 1.4.2.1, the first ~40 amino acids of CPE have an inhibitory effect on activity since truncation of the N-terminus using enzymatic (59, 60, 67) or molecular cloning (93)

methods doubles or triples its cytotoxicity. Analysis of secondary structure predictions reveals a large alpha helical structure followed by a unstructured loop section in this location (Fig 4.1). It is likely that this region is inhibitory because it slows or interferes with oligomerization, mediated by the adjacent NTCCS.

4.4.2 N-terminal core cytotoxicity sequence

Initially discovered by deletion mutagenesis (93), then fine-mapped by present Section 3.1 studies (190), this region contains five amino acids essential for the oligomerization of the toxin. Of the residues in this region, the aspartic acid at position 48 appears to be absolutely essential for formation of the CPE oligomer, whereas aliphatic hydrocarbon chains are preferred at position 51. Interestingly, all the amino acids of the NTCCS appear to be contained in a single beta strand (Fig. 4.1). Despite the proposed comparative functionality with the N-terminal latch of *S. aureus* alpha hemolysin, the latch in this toxin consists of mostly of an unstructured loop with N-terminal 5-7 amino acids having slight alpha helical structure (Fig 1.15).

4.4.3 Putative transmembrane domain

As the subject of Section 3.2 studies, amino acids 81-106 are essential for the insertion of the CPE oligomer into membranes and the formation of a pore. Though other potential functions do exist (including mediating protein-membrane or protein-protein interactions), it is likely that this region serves to form a beta hairpin structure during pore-formation. According to this model, the TMD beta hairpins from six CPE molecules would combine to form a membrane-penetrating beta barrel pore. Detailed above in Section 4.2, the putative TMD appears in this prediction to be alpha helical flanked by two beta strands, a pattern shared by both TMDs of perfringolysin O (Figs. 4.1 & 4.4).

4.4.4 Tight junction modulator region

While the C-CPE fragment of CPE (amino acids 184-319) has been shown to disrupt tight junctions and modulate paracellular permeability, the 220-319 fragment of C-CPE lacks this specific activity (105). Thus, amino acids 184-220 have been proposed to be responsible for this intestinal absorption enhancement activity. Secondary structure predictions of CPE project a large alpha helical structure between amino acids 190-220 to which the intestinal absorption activity could possibly be attributed (Fig. 4.1).

4.4.5 C-terminal binding domain

The 30 C-terminal amino acids of CPE have been conclusively demonstrated to fully contain the receptor binding activity of the toxin. Even a synthetic peptide corresponding to these 30 residues can compete for CPE-binding, possibly indicating that strict secondary structure requirements are probably not present in this domain. Correlating with this idea is the secondary structure predictions that project no dominant structural elements at the C-terminus of CPE (Fig. 4.1).

4.4.6 Latch binding site

The identification of the NTCCS and proposal that it acts as a latch to join together monomers in an oligomer necessitates that separate region of CPE functions to receive this latch. The dominant negative studies highlighted in Section 3.3.5 demonstrate that rCPE₁₆₈₋₃₁₉ fragment of CPE can act as a chain terminator, implying that the binding site for the NTCCS latch might exist between amino acids 168-319. While the identification of latch binding site remains to be

elucidated, it is nonetheless interesting to consider the alpha helical structure in the aforementioned tight junction modulator region as a potential candidate for such a site.

4.5 UPDATED MODEL FOR THE MOLECULAR MECHANISM OF ACTION OF CPE

The structure-function and oligomeric analyses of CPE in the present study has made several advances in the understanding of the molecular mechanism of action of CPE. It is clear from these studies that three distinct steps now exist within CPE action. Found below is a succinct description of these steps, each of which is graphically represented in Fig. 4.7.

4.5.1 Step 1 – Receptor binding and formation of the small complex

Mediated by its extreme C-terminus, CPE interacts with the second extracellular loop of receptor-claudins located within tight junctions. Claudins serving as CPE-receptors are likely to associate with (or already be associated with) other tight junction proteins, namely, additional receptor- or non-receptor claudins. This collection of proteins results in what has been described as the CPE small complex and is sensitive to denaturation with SDS (Fig. 4.7A).

4.5.2 Step 2 – Oligomerization of CPE and formation of the pre-pore

Six CPE small complexes self-assemble in an oligomerization event directly involving an interaction between the NTCCS latch and a latch binding pocket in C-terminal half of CPE. This association results in the formation of an SDS-resistant hexamer of CPE and contains several other copies of claudin (Fig. 4.7B). The CPE hexamer at this pre-pore stage is not resistant to soluble proteases and is subject to dissociation from the membrane as well as heat denaturation.

4.5.3 Step 3 – Pore-formation by membrane insertion

Conformational changes in CPE structure allow the coordinated insertion of a TMD from each monomer forming a beta barrel pore structure, resulting in the CH-1 complex (Fig. 4.7C). Should occludin be present, it may also associate with the CPE hexamer and form the CH-2 complex (Fig. 4.7D). Accompanying this insertion event is the protection of this oligomeric complex from proteolytic degradation as well the achievement of oligomer stability. Membrane penetration of the CH-1 and CH-2 complexes event permits an intracellular Ca^{2+} influx, causing the beginning of the cytotoxic and enteropathic effects of CPE action.

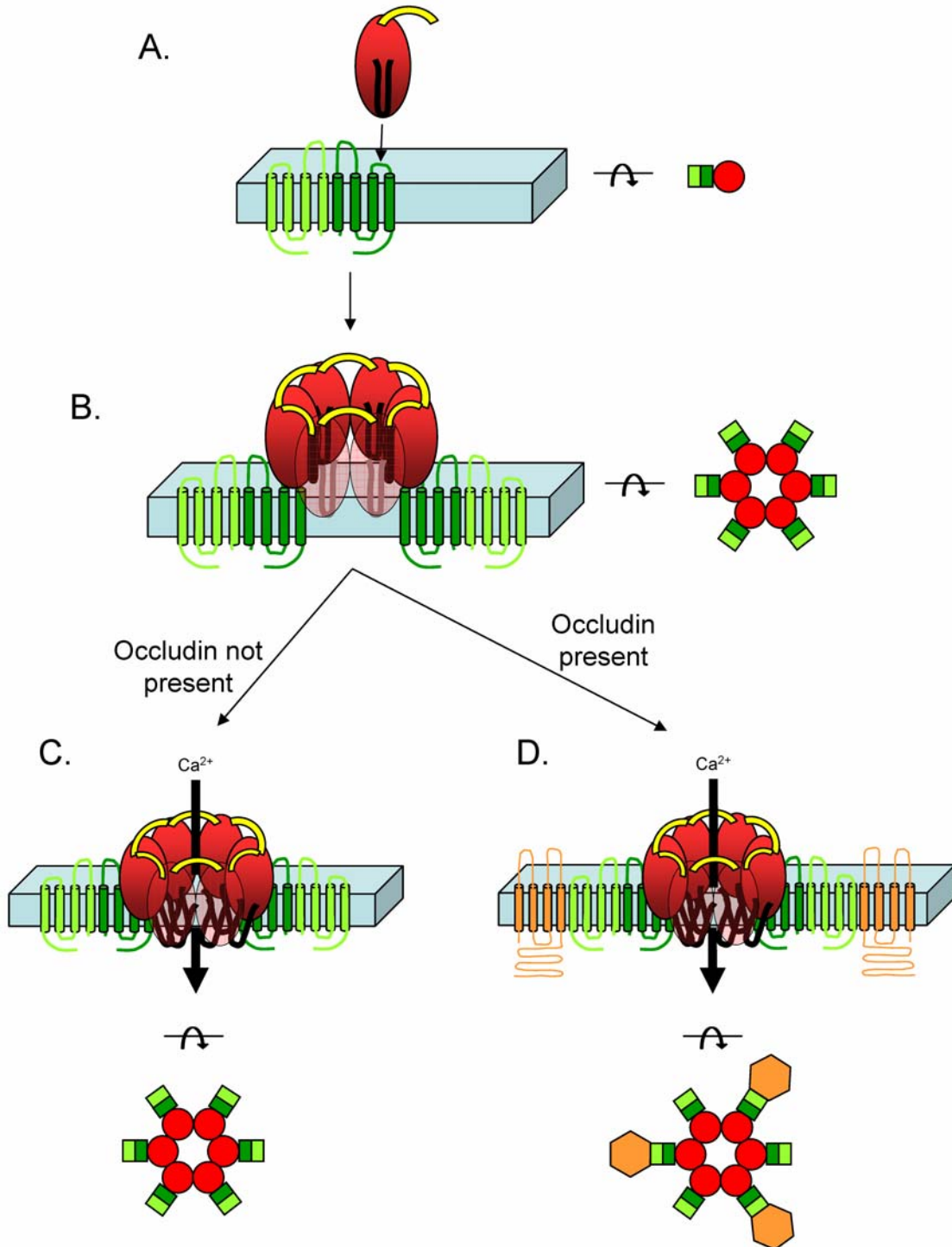


Figure 4.7 Model for the molecular mechanism of action of CPE. A, Binding of CPE to a receptor claudin (dark green) itself already associated with a carrier claudin (light green) results in the formation of the small complex. B, Oligomerization of small complexes mediated by the N-terminal cytototoxicity sequence results in the formation of a pre-pore, SDS-resistant hexamer uninserted into the membranes. C, In the absence of occludin, this hexamer (CH-1) penetrates the phospholipid bilayer with a beta barrel formed with six TMDs, allowing Ca^{2+} to penetrate the cell. D, If occludin is present during membrane insertion, it can also associate with this hexamer via an interaction with claudin, also resulting a CPE pore (CH-2).

4.6 FUTURE INVESTIGATIONS

4.6.1 NTCCS latch and binding site

Both the site-directed mutagenesis study in Section 3.1 and the dominant negative work in Section 3.3.4 illustrate that a crucial interaction takes place between the NTCCS of one CPE molecule to the latch binding site of a neighboring CPE molecule. There are several ways in which this interaction can be further evaluated. First, amino acids 184-220 is an appealing candidate for the latch binding site for the reasons delineated in Section 4.3.5.1. Attainment of a 220-319 deletion construct either as a gift from Masuyama *et al.* or by PCR cloning would be helpful in this regard (105). It would be predicted that if this 184-220 region contained the latch binding site, the 220-319 fragment would maintain binding activity but would not be dominant negative since it cannot receive a latch domain.

Another way to determine where the NTCCS binds would be to possibly use label-transfer reagents. These experiments would involve labeling CPE with a label-transfer tag near the NTCCS, then after allowing oligomerization to occur, performing a cross-linking step which would transfer the label near the putative latch binding site. Defining the specific location of label transfer could occur via several different methods, however, mass spectrometry of tryptic peptides of the oligomers would probably be the most precise method.

4.6.2 Confirming the putative TMD of CPE

Although Section 3.2 studies provide evidence consistent with amino acids 81-106 acting as a TMD, more direct analysis must now follow to formally establish that this region functions as predicted. Section 4.2.2.1.1 highlighted the fluorescence spectroscopic approach that will

probably be required to definitively show transmembrane status. Large initial strides have already been made for this strategy, including creating a cysteine-less background construct (C186A) and generation of the six Cys-variants V85C, N86C, F87C, E101C, Y102C, G103C. As mentioned above, follow-up studies of this strategy will probably have to involve making more single cysteine variants as well as better purification techniques to achieve 90-95% purity before labeling.

Another potential method to show that amino acids 81-106 serve as a transmembrane beta hairpin would be to swap this region with a bona fide TMD from another β -PFT. For example, restoring full pore-forming functionality to the TM1 deletion variant by cloning in the TMD of *S. aureus* alpha hemolysin would provide very strong evidence for the proposed functionality. While protein-folding issues may prohibit such an approach, this may be a worthwhile alternative should the fluorescence spectroscopy be unfruitful or ambiguous.

It is also worth mentioning that the second putative TMD of CPE between amino acids 238-265 could be investigated identically to the first putative TMD. Initial deletion mutagenesis by PCR splicing would rapidly show whether this region is specifically important and whether it also would form the pre-pore large complex similar to TM1. Additionally, fluorescence spectroscopy or TMD swapping could also be applied to this region if necessary.

4.6.3 Additional dominant negative analysis

The initial dominant negative studies described in Section 3.3.5 have yielded promising results regarding the inhibitive nature of some rCPE variants. This preliminary work must be followed up with more detailed analysis. For example, it is crucial to determine the extent of which (if any) binding inhibition contributes to the dominant negative effect seen by these variants. While it is unlikely that the dramatic inhibitory effects seen in these experiments result merely from

binding competition, this needs to be evaluated by performing careful binding competition experiments with a labeled toxin (possibly ^{125}I -CPE).

It would also be interesting to explore the protective effect of a co-incubation with one of these dominant negative variants. The ^{86}Rb release experiments in Section 3.3.5 demonstrate that pore formation in Caco-2 cells can be blocked nearly 100% after incubation of only a 1:1 ratio of rCPE₁₆₈₋₃₁₉:rCPE. Perhaps a co-treatment of Caco-2 cells with similar ratios of these two toxins would be able to provide extensive protection from morphologic damage. If such a protective effect is offered by co-treatment of rCPE with rCPE₁₆₈₋₃₁₉, it is conceivable that similar co-treatments could inhibit fluid accumulation in the rabbit ileal loop model, thus providing *in vivo* promise for a potential therapeutic for CPE.

4.6.4 Solving the three-dimensional structure of CPE

Impressive strides have recently been made in structure-function analysis of CPE, all in the absence of any three-dimensional information. Nonetheless, having detailed knowledge of secondary, tertiary and even quaternary elements of the structure of CPE and/or its oligomer would greatly propel investigations of how functional regions of the toxin contribute in the mechanism of action. An ongoing collaboration between our laboratory and Dr. Ajit Basak in the Department of Crystallography at Birkbeck College has generated several crystallized forms of native CPE as seen in Fig. 4.8. However, all crystals formed to date they have been either of poor quality or of heterogeneous unit cell to generate any meaningful structural information. While efforts are currently underway to grow crystals from highly-purified recombinant fragments of CPE (such as rCPE₁₆₈₋₃₁₉), it is critical that work geared towards solving the three-dimensional structure of CPE continue and be completed. This may involve using non-crystallographic means to generate structural information (NMR-based structure-mapping), however the end

result will greatly increase the pace at which knowledge of structure-function relationships can be attained.

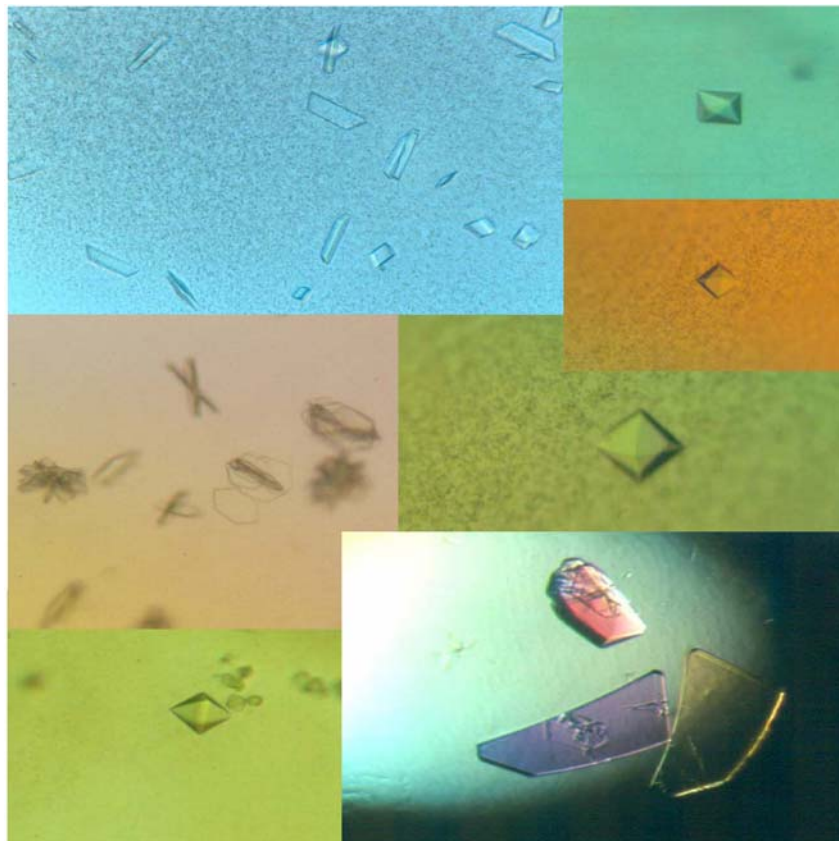


Figure 4.8 Montage of various crystal morphologies formed by CPE (Briggs, D. & Basak, A., unpublished observations).

4.7 FINAL SUMMATION

The research contained within this thesis dissertation has directly built upon previous investigations of the mechanism of action of CPE, the causative toxin of *C. perfringens* type A gastrointestinal diseases suffered by hundreds of thousands of people each year. Investigation of a distinct region at the N-terminus of the CPE resulted in identification of specific residues involved in toxin oligomerization. In addition, a novel pre-pore step in the molecular mechanism of action was discovered when a second CPE region was deleted that may potentially act as a transmembrane domain. Lastly, examination of the stoichiometry of CPE in its large SDS-resistant complexes resulted in the discovery that six copies of CPE are found within both of these complexes. Collectively these findings have uncovered new aspects of the mechanism of action of CPE and have demanded a reevaluation of molecular interactions that occur between CPE, host cell proteins, and the plasma membrane. Just as this present work has benefited greatly from the important studies performed earlier, the contributions here within can (and should) be extended to continue answering both fundamental and advanced questions regarding the role of CPE in *C. perfringens* type A gastrointestinal diseases.

4.8 ORIGINAL KNOWLEDGE CONTRIBUTED

This thesis dissertation has contributed the following works of original knowledge to structure-function analysis and examination of the molecular mechanism of action of CPE:

Smedley, J. G., 3rd, and B. A. McClane. 2004. Fine mapping of the N-terminal cytotoxicity region of *Clostridium perfringens* enterotoxin by site-directed mutagenesis. *Infect Immun* **72**:6914-23.

Smedley, J. G., 3rd, Uzal, F. A., McClane, B.A. 2007. Identification of a Pre-Pore Large Complex Stage in the Mechanism of Action of *Clostridium perfringens* Enterotoxin. *Infect Immun* In press.

Smedley, J. G., 3rd, and B. A. McClane. 2007. Identification and Analysis of the Hexameric Complexes Formed by *Clostridium perfringens* enterotoxin. Submitted for publication to *Cellular Microbiology*.

Smedley, J. G., 3rd, Saputo, J., Parker, J. C., Fernandez-Miyakawa, M. E., McClane, B. A., Uzal, F. A. 2007. Cytotoxicity is Required for the Enterotoxicity Induced by *Clostridium perfringens* Enterotoxin. Manuscript in preparation.

BIBLIOGRAPHY

1. **Abraham, C., R. J. Carman, H. Hahn, and O. Liesenfeld.** 2001. Similar frequency of detection of *Clostridium perfringens* enterotoxin and *Clostridium difficile* toxins in patients with antibiotic-associated diarrhea. *Eur J Clin Microbiol Infect Dis* **20**:676-677.
2. **Alouf, J. E.** 2006. Paradigms and classification of bacterial membrane-damaging toxins. *In* J. E. Alouf, Popoff, M.R. (ed.), *The Comprehensive Sourcebook of Bacterial Protein Toxins*, Third ed. Academic Press, London.
3. **Alouf, J. E., Popoff, M.R.** 2006. *The Comprehensive Sourcebook of Bacterial Protein Toxins*, Third ed. Academic Press, London.
4. **Arnaout, M. A., S. L. Goodman, and J. P. Xiong.** 2002. Coming to grips with integrin binding to ligands. *Curr Opin Cell Biol* **14**:641-651.
5. **Arnon, S. S.** 1997. Human Tetanus and Human Botulism. *In* J. I. Rood, McClane, B.A., Songer, J.G., Titball, R.W. (ed.), *The Clostridia: Molecular Biology and Pathogenesis*, vol. 95-115. Academic, London.
6. **Asha, N. J., D. Tompkins, and M. H. Wilcox.** 2006. Comparative analysis of prevalence, risk factors, and molecular epidemiology of antibiotic-associated diarrhea due to *Clostridium difficile*, *Clostridium perfringens*, and *Staphylococcus aureus*. *J Clin Microbiol* **44**:2785-2791.
7. **Awad, M. M., D. M. Ellemor, R. L. Boyd, J. J. Emmins, and J. I. Rood.** 2001. Synergistic effects of alpha-toxin and perfringolysin O in *Clostridium perfringens*-mediated gas gangrene. *Infect Immun* **69**:7904-7910.
8. **Baba Moussa, L., S. Werner, D. A. Colin, L. Mourey, J. D. Pedelacq, J. P. Samama, A. Sanni, H. Monteil, and G. Prevost.** 1999. Decoupling the Ca(2+)-activation from the pore-forming function of the bi-component Panton-Valentine leucocidin in human PMNs. *FEBS Lett* **461**:280-286.
9. **Bacciarini, L. N., P. Boerlin, R. Straub, J. Frey, and A. Grone.** 2003. Immunohistochemical localization of *Clostridium perfringens* beta2-toxin in the gastrointestinal tract of horses. *Vet Pathol* **40**:376-381.
10. **Ballard, J., J. Crabtree, B. A. Roe, and R. K. Tweten.** 1995. The primary structure of *Clostridium septicum* alpha-toxin exhibits similarity with that of *Aeromonas hydrophila* aerolysin. *Infect Immun* **63**:340-344.

11. **Ballard, J., Y. Sokolov, W. L. Yuan, B. L. Kagan, and R. K. Tweten.** 1993. Activation and mechanism of *Clostridium septicum* alpha toxin. *Mol Microbiol* **10**:627-634.
12. **Beaugerie, L., and J. C. Petit.** 2004. Microbial-gut interactions in health and disease. Antibiotic-associated diarrhoea. *Best Pract Res Clin Gastroenterol* **18**:337-352.
13. **Bhakdi, S., R. Fussle, and J. Tranum-Jensen.** 1981. Staphylococcal alpha-toxin: oligomerization of hydrophilic monomers to form amphiphilic hexamers induced through contact with deoxycholate detergent micelles. *Proc Natl Acad Sci U S A* **78**:5475-5479.
14. **Borriello, S. P., H. E. Larson, A. R. Welch, F. Barclay, M. F. Stringer, and B. A. Bartholomew.** 1984. Enterotoxigenic *Clostridium perfringens*: a possible cause of antibiotic-associated diarrhoea. *Lancet* **1**:305-307.
15. **Brett, M. M., J. C. Rodhouse, T. J. Donovan, G. M. Tebbutt, and D. N. Hutchinson.** 1992. Detection of *Clostridium perfringens* and its enterotoxin in cases of sporadic diarrhoea. *J Clin Pathol* **45**:609-611.
16. **Brynstad, S., M. R. Sarker, B. A. McClane, P. E. Granum, and J. I. Rood.** 2001. Enterotoxin plasmid from *Clostridium perfringens* is conjugative. *Infect Immun* **69**:3483-3487.
17. **Bueschel, D. M., B. H. Jost, S. J. Billington, H. T. Trinh, and J. G. Songer.** 2003. Prevalence of *cpb2*, encoding beta2 toxin, in *Clostridium perfringens* field isolates: correlation of genotype with phenotype. *Vet Microbiol* **94**:121-129.
18. **Carman, R. J.** 1997. *Clostridium perfringens* in spontaneous and antibiotic-associated diarrhoea of man and other animals. *Rev Med Microbiol* **8**:S43-S45.
19. **Chakrabarti, G., and B. A. McClane.** 2005. The importance of calcium influx, calpain and calmodulin for the activation of CaCo-2 cell death pathways by *Clostridium perfringens* enterotoxin. *Cell Microbiol* **7**:129-146.
20. **Chakrabarti, G., X. Zhou, and B. A. McClane.** 2003. Death pathways activated in CaCo-2 cells by *Clostridium perfringens* enterotoxin. *Infect Immun* **71**:4260-4270.
21. **Charles, P. D.** 2004. Botulinum neurotoxin serotype A: a clinical update on non-cosmetic uses. *Am J Health Syst Pharm* **61**:S11-23.
22. **Cheley, S., M. S. Malghani, L. Song, M. Hobaugh, J. E. Gouaux, J. Yang, and H. Bayley.** 1997. Spontaneous oligomerization of a staphylococcal alpha-hemolysin conformationally constrained by removal of residues that form the transmembrane beta-barrel. *Protein Eng* **10**:1433-1443.
23. **Colegio, O. R., C. Van Itallie, C. Rahner, and J. M. Anderson.** 2003. Claudin extracellular domains determine paracellular charge selectivity and resistance but not tight junction fibril architecture. *Am J Physiol Cell Physiol* **284**:C1346-1354.
24. **Collee, J. G.** 1954. Food poisoning due to *Cl. welchii*. *J R Army Med Corps* **100**:296-299.

25. **Collee, J. G.** 1955. A further outbreak of food poisoning due to *Cl. welchii*. J R Army Med Corps **101**:46-49.
26. **Collie, R. E., J. F. Kokai-Kun, and B. A. McClane.** 1998. Phenotypic Characterization of Enterotoxigenic *Clostridium perfringens* Isolates from Non-foodborne Human Gastrointestinal Diseases. Anaerobe **4**:69-79.
27. **Collie, R. E., and B. A. McClane.** 1998. Evidence that the enterotoxin gene can be episomal in *Clostridium perfringens* isolates associated with non-food-borne human gastrointestinal diseases. J Clin Microbiol **36**:30-36.
28. **Czczulin, J. R., R. E. Collie, and B. A. McClane.** 1996. Regulated expression of *Clostridium perfringens* enterotoxin in naturally cpe-negative type A, B, and C isolates of *C. perfringens*. Infect Immun **64**:3301-3309.
29. **Czczulin, J. R., P. C. Hanna, and B. A. McClane.** 1993. Cloning, nucleotide sequencing, and expression of the *Clostridium perfringens* enterotoxin gene in *Escherichia coli*. Infect Immun **61**:3429-3439.
30. **Deleage, G., and B. Roux.** 1987. An algorithm for protein secondary structure prediction based on class prediction. Protein Eng **1**:289-294.
31. **Duncan, C. L., and D. H. Strong.** 1969. Ileal loop fluid accumulation and production of diarrhea in rabbits by cell-free products of *Clostridium perfringens*. J Bacteriol **100**:86-94.
32. **Duncan, C. L., D. H. Strong, and M. Sebald.** 1972. Sporulation and enterotoxin production by mutants of *Clostridium perfringens*. J Bacteriol **110**:378-391.
33. **Duncan, C. L., H. Sugiyama, and D. H. Strong.** 1968. Rabbit ileal loop response to strains of *Clostridium perfringens*. J Bacteriol **95**:1560-1566.
34. **Ebihara, C., M. Kondoh, M. Harada, M. Fujii, H. Mizuguchi, S. I. Tsunoda, Y. Horiguchi, K. Yagi, and Y. Watanabe.** 2006. Role of Tyr306 in the C-terminal fragment of *Clostridium perfringens* enterotoxin for modulation of tight junction. Biochem Pharmacol.
35. **Ebihara, C., M. Kondoh, N. Hasuike, M. Harada, H. Mizuguchi, Y. Horiguchi, M. Fujii, and Y. Watanabe.** 2006. Preparation of a claudin-targeting molecule using a C-terminal fragment of *Clostridium perfringens* enterotoxin. J Pharmacol Exp Ther **316**:255-260.
36. **Enders, G. L., Jr., and C. L. Duncan.** 1976. Anomalous aggregation of *Clostridium perfringens* enterotoxin under dissociating conditions. Can J Microbiol **22**:1410-1414.
37. **Engstrom, B. E., C. Fermer, A. Lindberg, E. Saarinen, V. Baverud, and A. Gunnarsson.** 2003. Molecular typing of isolates of *Clostridium perfringens* from healthy and diseased poultry. Vet Microbiol **94**:225-235.

38. **Fagerlund, A., O. Ween, T. Lund, S. P. Hardy, and P. E. Granum.** 2004. Genetic and functional analysis of the cytK family of genes in *Bacillus cereus*. *Microbiology* **150**:2689-2697.
39. **Ferguson, K. A.** 1964. Starch-Gel Electrophoresis--Application to the Classification of Pituitary Proteins and Polypeptides. *Metabolism* **13**:SUPPL:985-1002.
40. **Fernandez-Miyakawa, M. E., Fisher, D.F, Poon, R., Sayeed, S., Adams, V., Rood, J, McClane, B.A., Uzal, F.A.** 2007. Both epsilon toxin and beta-toxin are important for the lethal properties of *Clostridium perfringens* type B isolates in the mouse intravenous injection model. *Infect Immun*.
41. **Fernandez Miyakawa, M. E., V. Pistone Creydt, F. A. Uzal, B. A. McClane, and C. Ibarra.** 2005. *Clostridium perfringens* enterotoxin damages the human intestine *in vitro*. *Infect Immun* **73**:8407-8410.
42. **Fisher, D. J.** 2006. *Clostridium perfringens* Beta2 Toxin: A Potential Accessory Toxin In Gastrointestinal Diseases of Humans and Domestic Animals. University of Pittsburgh School of Medicine, Pittsburgh.
43. **Fisher, D. J., M. E. Fernandez-Miyakawa, S. Sayeed, R. Poon, V. Adams, J. I. Rood, F. A. Uzal, and B. A. McClane.** 2006. Dissecting the contributions of *Clostridium perfringens* type C toxins to lethality in the mouse intravenous injection model. *Infect Immun* **74**:5200-5210.
44. **Fisher, D. J., K. Miyamoto, B. Harrison, S. Akimoto, M. R. Sarker, and B. A. McClane.** 2005. Association of beta2 toxin production with *Clostridium perfringens* type A human gastrointestinal disease isolates carrying a plasmid enterotoxin gene. *Mol Microbiol* **56**:747-762.
45. **Fujinaga, Y., K. Inoue, S. Shimazaki, K. Tomochika, K. Tsuzuki, N. Fujii, T. Watanabe, T. Ohyama, K. Takeshi, and et al.** 1994. Molecular construction of *Clostridium botulinum* type C progenitor toxin and its gene organization. *Biochem Biophys Res Commun* **205**:1291-1298.
46. **Fujita, H., H. Chiba, H. Yokozaki, N. Sakai, K. Sugimoto, T. Wada, T. Kojima, T. Yamashita, and N. Sawada.** 2006. Differential expression and subcellular localization of claudin-7, -8, -12, -13, and -15 along the mouse intestine. *J Histochem Cytochem* **54**:933-944.
47. **Fujita, K., J. Katahira, Y. Horiguchi, N. Sonoda, M. Furuse, and S. Tsukita.** 2000. *Clostridium perfringens* enterotoxin binds to the second extracellular loop of claudin-3, a tight junction integral membrane protein. *FEBS Lett* **476**:258-261.
48. **Furuse, M., K. Fujita, T. Hiiragi, K. Fujimoto, and S. Tsukita.** 1998. Claudin-1 and -2: novel integral membrane proteins localizing at tight junctions with no sequence similarity to occludin. *J Cell Biol* **141**:1539-1550.
49. **Furuse, M., H. Sasaki, and S. Tsukita.** 1999. Manner of interaction of heterogeneous claudin species within and between tight junction strands. *J Cell Biol* **147**:891-903.

50. **Furuse, M., and S. Tsukita.** 2006. Claudins in occluding junctions of humans and flies. *Trends Cell Biol* **16**:181-188.
51. **Garmory, H. S., N. Chanter, N. P. French, D. Bueschel, J. G. Songer, and R. W. Titball.** 2000. Occurrence of *Clostridium perfringens* beta2-toxin amongst animals, determined using genotyping and subtyping PCR assays. *Epidemiol Infect* **124**:61-67.
52. **Gershoni, J. M., and G. E. Palade.** 1982. Electrophoretic transfer of proteins from sodium dodecyl sulfate-polyacrylamide gels to a positively charged membrane filter. *Anal Biochem* **124**:396-405.
53. **Gibert, M., C. Jolivet-Reynaud, and M. R. Popoff.** 1997. Beta2 toxin, a novel toxin produced by *Clostridium perfringens*. *Gene* **203**:65-73.
54. **Gill, D. M.** 1982. Bacterial Toxins: a Table of Lethal Amounts. *Microbiological Reviews* **46**:86-94.
55. **Giugliano, L. G., M. F. Stringer, and B. S. Drasar.** 1983. Detection of *Clostridium perfringens* enterotoxin by tissue culture and double-gel diffusion methods. *J Med Microbiol* **16**:233-237.
56. **Gouaux, J. E., O. Braha, M. R. Hobaugh, L. Song, S. Cheley, C. Shustak, and H. Bayley.** 1994. Subunit stoichiometry of staphylococcal alpha-hemolysin in crystals and on membranes: a heptameric transmembrane pore. *Proc Natl Acad Sci U S A* **91**:12828-12831.
57. **Granum, P. E.** 1982. Inhibition of protein synthesis by a tryptic polypeptide of *Clostridium perfringens* type A enterotoxin. *Biochim Biophys Acta* **708**:6-11.
58. **Granum, P. E., Harbitz, O.** 1985. A circular-dichroism study of the enterotoxin from *Clostridium perfringens* type A. *J Food Biochem* **9**:137-146.
59. **Granum, P. E., and M. Richardson.** 1991. Chymotrypsin treatment increases the activity of *Clostridium perfringens* enterotoxin. *Toxicon* **29**:898-900.
60. **Granum, P. E., J. R. Whitaker, and R. Skjelkvale.** 1981. Trypsin activation of enterotoxin from *Clostridium perfringens* type A: fragmentation and some physicochemical properties. *Biochim Biophys Acta* **668**:325-332.
61. **Gray, G. S., and M. Kehoe.** 1984. Primary sequence of the alpha-toxin gene from *Staphylococcus aureus* wood 46. *Infect Immun* **46**:615-618.
62. **Gurcel, L., Iacovache, I., van der Goot, F.G.,** 2006. Aerolysin and related *Aeromonas* toxins. *In* J. E. Alouf, Popoff, M.R. (ed.), *The Comprehensive Sourcebook of Bacterial Protein Toxins*, Third ed. Academic Press, London.
63. **Gyobi, Y., Kodama, H.** 1978. Vero cell microcell culture technique for the detection of neutralization antibody against *Clostridium perfringens* enterotoxin and its application to sero-epidemiology. *J Food Hyg Soc Jap* **19**:294-298.

64. **Hall, T.** 1999. BioEdit: a user-friendly biological sequence alignment editor and analysis program for Windows 95/98/NT. Nucleic acids symposium series **41**:95-98.
65. **Hanna, P. C., and B. A. McClane.** 1991. A recombinant C-terminal toxin fragment provides evidence that membrane insertion is important for *Clostridium perfringens* enterotoxin cytotoxicity. Mol Microbiol **5**:225-230.
66. **Hanna, P. C., T. A. Mietzner, G. K. Schoolnik, and B. A. McClane.** 1991. Localization of the receptor-binding region of *Clostridium perfringens* enterotoxin utilizing cloned toxin fragments and synthetic peptides. The 30 C-terminal amino acids define a functional binding region. J Biol Chem **266**:11037-11043.
67. **Hanna, P. C., E. U. Wieckowski, T. A. Mietzner, and B. A. McClane.** 1992. Mapping of functional regions of *Clostridium perfringens* type A enterotoxin. Infect Immun **60**:2110-2114.
68. **Hanna, P. C., A. P. Wnek, and B. A. McClane.** 1989. Molecular cloning of the 3' half of the *Clostridium perfringens* enterotoxin gene and demonstration that this region encodes receptor-binding activity. J Bacteriol **171**:6815-6820.
69. **Harada, M., M. Kondoh, C. Ebihara, A. Takahashi, E. Komiya, M. Fujii, H. Mizuguchi, S. Tsunoda, Y. Horiguchi, K. Yagi, and Y. Watanabe.** 2007. Role of tyrosine residues in modulation of claudin-4 by the C-terminal fragment of *Clostridium perfringens* enterotoxin. Biochem Pharmacol **73**:206-214.
70. **Hardy, S. P., M. Denmead, N. Parekh, and P. E. Granum.** 1999. Cationic currents induced by *Clostridium perfringens* type A enterotoxin in human intestinal CaCO-2 cells. J Med Microbiol **48**:235-243.
71. **Hardy, S. P., T. Lund, and P. E. Granum.** 2001. CytK toxin of *Bacillus cereus* forms pores in planar lipid bilayers and is cytotoxic to intestinal epithelia. FEMS Microbiol Lett **197**:47-51.
72. **Hardy, S. P., C. Ritchie, M. C. Allen, R. H. Ashley, and P. E. Granum.** 2001. *Clostridium perfringens* type A enterotoxin forms mepacrine-sensitive pores in pure phospholipid bilayers in the absence of putative receptor proteins. Biochim Biophys Acta **1515**:38-43.
73. **Hauschild, A. H., and R. Hilsheimer.** 1971. Purification and characteristics of the enterotoxin of *Clostridium perfringens* type A. Can J Microbiol **17**:1425-1433.
74. **Hauschild, A. H., L. Niilo, and W. J. Dorward.** 1967. Experimental enteritis with food poisoning and classical strains of *Clostridium perfringens* type A in lambs. J Infect Dis **117**:379-386.
75. **Hedrick, J. L., and A. J. Smith.** 1968. Size and charge isomer separation and estimation of molecular weights of proteins by disc gel electrophoresis. Arch Biochem Biophys **126**:155-164.

76. **Heredia, N. L., R. G. Labbe, M. A. Rodriguez, and J. S. Garcia-Alvarado.** 1991. Growth, sporulation and enterotoxin production by *Clostridium perfringens* type A in the presence of human bile salts. *FEMS Microbiol Lett* **68**:15-21.
77. **Heuck, A. P., E. M. Hotze, R. K. Tweten, and A. E. Johnson.** 2000. Mechanism of membrane insertion of a multimeric beta-barrel protein: perfringolysin O creates a pore using ordered and coupled conformational changes. *Mol Cell* **6**:1233-1242.
78. **Horiguchi, Y., T. Akai, and G. Sakaguchi.** 1987. Isolation and function of a *Clostridium perfringens* enterotoxin fragment. *Infect Immun* **55**:2912-2915.
79. **Horiguchi, Y., T. Uemura, S. Kozaki, and G. Sakaguchi.** 1986. Effects of Ca²⁺ and other cations on the action of *Clostridium perfringens* enterotoxin. *Biochim Biophys Acta* **889**:65-71.
80. **Horton, R. M., H. D. Hunt, S. N. Ho, J. K. Pullen, and L. R. Pease.** 1989. Engineering hybrid genes without the use of restriction enzymes: gene splicing by overlap extension. *Gene* **77**:61-68.
81. **Huang, I. H., M. Waters, R. R. Grau, and M. R. Sarker.** 2004. Disruption of the gene (spo0A) encoding sporulation transcription factor blocks endospore formation and enterotoxin production in enterotoxigenic *Clostridium perfringens* type A. *FEMS Microbiol Lett* **233**:233-240.
82. **Hunter, S. E., J. E. Brown, P. C. Oyston, J. Sakurai, and R. W. Titball.** 1993. Molecular genetic analysis of beta-toxin of *Clostridium perfringens* reveals sequence homology with alpha-toxin, gamma-toxin, and leukocidin of *Staphylococcus aureus*. *Infect Immun* **61**:3958-3965.
83. **Ikigai, H., A. Akatsuka, H. Tsujiyama, T. Nakae, and T. Shimamura.** 1996. Mechanism of membrane damage by El Tor hemolysin of *Vibrio cholerae* O1. *Infect Immun* **64**:2968-2973.
84. **Ikigai, H., and T. Nakae.** 1985. Conformational alteration in alpha-toxin from *Staphylococcus aureus* concomitant with the transformation of the water-soluble monomer to the membrane oligomer. *Biochem Biophys Res Commun* **130**:175-181.
85. **Ishibashi, Y., D. A. Relman, and A. Nishikawa.** 2001. Invasion of human respiratory epithelial cells by *Bordetella pertussis*: possible role for a filamentous hemagglutinin Arg-Gly-Asp sequence and alpha5beta1 integrin. *Microb Pathog* **30**:279-288.
86. **Jayasinghe, L., and H. Bayley.** 2005. The leukocidin pore: evidence for an octamer with four LukF subunits and four LukS subunits alternating around a central axis. *Protein Sci* **14**:2550-2561.
87. **Justus, P. G., Mathias, J.R., Carlson, G.M., Martin, J.L., Formal, S., Shields, R.P.** 1980. The myoelectric activity of the small intestine in response to *Clostridium perfringens* A enterotoxin and *Clostridium difficile* culture filtrate., p. 379-386. *In* J. Christensen (ed.), *Gastrointestinal Mobility*. Raven Press, New York.

88. **Katahira, J., N. Inoue, Y. Horiguchi, M. Matsuda, and N. Sugimoto.** 1997. Molecular cloning and functional characterization of the receptor for *Clostridium perfringens* enterotoxin. *J Cell Biol* **136**:1239-1247.
89. **Katahira, J., H. Sugiyama, N. Inoue, Y. Horiguchi, M. Matsuda, and N. Sugimoto.** 1997. *Clostridium perfringens* enterotoxin utilizes two structurally related membrane proteins as functional receptors *in vivo*. *J Biol Chem* **272**:26652-26658.
90. **Katayama, S., B. Dupuy, G. Daube, B. China, and S. T. Cole.** 1996. Genome mapping of *Clostridium perfringens* strains with I-Ceul shows many virulence genes to be plasmid-borne. *Mol Gen Genet* **251**:720-726.
91. **Katic, R., M. Lompar, and Z. Vukicevic.** 1958. *Clostridium perfringens (welchii)* as a causative factor of toxico-infection in a military establishment. *Vojnosanit Pregl* **15**:163-167.
92. **Kokai-Kun, J. F., K. Benton, E. U. Wieckowski, and B. A. McClane.** 1999. Identification of a *Clostridium perfringens* enterotoxin region required for large complex formation and cytotoxicity by random mutagenesis. *Infect Immun* **67**:5634-5641.
93. **Kokai-Kun, J. F., and B. A. McClane.** 1997. Deletion analysis of the *Clostridium perfringens* enterotoxin. *Infect Immun* **65**:1014-1022.
94. **Kokai-Kun, J. F., and B. A. McClane.** 1996. Evidence that a region(s) of the *Clostridium perfringens* enterotoxin molecule remains exposed on the external surface of the mammalian plasma membrane when the toxin is sequestered in small or large complexes. *Infect Immun* **64**:1020-1025.
95. **Kominsky, S. L.** 2006. Claudins: emerging targets for cancer therapy. *Expert Rev Mol Med* **8**:1-11.
96. **Kondoh, M., A. Masuyama, A. Takahashi, N. Asano, H. Mizuguchi, N. Koizumi, M. Fujii, T. Hayakawa, Y. Horiguchi, and Y. Watanbe.** 2005. A novel strategy for the enhancement of drug absorption using a claudin modulator. *Mol Pharmacol* **67**:749-756.
97. **Kyte, J., and R. F. Doolittle.** 1982. A simple method for displaying the hydrophobic character of a protein. *J Mol Biol* **157**:105-132.
98. **Labbe, R. G.** 1989. *Clostridium perfringens*, p. 192-234. *In* M. P. Doyle (ed.), *Foodborne Bacterial Pathogens*. Marcel Dekker, New York.
99. **Leppla, S. H.** 2006. *Bacillus anthracis* toxins. *In* J. E. Alouf, Popoff, M.R. (ed.), *The Comprehensive Sourcebook of Bacterial Protein Toxins*, Third ed. Academic Press, London.
100. **Leppla, S. H.** 1988. Production and purification of anthrax toxin. *Methods Enzymol* **165**:103-116.
101. **Loffler, A., and R. Labbe.** 1986. Characterization of a parasporal inclusion body from sporulating, enterotoxin-positive *Clostridium perfringens* type A. *J Bacteriol* **165**:542-548.

102. **Loffler, A., Labbe, R.G.** 1986. Isolation of an inclusion body from sporulating, enterotoxin-positive *Clostridium perfringens*. FEMS Microbiol **27**:143-147.
103. **Manteca, C., G. Daube, T. Jauniaux, A. Linden, V. Pirson, J. Detilleux, A. Ginter, P. Coppe, A. Kaeckenbeeck, and J. G. Mainil.** 2002. A role for the *Clostridium perfringens* beta2 toxin in bovine enterotoxaemia? Vet Microbiol **86**:191-202.
104. **Masignani, V., Pizza, M., Rappuoli, R.** 2006. Molecular, functional, and evolutionary aspects of ADP-ribosylating toxins, p. 213-244. In J. E. Alouf, Popoff, M.R. (ed.), The Comprehensive Sourcebook of Bacterial Protein Toxins, Third ed. Academic Press, London.
105. **Masuyama, A., M. Kondoh, H. Seguchi, A. Takahashi, M. Harada, M. Fujii, H. Mizuguchi, Y. Horiguchi, and Y. Watanabe.** 2005. Role of N-terminal amino acids in the absorption-enhancing effects of the c-terminal fragment of *Clostridium perfringens* enterotoxin. J Pharmacol Exp Ther **314**:789-795.
106. **Matsuda, M., A. Kubo, M. Furuse, and S. Tsukita.** 2004. A peculiar internalization of claudins, tight junction-specific adhesion molecules, during the intercellular movement of epithelial cells. J Cell Sci **117**:1247-1257.
107. **Matsuda, M., K. Ozutsumi, H. Iwahashi, and N. Sugimoto.** 1986. Primary action of *Clostridium perfringens* type A enterotoxin on HeLa and Vero cells in the absence of extracellular calcium: rapid and characteristic changes in membrane permeability. Biochem Biophys Res Commun **141**:704-710.
108. **Matsuda, M., and N. Sugimoto.** 1979. Calcium-independent and dependent steps in action of *Clostridium perfringens* enterotoxin on HeLa and Vero cells. Biochem Biophys Res Commun **91**:629-636.
109. **McClain, M. S., P. Cao, and T. L. Cover.** 2001. Amino-terminal hydrophobic region of *Helicobacter pylori* vacuolating cytotoxin (VacA) mediates transmembrane protein dimerization. Infect Immun **69**:1181-1184.
110. **McClain, M. S., H. Iwamoto, P. Cao, A. D. Vinion-Dubiel, Y. Li, G. Szabo, Z. Shao, and T. L. Cover.** 2003. Essential role of a GXXXG motif for membrane channel formation by *Helicobacter pylori* vacuolating toxin. J Biol Chem **278**:12101-12108.
111. **McClane, B. A.** 2006. *Clostridium perfringens* enterotoxin. In J. E. Alouf, Popoff, M.R. (ed.), The Comprehensive Sourcebook of Bacterial Protein Toxins, Third ed. Academic Press, London.
112. **McClane, B. A.** 1994. *Clostridium perfringens* enterotoxin acts by producing small molecule permeability alterations in plasma membranes. Toxicology **87**:43-67.
113. **McClane, B. A.** 2000. *Clostridium perfringens* enterotoxin and intestinal tight junctions. Trends Microbiol **8**:145-146.
114. **McClane, B. A.** 1984. Osmotic stabilizers differentially inhibit permeability alterations induced in Vero cells by *Clostridium perfringens* enterotoxin. Biochim Biophys Acta **777**:99-106.

115. **McClane, B. A., and J. L. McDonel.** 1980. Characterization of membrane permeability alterations induced in Vero cells by *Clostridium perfringens* enterotoxin. *Biochim Biophys Acta* **600**:974-985.
116. **McClane, B. A., and J. L. McDonel.** 1979. The effects of *Clostridium perfringens* enterotoxin on morphology, viability, and macromolecular synthesis in Vero cells. *J Cell Physiol* **99**:191-200.
117. **McClane, B. A., and A. P. Wnek.** 1990. Studies of *Clostridium perfringens* enterotoxin action at different temperatures demonstrate a correlation between complex formation and cytotoxicity. *Infect Immun* **58**:3109-3115.
118. **McClane, B. A., A. P. Wnek, K. I. Hulkower, and P. C. Hanna.** 1988. Divalent cation involvement in the action of *Clostridium perfringens* type A enterotoxin. Early events in enterotoxin action are divalent cation-independent. *J Biol Chem* **263**:2423-2435.
119. **McDonel, J. L.** 1980. Binding of *Clostridium perfringens* [¹²⁵I]enterotoxin to rabbit intestinal cells. *Biochemistry* **19**:4801-4807.
120. **McDonel, J. L.** 1980. *Clostridium perfringens* toxins (type A, B, C, D, E). *Pharmacol Ther* **10**:617-655.
121. **McDonel, J. L.** 1974. *In Vivo* Effects of *Clostridium perfringens* Enteropathogenic Factors on the Rat Ileum. *Infect Immun* **10**:1156-1162.
122. **McDonel, J. L.** 1986. Toxins of *Clostridium perfringens* (types A, B, C, D, and E), p. 477-506. *In* F. Dorner, Drews, J. (ed.), *Pharmacology of Bacterial Toxins*. Pergamon Press, New York.
123. **McDonel, J. L., L. W. Chang, J. G. Pounds, and C. L. Duncan.** 1978. The effects of *Clostridium perfringens* enterotoxin on rat and rabbit ileum: an electron microscopic study. *Lab Invest* **39**:210-218.
124. **McDonel, J. L., and C. L. Duncan.** 1975. Histopathological effect of *Clostridium perfringens* enterotoxin in the rabbit ileum. *Infect Immun* **12**:1214-1218.
125. **McDonel, J. L., Duncan, C.L.** 1975. Presented at the 11th Joint Conference U.S.-Japan Cooperative Medical Science Program, Cholera Panel.
126. **McDonel, J. L., and B. A. McClane.** 1979. Binding versus biological activity of *Clostridium perfringens* enterotoxin in Vero cells. *Biochem Biophys Res Commun* **87**:497-504.
127. **McDonel, J. L., and B. A. McClane.** 1988. Production, purification, and assay of *Clostridium perfringens* enterotoxin. *Methods Enzymol* **165**:94-103.
128. **McKillop, E. J.** 1959. Bacterial contamination of hospital food with special reference to *Clostridium welchii* food poisoning. *J Hyg (Lond)* **57**:31-46.

129. **Meinhardt, S. W., W. Cheng, C. Y. Kwon, C. M. Donohue, and J. B. Rasmussen.** 2002. Role of the arginyl-glycyl-aspartic motif in the action of Ptr ToxA produced by *Pyrenophora tritici-repentis*. *Plant Physiol* **130**:1545-1551.
130. **Melton, J., Tweten, R.K.** 2006. *Clostridium septicum* pore-forming alpha toxin. In J. E. Alouf, Popoff, M.R. (ed.), *The Comprehensive Sourcebook of Bacterial Protein Toxins*, Third ed. Academic Press, London.
131. **Melton, J. A., M. W. Parker, J. Rossjohn, J. T. Buckley, and R. K. Tweten.** 2004. The identification and structure of the membrane-spanning domain of the *Clostridium septicum* alpha toxin. *J Biol Chem* **279**:14315-14322.
132. **Menestrina, G., M. D. Serra, and G. Prevost.** 2001. Mode of action of beta-barrel pore-forming toxins of the staphylococcal alpha-hemolysin family. *Toxicon* **39**:1661-1672.
133. **Menier, V., Bourrie, M., Berger, Y., Fabre, G.** 1995. The human intestinal epithelial cell line Caco-2; pharmacological and pharmacokinetic applications. *Cell Biology and Toxicology* **11**:187-194.
134. **Michelet, N., Granum, P.E., Mahillon, J.** 2006. *Bacillus cereus* enterotoxins, bi- and tri-component cytolytins, and other hemolysins. In J. E. Alouf, Popoff, M.R. (ed.), *The Comprehensive Sourcebook of Bacterial Protein Toxins*, Third ed. Academic Press, London.
135. **Michl, P., M. Buchholz, M. Rolke, S. Kunsch, M. Lohr, B. McClane, S. Tsukita, G. Leder, G. Adler, and T. M. Gress.** 2001. Claudin-4: a new target for pancreatic cancer treatment using *Clostridium perfringens* enterotoxin. *Gastroenterology* **121**:678-684.
136. **Mietzner, T. A., J. F. Kokai-Kun, P. C. Hanna, and B. A. McClane.** 1992. A conjugated synthetic peptide corresponding to the C-terminal region of *Clostridium perfringens* type A enterotoxin elicits an enterotoxin-neutralizing antibody response in mice. *Infect Immun* **60**:3947-3951.
137. **Miles, G., L. Movileanu, and H. Bayley.** 2002. Subunit composition of a bicomponent toxin: staphylococcal leukocidin forms an octameric transmembrane pore. *Protein Sci* **11**:894-902.
138. **Miller, C. J., J. L. Elliott, and R. J. Collier.** 1999. Anthrax protective antigen: prepore-to-pore conversion. *Biochemistry* **38**:10432-10441.
139. **Mitic, L. L., V. M. Unger, and J. M. Anderson.** 2003. Expression, solubilization, and biochemical characterization of the tight junction transmembrane protein claudin-4. *Protein Sci* **12**:218-227.
140. **Miyamoto, K., G. Chakrabarti, Y. Morino, and B. A. McClane.** 2002. Organization of the plasmid *cpe* locus in *Clostridium perfringens* type A isolates. *Infect Immun* **70**:4261-4272.
141. **Miyamoto, K., D. J. Fisher, J. Li, S. Sayeed, S. Akimoto, and B. A. McClane.** 2006. Complete sequencing and diversity analysis of the enterotoxin-encoding plasmids in

- Clostridium perfringens* type A non-food-borne human gastrointestinal disease isolates. J Bacteriol **188**:1585-1598.
142. **Miyamoto, K., Q. Wen, and B. A. McClane.** 2004. Multiplex PCR genotyping assay that distinguishes between isolates of *Clostridium perfringens* type A carrying a chromosomal enterotoxin gene (cpe) locus, a plasmid cpe locus with an IS1470-like sequence, or a plasmid cpe locus with an IS1151 sequence. J Clin Microbiol **42**:1552-1558.
 143. **Miyata, S., O. Matsushita, J. Minami, S. Katayama, S. Shimamoto, and A. Okabe.** 2001. Cleavage of a C-terminal peptide is essential for heptamerization of *Clostridium perfringens* epsilon-toxin in the synaptosomal membrane. J Biol Chem **276**:13778-13783.
 144. **Miyata, S., J. Minami, E. Tamai, O. Matsushita, S. Shimamoto, and A. Okabe.** 2002. *Clostridium perfringens* epsilon-toxin forms a heptameric pore within the detergent-insoluble microdomains of Madin-Darby canine kidney cells and rat synaptosomes. J Biol Chem **277**:39463-39468.
 145. **Moniatte, M., F. G. van der Goot, J. T. Buckley, F. Pattus, and A. van Dorselaer.** 1996. Characterisation of the heptameric pore-forming complex of the *Aeromonas* toxin aerolysin using MALDI-TOF mass spectrometry. FEBS Lett **384**:269-272.
 146. **Morita, K., M. Furuse, K. Fujimoto, and S. Tsukita.** 1999. Claudin multigene family encoding four-transmembrane domain protein components of tight junction strands. Proc Natl Acad Sci U S A **96**:511-516.
 147. **Mourez, M., M. Yan, D. B. Lacy, L. Dillon, L. Bentsen, A. Marpoe, C. Maurin, E. Hotze, D. Wigelsworth, R. A. Pimental, J. D. Ballard, R. J. Collier, and R. K. Tweten.** 2003. Mapping dominant-negative mutations of anthrax protective antigen by scanning mutagenesis. Proc Natl Acad Sci U S A **100**:13803-13808.
 148. **Mpamugo, O., T. Donovan, and M. M. Brett.** 1995. Enterotoxigenic *Clostridium perfringens* as a cause of sporadic cases of diarrhoea. J Med Microbiol **43**:442-445.
 149. **Myers, G. S., D. A. Rasko, J. K. Cheung, J. Ravel, R. Seshadri, R. T. DeBoy, Q. Ren, J. Varga, M. M. Awad, L. M. Brinkac, S. C. Daugherty, D. H. Haft, R. J. Dodson, R. Madupu, W. C. Nelson, M. J. Rosovitz, S. A. Sullivan, H. Khouri, G. I. Dimitrov, K. L. Watkins, S. Mulligan, J. Benton, D. Radune, D. J. Fisher, H. S. Atkins, T. Hiscox, B. H. Jost, S. J. Billington, J. G. Songer, B. A. McClane, R. W. Titball, J. I. Rood, S. B. Melville, and I. T. Paulsen.** 2006. Skewed genomic variability in strains of the toxigenic bacterial pathogen, *Clostridium perfringens*. Genome Res **16**:1031-1040.
 150. **Nagahama, M., S. Hayashi, S. Morimitsu, and J. Sakurai.** 2003. Biological activities and pore formation of *Clostridium perfringens* beta toxin in HL 60 cells. J Biol Chem **278**:36934-36941.
 151. **Naik, H. S., and C. L. Duncan.** 1978. Detection of *Clostridium perfringens* enterotoxin in human fecal samples and anti-enterotoxin in sera. J Clin Microbiol **7**:337-340.

152. **Nguyen, V. T., Y. Kamio, and H. Higuchi.** 2003. Single-molecule imaging of cooperative assembly of gamma-hemolysin on erythrocyte membranes. *EMBO J* **22**:4968-4979.
153. **Niilo, L.** 1974. Response of ligated intestinal loops in chickens to the enterotoxin of *Clostridium perfringens*. *Appl Microbiol* **28**:889-891.
154. **Nusrat, A., G. T. Brown, J. Tom, A. Drake, T. T. Bui, C. Quan, and R. J. Mrsny.** 2005. Multiple protein interactions involving proposed extracellular loop domains of the tight junction protein occludin. *Mol Biol Cell* **16**:1725-1734.
155. **Olsen, S. J., L. C. MacKinnon, J. S. Goulding, N. H. Bean, and L. Slutsker.** 2000. Surveillance for foodborne-disease outbreaks--United States, 1993-1997. *MMWR CDC Surveill Summ* **49**:1-62.
156. **Olson, R., H. Nariya, K. Yokota, Y. Kamio, and E. Gouaux.** 1999. Crystal structure of staphylococcal LukF delineates conformational changes accompanying formation of a transmembrane channel. *Nat Struct Biol* **6**:134-140.
157. **Parker, M. W., J. T. Buckley, J. P. Postma, A. D. Tucker, K. Leonard, F. Pattus, and D. Tsernoglou.** 1994. Structure of the *Aeromonas* toxin proaerolysin in its water-soluble and membrane-channel states. *Nature* **367**:292-295.
158. **Parker, M. W., and S. C. Feil.** 2005. Pore-forming protein toxins: from structure to function. *Prog Biophys Mol Biol* **88**:91-142.
159. **Petit, L., M. Gibert, A. Gouch, M. Bens, A. Vandewalle, and M. R. Popoff.** 2003. *Clostridium perfringens* epsilon toxin rapidly decreases membrane barrier permeability of polarized MDCK cells. *Cell Microbiol* **5**:155-164.
160. **Petit, L., E. Maier, M. Gibert, M. R. Popoff, and R. Benz.** 2001. *Clostridium perfringens* epsilon toxin induces a rapid change of cell membrane permeability to ions and forms channels in artificial lipid bilayers. *J Biol Chem* **276**:15736-15740.
161. **Prevost, G., Mourey, L., Colin, D.A., Monteil, H., Dalla Serra, M., Menestrina, G.** 2006. Alpha-helix and beta-barrel pore-forming toxins (leukocidins, alpha-, gamma-, and delta-cytolysins) of *Staphylococcus aureus*. In J. E. Alouf, Popoff, M.R. (ed.), *The Comprehensive Sourcebook of Bacterial Protein Toxins*, Third ed. Academic Press, London.
162. **Rahner, C., L. L. Mitic, and J. M. Anderson.** 2001. Heterogeneity in expression and subcellular localization of claudins 2, 3, 4, and 5 in the rat liver, pancreas, and gut. *Gastroenterology* **120**:411-422.
163. **Richard, J. F., L. Petit, M. Gibert, J. C. Marvaud, C. Bouchaud, and M. R. Popoff.** 1999. Bacterial toxins modifying the actin cytoskeleton. *Int Microbiol* **2**:185-194.
164. **Richardson, M., and P. E. Granum.** 1985. The amino acid sequence of the enterotoxin from *Clostridium perfringens* type A. *FEBS Lett* **182**:479-484.

165. **Richardson, M., and P. E. Granum.** 1983. Sequence of the amino-terminal part of enterotoxin from *Clostridium perfringens* type A: identification of points of trypsin activation. *Infect Immun* **40**:943-949.
166. **Robertson, S. L., Singh, U., Chakrabarti, G., Van Itallie, C.M., Anderson, J.M., McClane, B.A.** 2007. *Clostridium perfringens* enterotoxin interactions with claudins in naturally-sensitive Caco-2 cells and transfected fibroblasts. Submitted for publication.
167. **Rood, J. I.** 1997. Genetic analysis in *C. perfringens*, p. 65-72. *In* J. I. Rood, McClane, B.A., Songer, J.G., Titball, R.W. (ed.), *The Clostridia: Molecular Biology and Pathogenesis*. Academic, London.
168. **Rood, J. I.** 1998. Virulence genes of *Clostridium perfringens*. *Annu Rev Microbiol* **52**:333-360.
169. **Rossjohn, J., S. C. Feil, W. J. McKinstry, R. K. Tweten, and M. W. Parker.** 1997. Structure of a cholesterol-binding, thiol-activated cytolysin and a model of its membrane form. *Cell* **89**:685-692.
170. **Rost, B., and C. Sander.** 1993. Prediction of protein secondary structure at better than 70% accuracy. *J Mol Biol* **232**:584-599.
171. **Ruoslahti, E.** 1996. RGD and other recognition sequences for integrins. *Annu Rev Cell Dev Biol* **12**:697-715.
172. **Sakurai, J., M. Nagahama, and M. Oda.** 2004. *Clostridium perfringens* alpha-toxin: characterization and mode of action. *J Biochem (Tokyo)* **136**:569-574.
173. **Salinovich, O., W. L. Mattice, and E. W. Blakeney, Jr.** 1982. Effects of temperature, pH and detergents on the molecular conformation of the enterotoxin of *Clostridium perfringens*. *Biochim Biophys Acta* **707**:147-153.
174. **Santin, A. D., S. Cane, S. Bellone, M. Palmieri, E. R. Siegel, M. Thomas, J. J. Roman, A. Burnett, M. J. Cannon, and S. Pecorelli.** 2005. Treatment of chemotherapy-resistant human ovarian cancer xenografts in C.B-17/SCID mice by intraperitoneal administration of *Clostridium perfringens* enterotoxin. *Cancer Res* **65**:4334-4342.
175. **Sarker, M. R., R. J. Carman, and B. A. McClane.** 1999. Inactivation of the gene (*cpe*) encoding *Clostridium perfringens* enterotoxin eliminates the ability of two *cpe*-positive *C. perfringens* type A human gastrointestinal disease isolates to affect rabbit ileal loops. *Mol Microbiol* **33**:946-958.
176. **Sasaki, H., C. Matsui, K. Furuse, Y. Mimori-Kiyosue, M. Furuse, and S. Tsukita.** 2003. Dynamic behavior of paired claudin strands within apposing plasma membranes. *Proc Natl Acad Sci U S A* **100**:3971-3976.
177. **Sayeed, S., M. E. Fernandez-Miyakawa, D. J. Fisher, V. Adams, R. Poon, J. I. Rood, F. A. Uzal, and B. A. McClane.** 2005. Epsilon-toxin is required for most *Clostridium perfringens* type D vegetative culture supernatants to cause lethality in the mouse intravenous injection model. *Infect Immun* **73**:7413-7421.

178. **Sellman, B. R., M. Mourez, and R. J. Collier.** 2001. Dominant-negative mutants of a toxin subunit: an approach to therapy of anthrax. *Science* **292**:695-697.
179. **Shatursky, O., R. Bayles, M. Rogers, B. H. Jost, J. G. Songer, and R. K. Tweten.** 2000. *Clostridium perfringens* beta-toxin forms potential-dependent, cation-selective channels in lipid bilayers. *Infect Immun* **68**:5546-5551.
180. **Shatursky, O., A. P. Heuck, L. A. Shepard, J. Rossjohn, M. W. Parker, A. E. Johnson, and R. K. Tweten.** 1999. The mechanism of membrane insertion for a cholesterol-dependent cytolysin: a novel paradigm for pore-forming toxins. *Cell* **99**:293-299.
181. **Shepard, L. A., A. P. Heuck, B. D. Hamman, J. Rossjohn, M. W. Parker, K. R. Ryan, A. E. Johnson, and R. K. Tweten.** 1998. Identification of a membrane-spanning domain of the thiol-activated pore-forming toxin *Clostridium perfringens* perfringolysin O: an alpha-helical to beta-sheet transition identified by fluorescence spectroscopy. *Biochemistry* **37**:14563-14574.
182. **Sherman, S., E. Klein, and B. A. McClane.** 1994. *Clostridium perfringens* type A enterotoxin induces tissue damage and fluid accumulation in rabbit ileum. *J Diarrhoeal Dis Res* **12**:200-207.
183. **Shimizu, T., K. Ohtani, H. Hirakawa, K. Ohshima, A. Yamashita, T. Shiba, N. Ogasawara, M. Hattori, S. Kuhara, and H. Hayashi.** 2002. Complete genome sequence of *Clostridium perfringens*, an anaerobic flesh-eater. *Proc Natl Acad Sci U S A* **99**:996-1001.
184. **Sigrist, H., P. Ronner, and G. Semenza.** 1975. A hydrophobic form of the small-intestinal sucrase-isomaltase complex. *Biochim Biophys Acta* **406**:433-446.
185. **Singh, U., L. L. Mitic, E. U. Wieckowski, J. M. Anderson, and B. A. McClane.** 2001. Comparative biochemical and immunocytochemical studies reveal differences in the effects of *Clostridium perfringens* enterotoxin on polarized CaCo-2 cells versus Vero cells. *J Biol Chem* **276**:33402-33412.
186. **Singh, U., C. M. Van Itallie, L. L. Mitic, J. M. Anderson, and B. A. McClane.** 2000. CaCo-2 cells treated with *Clostridium perfringens* enterotoxin form multiple large complex species, one of which contains the tight junction protein occludin. *J Biol Chem* **275**:18407-18417.
187. **Singh, Y., K. R. Klimpel, N. Arora, M. Sharma, and S. H. Leppla.** 1994. The chymotrypsin-sensitive site, FFD315, in anthrax toxin protective antigen is required for translocation of lethal factor. *J Biol Chem* **269**:29039-29046.
188. **Skjelkvale, R., and C. L. Duncan.** 1975. Characterization of enterotoxin purified from *Clostridium perfringens* type C. *Infect Immun* **11**:1061-1068.
189. **Skjelkvale, R., and T. Uemura.** 1977. Experimental Diarrhoea in human volunteers following oral administration of *Clostridium perfringens* enterotoxin. *J Appl Bacteriol* **43**:281-286.

190. **Smedley, J. G., 3rd, and B. A. McClane.** 2004. Fine mapping of the N-terminal cytotoxicity region of *Clostridium perfringens* enterotoxin by site-directed mutagenesis. *Infect Immun* **72**:6914-6923.
191. **Smedley, J. G., Uzal, F. A., 3rd, McClane, B.A.** 2007. Identification of a Pre-Pore Large Complex Stage in the Mechanism of Action of *Clostridium perfringens* Enterotoxin. *Infect Immun* **5**:In press.
192. **Song, L., M. R. Hobaugh, C. Shustak, S. Cheley, H. Bayley, and J. E. Gouaux.** 1996. Structure of staphylococcal alpha-hemolysin, a heptameric transmembrane pore. *Science* **274**:1859-1866.
193. **Songer, J. G.** 1996. Clostridial enteric diseases of domestic animals. *Clin Microbiol Rev* **9**:216-234.
194. **Songer, J. G., and F. A. Uzal.** 2005. Clostridial enteric infections in pigs. *J Vet Diagn Invest* **17**:528-536.
195. **Sonoda, N., M. Furuse, H. Sasaki, S. Yonemura, J. Katahira, Y. Horiguchi, and S. Tsukita.** 1999. *Clostridium perfringens* enterotoxin fragment removes specific claudins from tight junction strands: Evidence for direct involvement of claudins in tight junction barrier. *J Cell Biol* **147**:195-204.
196. **Stark, R. L., and C. L. Duncan.** 1971. Biological characteristics of *Clostridium perfringens* type A enterotoxin. *Infect Immun* **4**:89-96.
197. **Stewart, J. J., J. T. White, X. Yan, S. Collins, C. W. Drescher, N. D. Urban, L. Hood, and B. Lin.** 2006. Proteins associated with Cisplatin resistance in ovarian cancer cells identified by quantitative proteomic technology and integrated with mRNA expression levels. *Mol Cell Proteomics* **5**:433-443.
198. **Stockbauer, K. E., L. Magoun, M. Liu, E. H. Burns, Jr., S. Gubba, S. Renish, X. Pan, S. C. Bodary, E. Baker, J. Coburn, J. M. Leong, and J. M. Musser.** 1999. A natural variant of the cysteine protease virulence factor of group A *Streptococcus* with an arginine-glycine-aspartic acid (RGD) motif preferentially binds human integrins alphavbeta3 and alphallbeta3. *Proc Natl Acad Sci U S A* **96**:242-247.
199. **Strong, D. H., C. L. Duncan, and G. Perna.** 1971. *Clostridium perfringens* Type A Food Poisoning II. Response of the Rabbit Ileum as an Indication of Enteropathogenicity of Strains of *Clostridium perfringens* in Human Beings. *Infect Immun* **3**:171-178.
200. **Stultz, C. M., Nambudripad, R., Lathrop, R.H., White, J.V.** 1997. Predicting Protein Structure with Probabilistic Models., p. 447-506. *In* E. E. Bittar (ed.), *Advances in Molecular and Cell Biology*, vol. 22B. JAI Press, Greenwich.
201. **Stultz, C. M., J. V. White, and T. F. Smith.** 1993. Structural analysis based on state-space modeling. *Protein Sci* **2**:305-314.
202. **Sugawara, N., T. Tomita, and Y. Kamio.** 1997. Assembly of *Staphylococcus aureus* gamma-hemolysin into a pore-forming ring-shaped complex on the surface of human erythrocytes. *FEBS Lett* **410**:333-337.

203. **Sugimoto, N., K. Ozutsumi, and M. Matsuda.** 1985. Morphological alterations and changes in cellular cations induced by *Clostridium perfringens* type A enterotoxin in tissue culture cells. *Eur J Epidemiol* **1**:264-273.
204. **Takahashi, A., M. Kondoh, A. Masuyama, M. Fujii, H. Mizuguchi, Y. Horiguchi, and Y. Watanabe.** 2005. Role of C-terminal regions of the C-terminal fragment of *Clostridium perfringens* enterotoxin in its interaction with claudin-4. *J Control Release* **108**:56-62.
205. **Tamai, E., T. Ishida, S. Miyata, O. Matsushita, H. Suda, S. Kobayashi, H. Sonobe, and A. Okabe.** 2003. Accumulation of *Clostridium perfringens* epsilon-toxin in the mouse kidney and its possible biological significance. *Infect Immun* **71**:5371-5375.
206. **Thelestam, M., and R. Mollby.** 1975. Sensitive assay for detection of toxin-induced damage to the cytoplasmic membrane of human diploid fibroblasts. *Infect Immun* **12**:225-232.
207. **Tilley, S. J., and H. R. Saibil.** 2006. The mechanism of pore formation by bacterial toxins. *Curr Opin Struct Biol* **16**:230-236.
208. **Tobkes, N., B. A. Wallace, and H. Bayley.** 1985. Secondary structure and assembly mechanism of an oligomeric channel protein. *Biochemistry* **24**:1915-1920.
209. **Todd, E. C. D.** 1989. Preliminary estimates of costs of food-borne disease in the United States. *J. Food Prot.* **52**:595-601.
210. **Torres, V. J., M. S. McClain, and T. L. Cover.** 2006. Mapping of a domain required for protein-protein interactions and inhibitory activity of a *Helicobacter pylori* dominant-negative VacA mutant protein. *Infect Immun* **74**:2093-2101.
211. **Tsai, C. C., and H. P. Riemann.** 1975. Food poisoning signs in mice induced orally by *Clostridium perfringens* type A enterotoxin. *Taiwan Yi Xue Hui Za Zhi* **74**:310-315.
212. **Tsai, C. C., and H. P. Riemann.** 1975. Oral infection and food poisoning syndrome in mice by enterotoxigenic *Clostridium perfringens* type A. *Taiwan Yi Xue Hui Za Zhi* **74**:361-371.
213. **Tsitrin, Y., C. J. Morton, C. el-Bez, P. Paumard, M. C. Velluz, M. Adrian, J. Dubochet, M. W. Parker, S. Lanzavecchia, and F. G. van der Goot.** 2002. Conversion of a transmembrane to a water-soluble protein complex by a single point mutation. *Nat Struct Biol* **9**:729-733.
214. **Tweten, R. K.** 2005. Cholesterol-dependent cytolysins, a family of versatile pore-forming toxins. *Infect Immun* **73**:6199-6209.
215. **Valeva, A., J. Pongs, S. Bhakdi, and M. Palmer.** 1997. Staphylococcal alpha-toxin: the role of the N-terminus in formation of the heptameric pore -- a fluorescence study. *Biochim Biophys Acta* **1325**:281-286.
216. **Van Itallie, C. M., and J. M. Anderson.** 2006. Claudins and epithelial paracellular transport. *Annu Rev Physiol* **68**:403-429.

217. **Van Itallie, C. M., and J. M. Anderson.** 2004. The molecular physiology of tight junction pores. *Physiology (Bethesda)* **19**:331-338.
218. **Van Itallie, C. M., A. S. Fanning, and J. M. Anderson.** 2003. Reversal of charge selectivity in cation or anion-selective epithelial lines by expression of different claudins. *Am J Physiol Renal Physiol* **285**:F1078-1084.
219. **Varga, J. J., V. Nguyen, D. K. O'Brien, K. Rodgers, R. A. Walker, and S. B. Melville.** 2006. Type IV pili-dependent gliding motility in the Gram-positive pathogen *Clostridium perfringens* and other clostridia. *Mol Microbiol* **62**:680-694.
220. **Vinion-Dubiel, A. D., M. S. McClain, D. M. Czajkowsky, H. Iwamoto, D. Ye, P. Cao, W. Schraw, G. Szabo, S. R. Blanke, Z. Shao, and T. L. Cover.** 1999. A dominant negative mutant of *Helicobacter pylori* vacuolating toxin (VacA) inhibits VacA-induced cell vacuolation. *J Biol Chem* **274**:37736-37742.
221. **Wai, S. N., M. Westermark, J. Oscarsson, J. Jass, E. Maier, R. Benz, and B. E. Uhlin.** 2003. Characterization of dominantly negative mutant ClyA cytotoxin proteins in *Escherichia coli*. *J Bacteriol* **185**:5491-5499.
222. **Walker, B., and H. Bayley.** 1995. Key residues for membrane binding, oligomerization, and pore forming activity of staphylococcal alpha-hemolysin identified by cysteine scanning mutagenesis and targeted chemical modification. *J Biol Chem* **270**:23065-23071.
223. **Walker, B., M. Krishnasastri, L. Zorn, and H. Bayley.** 1992. Assembly of the oligomeric membrane pore formed by Staphylococcal alpha-hemolysin examined by truncation mutagenesis. *J Biol Chem* **267**:21782-21786.
224. **Weiss, K. F., D. H. Strong, and R. A. Groom.** 1966. Mice and monkeys as assay animals for *Clostridium perfringens* food poisoning. *Appl Microbiol* **14**:479-485.
225. **Wen, Q., K. Miyamoto, and B. A. McClane.** 2003. Development of a duplex PCR genotyping assay for distinguishing *Clostridium perfringens* type A isolates carrying chromosomal enterotoxin (*cpe*) genes from those carrying plasmid-borne enterotoxin (*cpe*) genes. *J Clin Microbiol* **41**:1494-1498.
226. **Whitaker, J. R.** 1963. Determination of the molecular weights of proteins by gel filtration on Sephadex. *Anal Chem* **35**:1950-1953.
227. **White, J. V., C. M. Stultz, and T. F. Smith.** 1994. Protein classification by stochastic modeling and optimal filtering of amino-acid sequences. *Math Biosci* **119**:35-75.
228. **Wieckowski, E. U., J. F. Kokai-Kun, and B. A. McClane.** 1998. Characterization of membrane-associated *Clostridium perfringens* enterotoxin following pronase treatment. *Infect Immun* **66**:5897-5905.
229. **Wieckowski, E. U., A. P. Wnek, and B. A. McClane.** 1994. Evidence that an approximately 50-kDa mammalian plasma membrane protein with receptor-like properties mediates the amphiphilicity of specifically bound *Clostridium perfringens* enterotoxin. *J Biol Chem* **269**:10838-10848.

230. **Wilmsen, H. U., K. R. Leonard, W. Tichelaar, J. T. Buckley, and F. Pattus.** 1992. The aerolysin membrane channel is formed by heptamerization of the monomer. *Embo J* **11**:2457-2463.
231. **Wnek, A. P., and B. A. McClane.** 1983. Identification of a 50,000 Mr protein from rabbit brush border membranes that binds *Clostridium perfringens* enterotoxin. *Biochem Biophys Res Commun* **112**:1099-1105.
232. **Wnek, A. P., and B. A. McClane.** 1989. Preliminary evidence that *Clostridium perfringens* type A enterotoxin is present in a 160,000-Mr complex in mammalian membranes. *Infect Immun* **57**:574-581.
233. **Wnek, A. P., R. J. Strouse, and B. A. McClane.** 1985. Production and characterization of monoclonal antibodies against *Clostridium perfringens* type A enterotoxin. *Infect Immun* **50**:442-448.
234. **Yamamoto, K., Y. Ichinose, H. Shinagawa, K. Makino, A. Nakata, M. Iwanaga, T. Honda, and T. Miwatani.** 1990. Two-step processing for activation of the cytolysin/hemolysin of *Vibrio cholerae* O1 biotype El Tor: nucleotide sequence of the structural gene (*hlyA*) and characterization of the processed products. *Infect Immun* **58**:4106-4116.
235. **Yamamoto, K., A. C. Wright, J. B. Kaper, and J. G. Morris, Jr.** 1990. The cytolysin gene of *Vibrio vulnificus*: sequence and relationship to the *Vibrio cholerae* E1 Tor hemolysin gene. *Infect Immun* **58**:2706-2709.
236. **Yamanaka, H., T. Satoh, T. Katsu, and S. Shinoda.** 1987. Mechanism of haemolysis by *Vibrio vulnificus* haemolysin. *J Gen Microbiol* **133**:2859-2864.
237. **Yan, M., and R. J. Collier.** 2003. Characterization of dominant-negative forms of anthrax protective antigen. *Mol Med* **9**:46-51.
238. **Zhao, Y., and S. B. Melville.** 1998. Identification and characterization of sporulation-dependent promoters upstream of the enterotoxin gene (*cpe*) of *Clostridium perfringens*. *J Bacteriol* **180**:136-142.
239. **Zinevich, L. S., M. M. Gasilina, and M. V. Sidorova.** 1972. [Pigeons as models for the study of food poisoning caused by *Clostridium perfringens* type A]. *Gig Sanit* **37**:70-73.
240. **Zitzer, A., O. Zitzer, S. Bhakdi, and M. Palmer.** 1999. Oligomerization of *Vibrio cholerae* cytolysin yields a pentameric pore and has a dual specificity for cholesterol and sphingolipids in the target membrane. *J Biol Chem* **274**:1375-1380.